# POLITECNICO DI TORINO

**Master of Science in Automotive Engineering**

Master's degree thesis

# Development and calibration of a predictive 1D CNG heavy duty engine model

**Supervisor**

Prof. Daniela Anna Misul

**Co-supervisor**

Dr. Eng. Carlo Beatrice[1]

Eng. Dario Di Maio[1]

**Candidate**

Andrea Rossini

1. CNR-Istituto Motori, Napoli

April 2019

# Ringraziamenti

Tengo a ringraziare la prof.ssa Daniela Anna Misul, relatrice di questa tesi e l'Ing. Carlo Beatrice, co-relatore e punto di riferimento per tutto il lavoro svolto presso l'Istituto Motori CNR di Napoli. Vorrei inoltre ringraziare l'Ing. Dario Di Maio, per avermi guidato nella realizzazione di questa tesi, con professionalità e dedizione, senza il cui aiuto non avrei raggiunto i risultati ottenuti.

Un ringraziamento sentito va agli amici che mi sono rimasti accanto durante questo periodo, e che lo sono ancora, per avermi sopportato e sostenuto lontano da casa; una vera e propria famiglia, a volte anche di più.

Grazie ai miei colleghi di università più vicini, dell'aiuto e della pazienza che mi hanno riservato, senza i quali non avrei certo terminato questo percorso in tempi dignitosi.

Grazie a mia Madre, a mio Padre e a mia sorella che nonostante la distanza e i momenti difficili, non hanno mai smesso di credere in me e mi hanno sostenuto in maniera incondizionata. Il vostro esempio e i vostri insegnamenti sono stati e saranno sempre un faro nel cammino che ho completato e che dovrò affrontare.

Grazie dunque per l'affetto, il sostegno e l'aiuto dedicatomi, in fondo la grandezza di un uomo la si giudica da coloro che lo accompagnano ed io, senza di voi, non sarei che una persona.

IV

# Contents

# List of Figures

# Nomenclature

| | |
|---|---|
| AFOLU | agriculture, forestry and other land use (emissions) |
| BDC | Bottom dead center |
| BMEP | Breake mean effective pressure |
| CAC | Charge-Air-Cooler |
| CI | Compression Ignition |
| CNG | Compressed natural gas |
| CR | Compression Ratio |
| DI | Direct Injection |
| DOE | Design of Experiment |
| ECU | Electronic Control Unit |
| FMEP | (total) Friction mean effective pressure |
| GHG | Greenhouse gas |
| GtCO2 | Gigatonne carbon dioxide equivalent |
| HC | Unburnt Hydrocarbon |
| HRR | Heat release rate |
| HTR | Heat transfer rate |
| ICE | Internal Combustion Engine |
| IMEP | Indicated Mean Effective Pressure |
| IVC | Intake valve closing |
| KI | Knock Index |

LHV             Lower Heating Value

LNG             Liquified Natural Gas

MPI             Multi-Point Injection

NG              Natural gas

$NO_x$          Nitrous Oxides

PM              Particulate matter

RON             Research Octane Number

SA              Spark advance

SI              Spark Ignition

SMOG            Smoke Fog

SOx             Sulphur Oxide

SPI             Single-Point Injection

TC              Turbo Compressor

TDC             Top Dead Center

THC             Total Hydrocarbons

TPA             Three-Pressure Analysis

TWC             Three-way Catalytic Converter

UEGO            Universal Exhaust Gas Oxigen

UV              Ultraviolet (radiation)

WEO             World Energy Outlook

WHTC            World Harmonized Transient Cycle

WG              Wastegate

| | |
|---|---|
| WOT | Wide open throttle |
| ZFAS-U | Zirconia Film Automotive Sensor - UEGO |

# Symbols

| | |
|---|---|
| A | cross-sectional area |
| $A_s$ | heat transfer surface area |
| $C_f$ | fanning friction factor |
| D | equivalent diameter |
| dx | length of mass element in the flow direction |
| dp | pressure differential acting across dx |
| e | total specific internal energy (internal energy plus kinetic energy per unit mass) |
| H | total specific enthalpy |
| h | heat transfer coefficient |
| $h_f$ | enthalpy of fuel mass |
| $h_a$ | enthalpy of air mass |
| $h_{f,i}$ | enthalpy of injected fuel mass |
| $K_p$ | pressure loss coefficient |
| m | mass |
| $m_a$ | air mass |
| $m_b$ | burned gas mass |

$m_{f,i}$         injected fuel mass

$m_u$         unburned gas mass

$\dot{m}$         boundary mass flux into the volume

$n$         Engine speed [rpm]

$p$         pressure

$Q_u$         unburned zone heat transfer rate

$T_{fluid}$         fluid temperature

$T_{wall}$         wall temperature

$u$         fluid velocity at the bondaries

$V$         volume

$V_u$         unburned zone volume

$\rho$         density

$\omega$         Engine speed [rad/s].

XIV

# 1. Introduction

## 1.1 Greenhouse Gases Emissions and Heavy-Duty transport

The interest on global warming consequent from Greenhouse Gases (GHG) emissions has never been so high as in this period. Anthropogenic GHG emissions, in fact, have increased steadily from the second half of the 18th century, when the industrial revolution starts, driven mostly by economic and population growth and are now higher than ever. This has led to atmospheric concentrations of carbon dioxide ($CO_2$), methane ($CH_4$) and nitrous oxide ($N_2O$) that are unprecedented in at least the last 800,000 years [1]; in the last few decades, especially, GHG emissions have largely increased reaching half of the total cumulative emissions of $CO_2$ since 1750 (Fig. 1.1) [1]. Despite a growing number of climate change mitigation policies, annual GHG emissions grew on average by 1.0 GtCO2-eq (2.2%) per year, from 2000 to 2010, compared to 0.4 GtCO2-eq (1.3%) per year, from 1970 to 2000 (Fig. 1.2) [1].
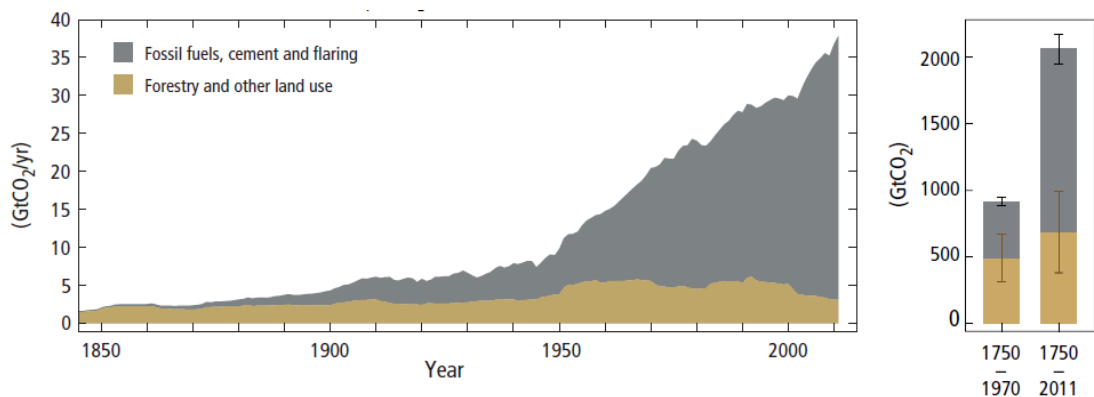


Figure 1.1: Global anthropogenic CO2 emissions over the years

Total annual anthropogenic GHG emissions have increased by about 10 GtCO2-eq between 2000 and 2010. This increase directly came from the energy (47%), industry (30%), transport (11%) and building (3%) sectors. When emissions from electricity and heat production are attributed to the sectors that use the final energy (i.e., indirect emissions), the shares of the industry and building sectors in global GHG emissions are increased to 31% and 19%, respectively (Fig. 1.3) [1]. The circle shows the shares of direct GHG emissions (in % of total anthropogenic GHG emissions). The pull-out shows how shares of indirect

CO2 emissions (in % of total anthropogenic GHG emissions) from electricity and heat production are attributed to sectors of final energy use.
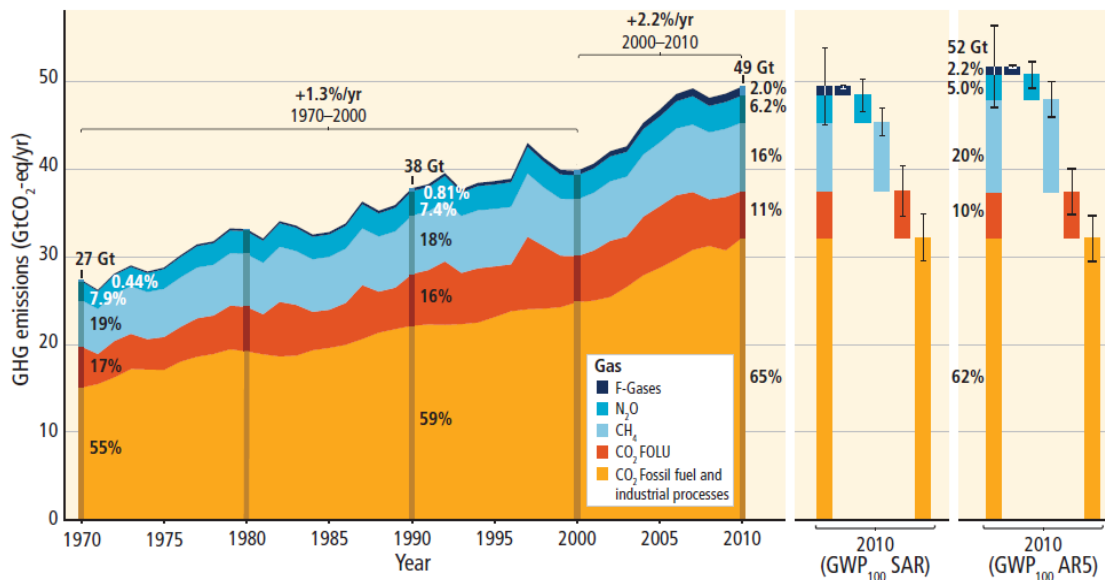


Figure 1.2: Total annual anthropogenic GHG emissions by gases 1970–2010
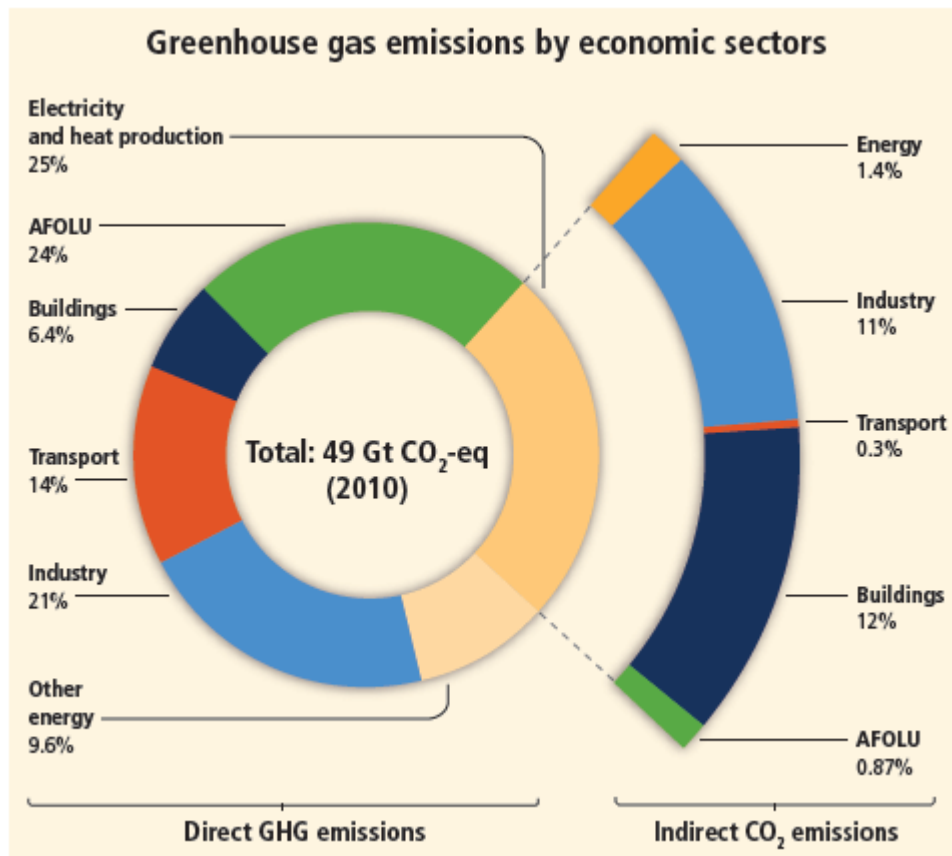


Figure 1.3: Total anthropogenic GHG emissions (GtCO2-eq/year) from economic sectors in 2010

In 2014, 29% of the energy mix came from coal, 31% from oil, 21% from gas, 5% from nuclear, 3% from hydro, 10% from bioenergy and 1% from renewables; therefore, the fossil fuel share among different sectors was still considerable and equal to 81% [2].

Since it'll be likely impossible, in the near future, to substitute all the energy sources with renewable ones, the differentiation among sectors remains the only sustainable path, in order to reduce the GHG emissions without impacting too much on the economic structure of our society. Hence, considering that transport sector is still almost completely dependent on fossil fuels and its complete electrification remains inapplicable on large scales with current technologies, the Natural Gas (NG) became more and more attractive as alternative fuel.

GHG have to be evaluated on the global scale due to the high volatility of the gases themselves which can spread out around the planet. The light traffic, mostly concentrated in urban areas, is the main cause of poor air quality but not as much as influent on the global warming topic as the heavy (goods) transports. The high urban air pollution, that remains the most perceived by population, is mainly due to the nitrous oxides ($NO_x$), unburned hydrocarbons (HC) and particulate matter (PM) emissions. The first two, thanks to UV radiations emitted by the sun, can combine with ozone ($O_3$) creating the well-known SMOG, while the latter is a very little dust that, if under certain dimensions, cannot be filtered by the human breathing system, being very dangerous for health; these compounds haven't the spreading capability of $CO_2$ and tend to accumulate in smaller areas. Hence, they're for sure accounted for the quality of the air but not from global perspective and, above all, not for global warming issue since they aren't GH compounds (exception has to be made for HC that are in fact GHG but only if not combined to form SMOG). For these reasons heavy-duty engines, that have much more fuel consumption and consequently more $CO_2$ production, are the most suited to be replaced by newer systems that can substitute conventional fuels with alternative and less $CO_2$ emitting ones, like NG.

## 1.2   Internal Combustion Engines (ICE) Fundamentals

Internal combustion engines are volumetric machines, i.e. machines that exploit volume changes of a mass of gas in order to produce power. The most common type in the automotive field is the 4-stroke in which four different phases are repeated continuously. Gasoline engines, in which the charge is ignited by a spark plug (Spark Ignition, SI) exploit the so-called Otto cycle, while diesel, which instead ignite the charge only by compression (Compression Ignition, CI), use the homonymous Diesel cycle. The Otto cycle is reported below, in Figure 1.4, where the piston and valve movement are shown; the four phases (strokes) are called:

*(a)* Intake: air-fuel mixture (charge) is inducted into the engine through the open intake valves while the piston moves down toward its lower position, called bottom dead centre (BDC).

*(b)* Compression: intake valves close and the piston moves upwards compressing the charge inside the chamber. When the piston is close to its top dead centre (TDC) the charge is ignited by the spark plug, with different timings depending on the speed and load conditions.

*(c)* Expansion: Due to the occurring of the combustion, the pressure has a step increase that pushes the piston downwards; this is the only phase in which work is produced.
Usually the combustion starts before the piston reaches the TDC and ends in the very first part of the expansion stroke.

*(d)* Exhaust: As soon as the piston approaches again the BDC, the exhaust valve is opened and the pressure, in the first part, as well as the movement upwards of the piston, during the stroke, expel the gases into the exhaust manifold.

The differences of the Diesel cycle with respect to the Otto cycle are not about the phases above mentioned, but in the way with which the mixture is obtained and then ignited. In the former the mixture is heterogeneous, since the fuel is injected directly (Direct Injection, DI) inside the chamber at the end of the compression stroke, giving little time to the charge to mix well, while in the latter is (usually) homogeneous, since the injection is made in the intake port (Port Fuel Injection, PFI) during the intake stroke, leaving a lot more time to the charge to well mix. In the latest years, also for gasoline engines are

arising models with direct injection (Gasoline Direct Injection, GDI) because of the numerous advantages on the engine control strategies, aimed to reduce fuel consumption without losing performances, that they allow if compared with traditional PFI ones.
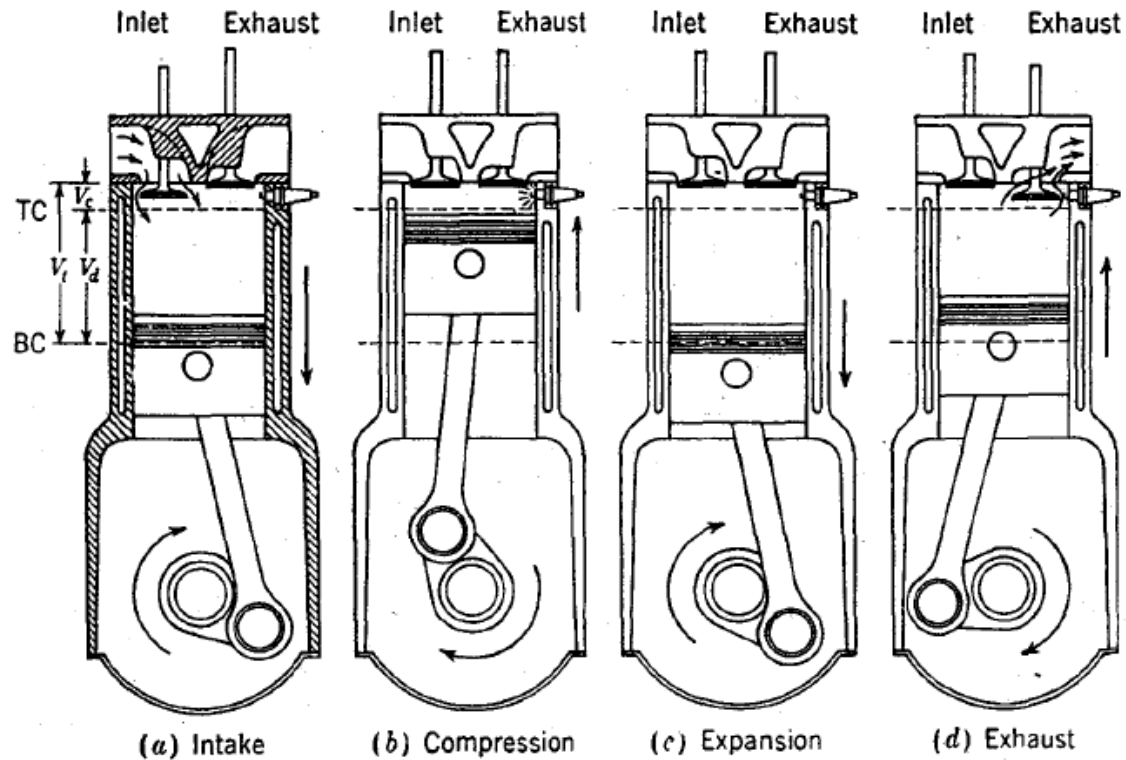


Figure 1.4 Four stroke SI operating cycle [3].

The bigger limitation about SI gasoline engines is the maximum compression ratio (CR) achievable. The CR, that is defined as:

$CR = \frac{V_d + V_c}{V_c}$, with $V_d$ the displacement volume and $V_c$ the clearance volume (Fig. 1.4),

is in fact the core of the volumetric machines: higher is the CR, higher the efficiency of the machine itself. But at high compression ratios (for PFI over 12:1) gasoline tends to undergo the so-called knocking, an unwanted phenomenon that negatively affect the lifespan of the engine. "*Its name comes from the noise that results from the autoignition of a portion of the fuel air, residual gas mixture ahead of the advancing flame. As the flame propagate across the combustion chamber, the unburned mixture ahead of the flame called the-end gas is compressed, causing its pressure, temperature, and density to increase. Some of the end-gas fuel-air mixture may undergo chemical reactions prior to normal combustion. The products of these reactions may then autoignite: i.e., spontaneously and rapidly release a large part or all of their chemical energy. When this happens,*

*the end gas burns very rapidly, releasing its energy at a rate 5 to 25 times that charac-teristic of normal combustion. This causes high frequency pressure oscillations inside the cylinder that produce the sharp metallic noise called knock.*" [3, page 375].

Natural gas engines are usually obtained by conversion from gasoline SI ones of which are maintained the geometrical and structural characteristics. As explained in the follow-ing, this is a largely impacting on the performances of those engines.

## 1.3    Natural Gas as engine fuel

Natural Gas is colourless, odourless, tasteless, shapeless, and lighter than air (see Table 1.1) and is sold after appropriate treatment for acid gas reduction, odorization, and hy-drocarbon and moisture dew point adjustment [4]. It is a mixture of different hydrocar-bons, mainly composed by methane ($CH_4$), the alkane with the highest hydrogen-to-car-bon ratio, and short chain compounds like ethane ($C_2H_6$), propane ($C_3H_8$) and butane ($C_4H_{10}$) as well as other more complex alkanes and alkenes but in lower percentages. Differently from common fossil fuels like gasoline and diesel, whose hydrogen-to-carbon ratio is typically equal to 1.85, NG has the lowest $CO_2$ emissions per units of energy produced (Table 1.2), although more energy per unit mass stored [5].

Saw from this only perspective, NG seems to be an excellent substitute for conventional fuels in automotive sector and there are no reasons why it isn't so widespread as vehicles fuel. Biggest issue, however, has to be ascribed to the storage technology both inside the vehicle and in refuelling stations.

**Table 1-1 Properties of Natural Gas [4]**

| Properties | Values |
|---|---|
| Carbon content, weight % | 73.3 |
| Hydrogen content, weight % | 23.9 |
| Oxygen content, weight % | 0.4 |
| Hydrogen/carbon atomic ratio | 3.0 – 4.0 |
| Relative density, 15 ℃ | 0.72 – 0.81 |
| Boiling point, ℃ | -162 |
| Autoignition temperature, ℃ | 540 – 560 |
| Octane number (RON) | 120 – 130 |

| | |
|---|---|
| Stoichiometric air/fuel ratio, weight | 17.2 |
| Lower heating value, MJ/kg | 38 – 50 |
| Stoichiometric lower heating value, MJ/kg | 2.75 |
| Methane concentration, volume % | 80 – 99 |
| Ethane concentration, volume % | 2.7 – 4.6 |
| Nitrogen concentration, volume % | 0.1 – 15 |
| Carbon dioxide concentration, volume % | 1 – 5 |
| Specific $CO_2$ formation, g/MJ | 38 – 50 |

**Table 1-2 Carbon dioxide emissions per units of energy [5]**

| Fuel | CO2 emissions per units of energy [kg/kWh] |
|---|---|
| Coal | 0.334 |
| Diesel fuel and heating oil | 0.250 |
| Gasoline (without ethanol) | 0.243 |
| Propane | 0.215 |
| Natural Gas | 0.181 |

**Table 1-3 Specific energy density by fuels [6]**

| Fuel | Specific Energy [MJ/kg] |
|---|---|
| Coal | 25 |
| Diesel fuel and heating oil | 44.8 |
| Gasoline (without ethanol) | 47.3 |
| Methane | 55.6 |
| Ethane | 51.8 |
| Propane | 50.3 |

To make it clear, a simple example is reported: consider the volume of a typical car fuel tank of a 45 $dm^3$, due to the NG characteristics reported above, the total amount of stored mass at environmental conditions (1bar and 20 ℃) is three order of magnitude lower than that of gasoline, 3e-2 kg for the former vs 30.6 kg for the latter. Considering the amount of available energy stored inside the tank, it is then three order of magnitude less as well. In order to increase the amount of available energy, some solutions have been developed.

As soon as the gas is refined need to be transported because of the its nature (gaseous at environment conditions) and consequence storage difficulties. The are several options for transporting natural gas energy from oil and gas fields to market but the most used until now are pipelines, liquefied natural gas (LNG), compressed natural gas (CNG) [4]. Pipelines are maybe the most convenient method of transport it but aren't flexible as the gas will leave the source and arrive at its (only) destination; this is in fact the method used for transport gas to buildings and, more generally, to cities, where a great amount of it is requested to be used for different purposes, for example cooking or heating. If for transport purposes this technology isn't suitable for obvious reasons, for refuelling stations could be a solution, however the cost of building a dedicated pipeline is generally very high and not convenient.

LNG, as the name itself says, is the liquid form of natural gas: when cooled under approximately -162 ℃, liquifies and reduces its volume of about 1/600 that of gas at room temperature. The increased density to approximately 0.42 kg/dm$^3$, similar to that of diesel and gasoline, allows to store much more energy inside the same tank, so making the vehicle reaching acceptable ranges. Anyway, LNG technology is typically used to facilitate transport of natural gas and not as solutions for tanks due to the complex systems required for liquefying natural gas. In the transport sector it is adopted in over-the-road trucks due to large cryogenic tank need. Even so, liquefied natural gas must be stored for periods of time (months) without significant boil-off losses, which is difficult.

CNG is an easier solution with respect to LNG, since natural gas is simply compressed, typically up to 250 bar, inside specifically designed containers; the increased density resulting from this process allows to store more mass of gas inside the tanks, so increasing the amount of energy available. Compressed natural gas technology provides an effective way for shorter-distance transport of gas and is the only suitable solution for light duty vehicles, although stringent regulations for tanks are necessary for safety reasons [7].

Considering instead the technical aspects of the natural gas engines, there are many advantages over traditional one [8]:

- **Thermal Efficiency**. Thermal efficiency of the engines is function of various parameters but perhaps most important is the compression ratio of the engine. Higher the compression ratio higher would be theoretical and also actual efficiency. Since, as previously reported, the octane number of natural gas is ranging

from 120 to130, the engine could function at compression ratio up to 16:1, without knocking, allowing a dedicated CNG engine to use higher compression ratio to enhance engine thermal efficiency of about 10% above than that of gasoline engine. A dedicated CNG engines may therefore have the efficiency up to 35% in contrast to 25% for that of gasoline engine.

- **Mixing Advantage.** Being a light weight and gaseous at normal atmospheric conditions fuel, natural gas can produce much better homogeneous air–fuel mixture. Moreover, because liquid fuel needs time for complete atomization and vaporization to form a homogeneous mixture, it has the inherent advantage of high level of miscibility and diffusion with gaseous air, which is essential for good combustion. On the other and, the lack of vaporization means that the air – CNG mixture will have higher temperature if compared to air – gasoline mixture (liquid fuel take heat from the surrounding air to complete the vaporization phase), reducing the volumetric efficiency. This, anyway, only if natural aspirated engines are considered, whereas turbo compressed ones can easily overcome it by simply increasing the boost pressure in the intake phase.

- **Maintenance Advantage.** Always because CNG comes into the engine in gaseous form it cannot dilute with the lubricating oil of the piston rings region, as instead gasoline and diesel do, preserving the oil lubrication characteristics for much more cycles. Therefore, CNG cuts the maintenance costs and prolongs engine useful life. Furthermore, the absence of lead concentration in CNG contributes to avoid lead fouling of spark plugs, thus extending the life of piston rings and plugs. On the other side, CNG engines require low sulfated ash oil, because it is dry and provide absolutely no lubricant value, conducing to sulfated ash deposits on exhaust valves. Those deposits contain metal sulfates, including barium, calcium, magnesium, zinc, potassium, sodium and tin that, if present in large quantities, can result in reduced heat transfer, detonation, valve burning and ring sticking or breaking.

Despite the big issue of the storage, the NG demand in transport sector has continuously increased in the last decades, mostly because of both the lower cost with respect of conventional fuels and the always more stringent emissions regulation. In fact, considering the global gas demand projection for different scenarios it will nearly double up in the next two decades with road transport that will account for two – thirds of the growth. The

key point will be for sure the enhancement of the refilling station infrastructure, increasing the coverage over the territory so making the natural gas vehicle more attractive than today [2].

## 1.4    Natural gas engine typologies

Natural gas engine technology is not new, first engines of this type in fact has been developed even before the gasoline one, with the main examples of the Lenoir (1860) and Otto (1867). Those engines, however, were suffering of low power density and generally high fuel consumption (even more than others of same period) and were not suitable for propulsion of vehicles considering that NG, at the time, was stored at atmospheric or slightly higher pressures. That technology was hence abandoned after the invention of the 4-stroke gasoline engine, due to its considerably higher power density and lower fuel consumption, and only during the beginning of the $20^{th}$ century natural gas was re-discovered as engine fuel. The use of CNG as a vehicular fuel was discovered back in early 1930 in Italy, but a larger interest grows up only in the 1970s, when natural gas was witnessed as a promising fuel aftermath of the oil crisis. This time, however, the engines were developed through conversions from previous gasoline or diesel platforms and not created by scratches, since the known technology on the formers were a lot more advanced. Current NG vehicles are still provided with those type of engines, named "bi-fuel" if gasoline-NG SI type, "dual-fuel" if diesel-NG CI type. The differences between them are not only in the engine cycle but also in the supply system and how the mixture of air and fuel is made.

In the bi-fuel configuration, the CNG supply system is mainly composed by a tank, a safe valve to ensure non-exceeding pressures, pressure regulator(s), a rail connected to the injectors and a fuel switch, that can be manual or automatic (Figure 1.5). The mixture is therefore performed in the intake runners and enters in the cylinder with homogeneous composition where is ignited by the spark plug. A highly criticized aspect of the bi-fuel engines is the lower performances in CNG mode if compared with gasoline mode, and so if compared to a traditional engine. This is a direct consequence of the current storage technologies and, moreover, of the poor refuelling infrastructure coverage. These engines are in fact designed following the gasoline characteristics: the higher tendency of it to auto-ignite if compared with methane (Research Octane Number: $RON_{gasoline} = 95$, $RON_{methane} = 120 - 130$) make mandatory to give special attention to the combustion

chamber [6], that is only optimized for gasoline. Therefore, in order to mitigate knock event for gasoline propulsion, the efficiency of the engine running with CNG is poor and the performances theoretically allowed by it, is not fully exploited.



| | |
|---|---|
| CAN, SENT LIN | |
| Diagnostic lamp | |
| Diagnostic interface | |
| Immobilizer | |
| Ambient pressure sensor | |

E  Exhaust gas
A  Fresh air
G  Natural-gas supply
F  Fuel
—  Electrical connection
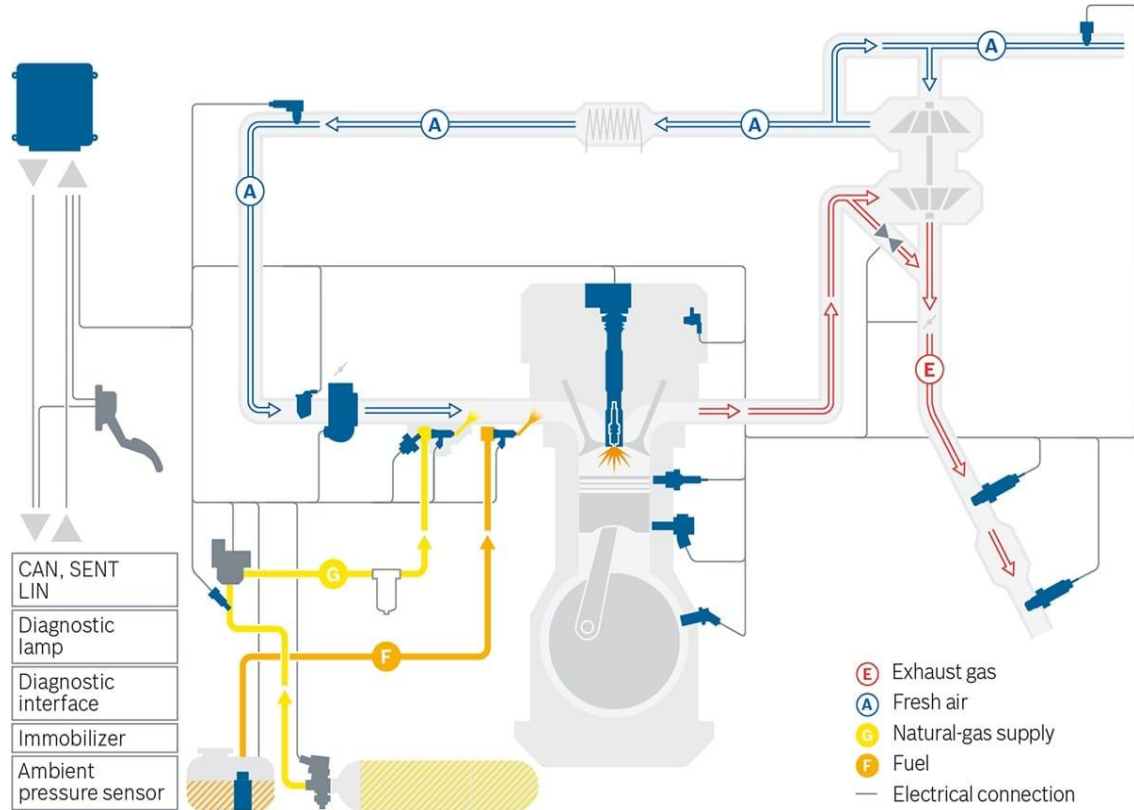
Figure 1.5 Bi-fuel CNG SI engine scheme with supply system [9]

Two completely different approaches instead can be found in the dual-fuel layout: in the first, the air-NG mixture is created in the intake manifold, as the previous layout, but it is ignited with a diesel pilot injection (Fig. 1.6); two different supply systems are necessary, one for the CNG, with injector(s) in the manifold, and one for the diesel, with the injector inside the cylinder head. The second option, technically and architecturally more complex, consist in a direct injection of CNG at the end of the compression stroke, like in conventional diesel engines, close to a hot surface that usually consist in special glow plugs. The most important advantages of this concept are high specific power and thermal efficiency without the limitation of combustion knock (Figure 1.7) [10].

These two more elaborated systems are needed because, even though CI engines present higher compression ratios (CR) by design, it is still not enough to auto ignite the methane simply by compressing it.
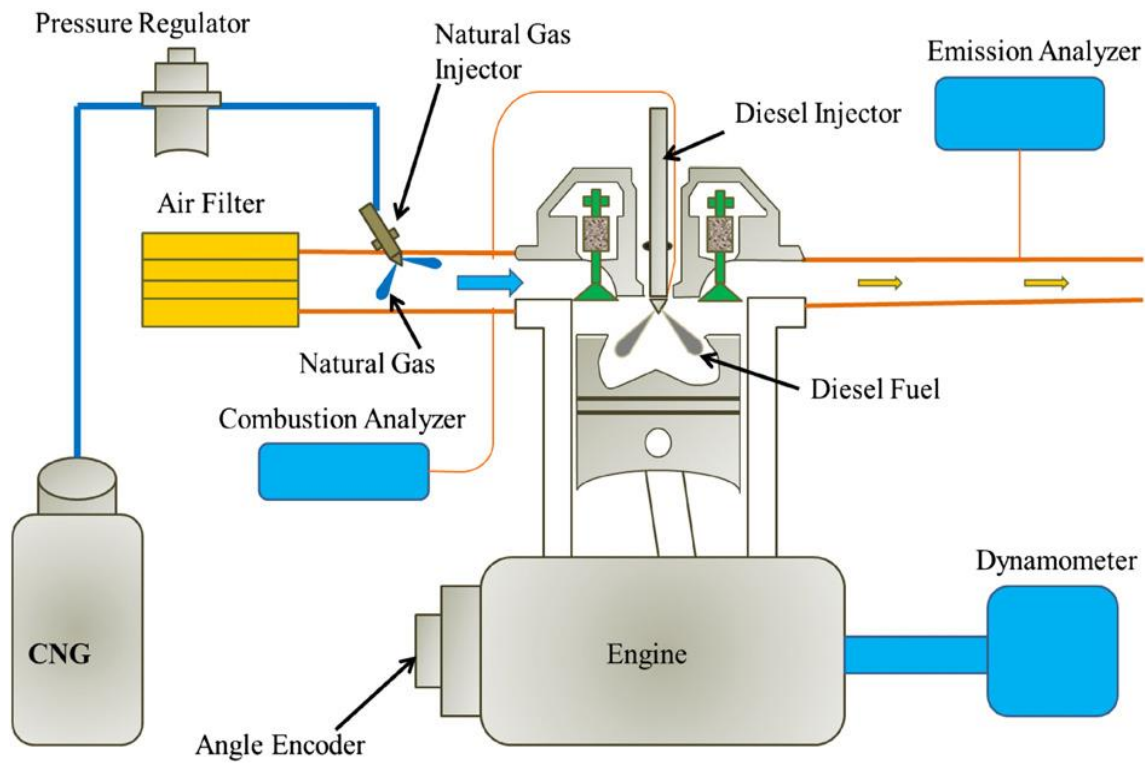
Figure 1.6 Schematic diagram of a dual fuel system [10]
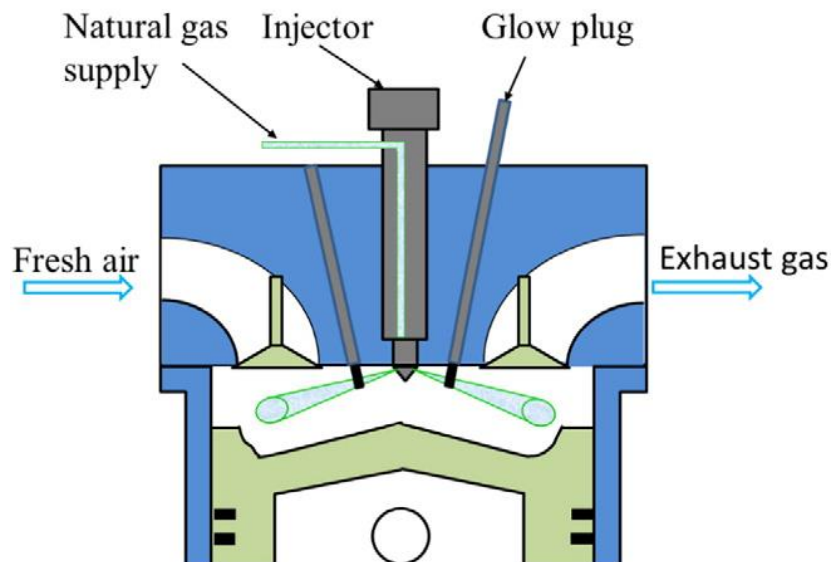


Figure 1.7 Schematic diagram of hot surface assisted compression ignition [10]

Finally, dedicated natural gas vehicles can be found in road transport market equipped with CNG or LNG supply system depending on vehicle size, CNG typically for light duty

vehicles, while LNG mostly for heavy-duty ones. Those engines are SI type that are operated only on natural gas, designed on its characteristics, so optimized to exploit the advantages exposed before. Furthermore, they are designed keeping the combustion properties of natural gas, so that the vehicle produces very less emission pollutant. Only this configuration is capable to totally exploit the potential of natural gas.

The following work will be focused on this last type of engine, more specifically on a heavy-duty SI CNG engine.

## 1.5   Simulation introduction and description of the used software: GT-Power

The simulation models are largely studied because they offer great advantage and a substitute when real-life testing is expensive, time consuming, difficult or not feasible. The most beneficial aspect over the actual test rig is the possibility, once the model has been accurately calibrated, to perform iterative tests and investigate the influence of different parameters on the results without requiring the re-setup of the whole rig, saving a lot of time and money.

The drawbacks of the models would be the time consumption for the calibration itself and also the simulation time. The models might not yield the same results as the test rig results due to the several factors but calibrating and validating the models against the test rig data would yield close enough results which can be relied upon.

GT-POWER is a one-dimensional simulation tool included in the GT-SUITE program from Gamma Technology. It is suitable for analysis of a wide range of vehicle and engine performance issues, from the combustion inside the cylinder, to the cooling and lubrication of the engine, as well as more mechanical focused parts like the valvetrain and cranktrain. The solution is based on one-dimensional fluid dynamics, representing the flow and heat transfer in the piping and other flow components of an engine system.

The tool is designed to allow the construction of the engine model by dragging and dropping objects representing the engine parts in the graphical user interface of GT-POWER from the GT-SUITE libraries, where a large database offers a broad range of different

objects. After having positioned all the components, the user may define specific proper-ties for each one, like geometrical and material characteristics as well as setting up simu-lation options such as convergence criteria and specify desired output plots. Finally, the user can link all the defined components by the connection object, simulating the actual connection between them.

- **Flow modelling [11]**. The flow model involves the solution of the conservation of continuity, momentum and energy equations, also known as "Navier-Stokes equations". As already explained, these equations are solved in one dimension, which means that all quantities are averages across the flow direction. There are two choices of time integration methods: an explicit method and an implicit method. The primary solution variables in the explicit method are mass flow, den-sity and internal energy, while those of the implicit method are mass flow, pres-sure and total enthalpy.

  Every pipe is discretized into one or more volumes, depending on the discretiza-tion length chosen by the user, while each flowsplit is represented by a single volume (Fig. 1.8). These volumes are connected by boundaries for which the vec-tor variables (mass flux, velocity, mass fraction fluxes, etc.) are calculated, whereas scalar variables (pressure, temperature, density, internal energy, en-thalpy, species concentrations, etc.) are assumed to be uniform over each volume. This type of discretization is referred to as a "staggered grid".
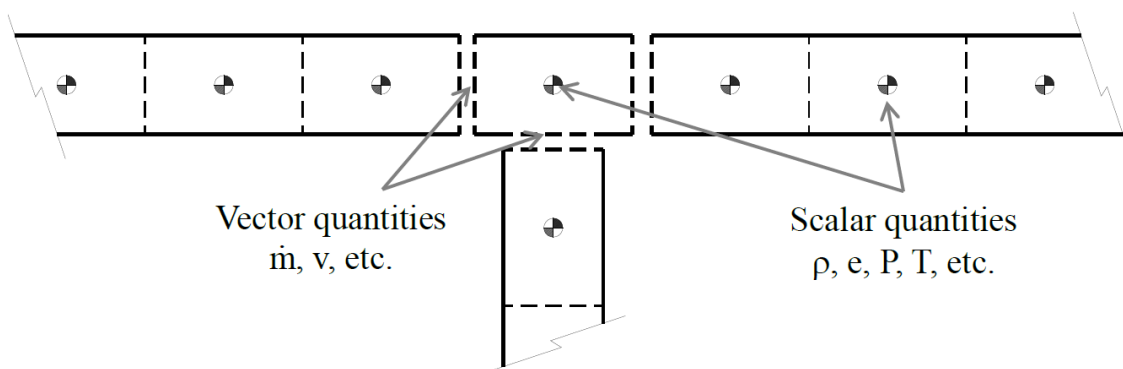


Figure 1.8 Schematic of staggered grid approach [11].

The conservation equations solved by GT-SUITE are shown below:

Continuity:

$$\frac{dm}{dt} = \sum_{boundaries} \dot{m}$$

Energy:

$$\frac{d(me)}{dt} = -p\frac{dV}{dt} + \sum_{boundaries} (\dot{m}H) - hA_s(T_{fluid} - T_{wall})$$

Enthalpy:

$$\frac{d(\rho HV)}{dt} = \sum_{boundaries} (\dot{m}H) + V\frac{dp}{dt}(T_{fluid} - T_{wall})$$

Momentum:

$$\frac{d\dot{m}}{dt} = \frac{dpA + \sum_{boundaries}(\dot{m}u) - 4C_f\frac{\rho u|u|}{2}\frac{dxA}{D} - K_p\left(\frac{\rho u|u|}{2}\right)A}{dx}$$

- **Combustion modelling [11]**. Combustion modelling in GT-Power is performed following the so called "Two-Zone Combustion" methodology. It means that the air-fuel mixture present inside the chamber is divided into two zones: the unburned zone and the burned zone. Before the start of the combustion, all the charge content is of course in the unburned zone whereas the burned zone is empty. From the start of combustion (the spark in the SI engine, or the start of injection in the DI engine) and for each following timestep, a portion of the air-fuel mixture is transferred to the burned zone, depending on the burn rate (imposed or calculated by the combustion model). Once the unburned mixture has been transferred from the unburned zone to the burned zone in a given time step, a chemical equilibrium calculation is carried out for the entire "lumped" burned zone. The equilibrium concentrations of the species depend strongly on the current burned zone temperature and to a lesser degree, on the pressure. Once the new composition of the burned zone has been obtained, the internal energy of each species is calculated. Then, the energy of the whole burned zone is obtained by summation over all the species. Applying the principle that energy is conserved, the new unburned and burned zone temperatures and cylinder pressure are obtained.

For each time step, and corresponding to the two zone, the following energy equations are solved:

- Unburned Zone:

$$\frac{d(m_u e_u)}{dt} = -p\frac{dV_u}{dt} - Q_u + \left(\frac{dm_f}{dt}h_f + \frac{dm_a}{dt}h_a\right) + \frac{dm_{f,i}}{dt}h_{f,i}$$

where subscript "u" denotes unburned zone,

- Burned Zone:

$$\frac{d(m_b e_b)}{dt} = -p\frac{dV_b}{dt} - Q_b + \left(\frac{dm_f}{dt}h_f + \frac{dm_a}{dt}h_a\right)$$

where subscript "b" denotes burned zone.

The algorithm and equations mentioned above are common for all the combustion models available in GT-Power. In the software, in fact, different combustion modelling alternatives for both SI and diesel engines are available, divided in Predictive, Semi-Predictive and Non-Predictive Combustion models. The three typologies are substantially different in how they operate with the burn rate and it is important to understand when each model is more appropriate than another.

In a **non-predictive** combustion model, the burn rate is imposed by the user as a function of the crank angle. The simulation follows this prescribed burn rate assuming enough fuel is available regardless of the cylinder conditions. Therefore, the residual fraction and the injection timing doesn't have any influence on the burn rate during the simulation. Hence non-predictive combustion model can be used for studying variables which has a very small influence on the burn rate, for example how the intake manifold runner length acts on volumetric efficiency or to study the acoustic performance of different muffler designs [11]. When instead the accounted variable is greatly influenced by the burn rate non-predictive combustion models are not desired and these situations can be handled by semi-predictive and predictive combustion models.

In **predictive combustion** models the burn rate is calculated each timestep starting from initial conditions of the model (usually corresponding to experimental data from the actual testing rig) and varies accordingly to any change in the parameters which have influence on it. Hence the computation time of these models is significantly higher because of

the added complexity in calculations, moreover predictive models requires calibration against measured data to provide accurate results which is time consuming [11].

A **semi-predictive** combustion model may be a good substitute for a predictive model in some cases. A semi-predictive combustion model is sensitive to the significant variables that influence combustion rate, and responds appropriately to changes in those variables, but does not use any physical models to predict that response, relying instead on non-predictive methodology (Wiebe) to impose the burn rate through lookups parameters.

## 1.6    Aim of the thesis

The thesis is focused on the calibration of a 1D model for a commercial turbocharged heavy-duty SI CNG engine, built on GT-Power, both in stationary and transient conditions with the aim of simulates as accurately as possible the thermodynamics, emissions and consumption of the real engine over transient cycles like the WHTC and RDE ones. The work is in fact developed in order to build a tool than can substitute the test bench in the first stage of the design of new engine components or on the development of new enhanced geometries. The work is divided in two main sections:

1. **Steady State**. Development and calibration of 1D model in steady state conditions with the implementation of a predictive combustion model. The objective of this first section is that of reproduce as close as possible the engine behaviour, in stationary conditions, over the whole available engine map. After the matching of the flows in pipes, of the amount of fuel injected and of the turbocharging system, work concentrate on the combustion itself. Finally, thermal exchanges and temperatures are accounted for.

   A large part of the section will be dedicated to the combustion process because, as will be exposed, several encountered criticalities have obliged to momentarily abandon the predictivity of the model.

2. **Transient**. Implementation and further calibration of the model over a WHTC cycle in order to achieve a good simulation of the whole engine behaviour under transient conditions and, in particular, an accurate estimation of the consumptions and emissions of $CO_2$, CO and $NO_x$ at the engine out (before the aftertreatment system).

## 1.7   References

[1]        IPCC: Climate Change 2014 Synthesis Report, 2.1 Emissions of long-lived
           GHGs. https://www.ipcc.ch/report/ar5/syr/, accessed.

[2]        IEA (2017), *World Energy Outlook* 2017, OECD Publishing, Paris/IEA,
           Paris. http://dx.doi.org/10.1787/weo-2017-en.

[3]        Heywood, J. B. (1988). Internal combustion engine fundamentals (Vol. 930).
           New York: Mcgraw-hill.

[4]        Mokhatab S., Poe W. A., Speight J. G. (2006). Handbook of Natural Gas
           Transmission and Processing, Gulf Professional Publishing, Burlington, USA

[5]        EIA: 2018, International Energy Outlook, Washington, DC, US Department
           of Energy, Energy Information Administration, DOE/EIA-0484(2018).

[6]        Specific energy and energy density of fuel, March 26 2014, Neutrium,
           https://neutrium.net/properties/specific-energy-and-energy-density-of-fuels/

[7]        International Organization for Standardization. (2013). Gas cylinders – High
           pressure cylinders for the on board storage of natural gas as a fuel for auto-
           motive vehicles (ISO 11439:2013).

[8]        Muhammad I. K., TabassumY., Abdul S., "Technical overview of com-
           pressed natural gas (CNG) as a transport fuel", *Renewable and Sustainable
           Energy Reviews*, 51 (2015) 785 – 797.

[9]        [website] https://www.bosch-mobility-solutions.com/media/global/products-
           and-services/passenger-cars-and-light-commercial-vehicles/powertrain-so-
           lutions/compressed-natural-gas/systemgraphic_cng.jpg.

[10]       LijiangWei, Peng Geng, "A review on natural gas/diesel dual fuel combus-
           tion, emissions and performance", *Fuel Processing Technology,* 142 (2016)
           264–278.

[11]       GT-Suite v2016, *Engine Performance Application manual*, Gamma Technol-
           ogies.

# 2. Engine model calibration

In this section is explained how the engine model is developed and the calibration phases that have been performed to achieve good simulating results.

The geometries, material properties and all the specifications, including the maps of the turbocharging system, have been provided directly from the OEM as well as the experimental data. All the work is based on that material, taken it as already corrected and verified, so possible errors in the acquisitions hasn't been specifically corrected, even if all the assumptions have been taken with reasonably confidence.

## 2.1   Engine model description

The study has been performed on a heavy-duty, turbocharged, CNG only, SI engine of which some characteristics are reported below (Table 2-1).

**Table 2-1 Engine Specifications**

| Engine Specifications | Values |
| --- | --- |
| Type | Turbocharged, CNG, SI |
| Cylinder Arrangement | 6L (in-line) vertical |
| Valves per cylinder | 4 |
| Injection System | Multi Point Injection (MPI) |
| After Treatment System (ATS) | Three Way Catalyst |

For almost every part of the actual engine is possible to create one or more elements starting from the objects already present in the internal library of GT-Power. An elementary object can be customized in order to mostly reconstruct the actual characteristics of that real object. The cylinders, the intake and exhaust valves, the crank train subsystem and the turbocharging system have one or more default elements on which is possible to choose, so to reproduce as much as possible the real engine element.

In case there isn't a pre-defined element, like for the Charge-Air-Cooler, it is always possible to simulate it as a combination of elementary objects modifying the geometry, the thermal and the material characteristics. CAC, in fact, is reproduced in this model like a

single elementary pipe on which length, material and thermal constraints have been imposed so to imitate the actual behaviour (Fig. 2.1).
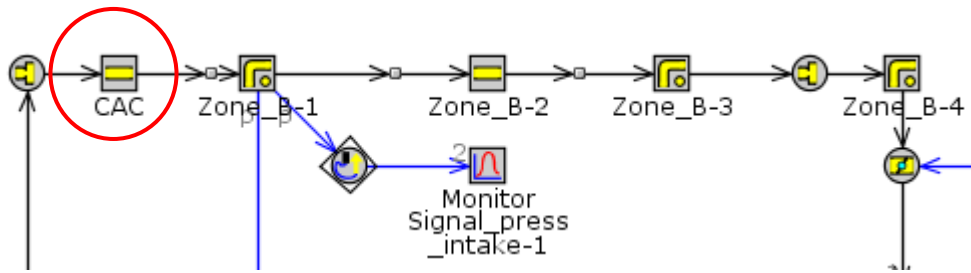


Figure 2.1 Detail of the Charge-Air-Cooler model

An important aspect of the model are the injectors: the elements used for them is the so called "InjAF-RatioConn" and allow to set only the value of A/F ratio, or the air index lambda ($\frac{A/F}{A/F_{st}}$) or phi (1/lambda), hence leaving the absolute quantity of air and fuel free to adjust based on the torque or the IMEP requested (Fig 2.2). This injector model decides the amount of fuel needed sensing the air flow that passes through it. This solution has been chosen because the experimental data of air flow and fuel flow were much more sensitive to errors than the those of lambda.



Figure 2.2 Control panel of the injector element "InjAF-RatioConn"

The controller of the entire model is based on two elements called Throttle Controller and Wastegate Controller (Fig. 2.3). The former controls the opening and closing of the element simulating the throttle valve (on the left edge of the left figure) through two sensors, one for the speed and one for the torque (or the IMEP, depending on the applications), linked to the crank train element. Doing so, it can control the load applied on the model itself. The latter, similarly, controls the travel of the wastegate in accordance with the need of the engine model in that instant, given the boost pressure as input (input signal

given by the sensor on the left edge of the right figure). The wastegate valve is intrinsically present as parameter in the "turbine" element and not available as independent object like the throttle valve.
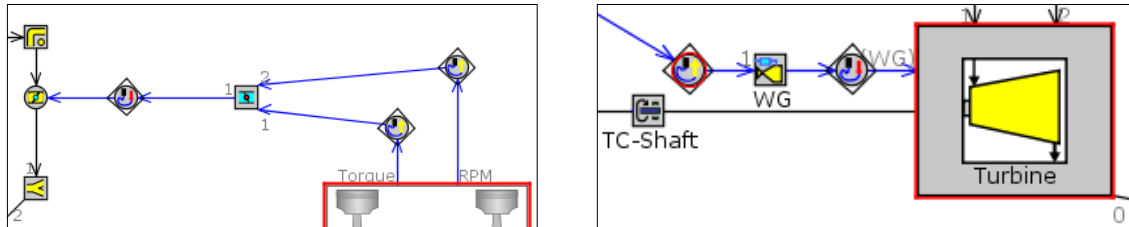


Figures 2.3 Throttle controller and Wastegate controller setup (respectively on the left and on the right)

## 2.2    Preliminary statements

First approach to the model has been to run it searching for errors and checking the integrity of the model itself. GT-Power, in fact, advise the user in case of encountered errors both during the actual model building, pointing out incomplete definitions of some elements, and in the simulation register, indicating more precisely what type of error has been encountered. Thanks to this, it is much easier to debug the entire model without double check every single element and parameter.

In this preliminary phase only a case at high load and medium speed has been considered, with a non-predictive combustion model based on the Wiebe relation. Doing so it has been possible to understand how the model worked without paying too much attention on the simulation results, both of flow and combustion. After the first check of the model the actual process of calibration started.

The available data from experimental tests were taken over 25 points of the engine map (see Fig. 2.4), from medium to high speed and from low to high load. Indicated crank resolved pressure cycles were available for the in-cylinder pressure while all the other thermodynamic data, like pressures and temperatures on intake and exhaust pipes, lambda values, emissions of CO, $CO_2$ and NOx, were given cycle averaged.

The 25 steady state conditions with corresponding experimental values have been implemented on it, and in particular the main inputs for the model were:

- speed (constraint)

- imep/torque (target);

- lambda (constraint);

- environmental pressures and temperatures (constraint)

- boost pressure (target);

- fuel composition (constraint).

Moreover, all the design specifications of the engine have been implemented inside the characteristics of each model element.
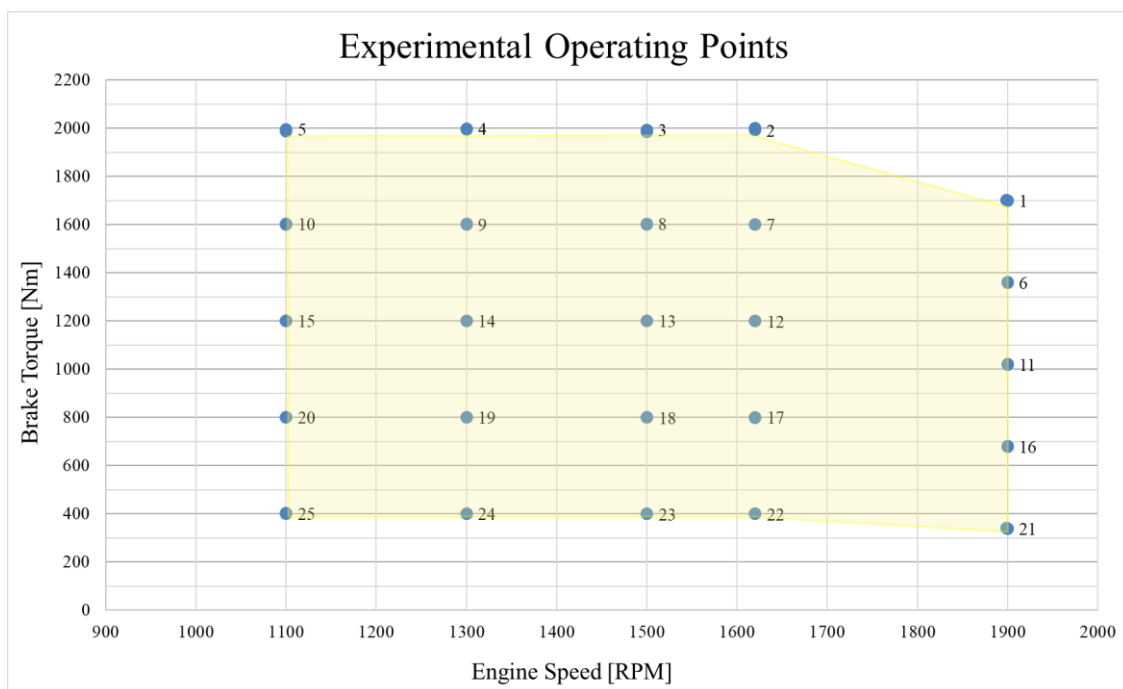


Figure 2.4 Experimental acquired points on engine map

A central aspect of the entire work has been to properly account for the lambda since both the fuel and air mass flow rates, although present among the experimental values, weren't directly used into the model. Lambda was in fact more precise and easier to implement on the injectors. Lambda values available on the experimental data sheet were several, taken from different sensors over the test bench. The selection of one value over the others and the reasons of the choice is described in the following chapter.

## 2.3    Lambda selection and air/fuel flow check

The chosen lambda has been selected among three available values, two of them obtained directly from dedicated sensors and one based on a relation with the exhaust gas composition at the engine out. The sensors were a **Smart NO$_x$ Sensor (SNS) 120** by Continental™ and a **Universal Lambda Sensor (ZFAS-U)** by NGK™ whereas the relation was obtained from the **R-49 regulation**.

### 2.3.1.  Smart NO$_x$ Sensor (SNS) 120

The SNS is used for catalyst management in vehicles with gasoline or diesel engines. Gasoline engines and CNG engines are pretty similar to each other, as already explained in the introduction, so it is possible to use the SNS also with CNG engines, taking into account that for both it's used the same ATS, the TWC. The smart NO$_x$ sensors consists of a ceramic sensor element and an electronic control unit, as shown in the assembly below (Fig. 2.5). It measures the NO$_x$ concentration, air/fuel ratio (A/F ratio) and equilibrium oxygen partial pressure in the exhaust gas, for this reason it must be mounted downstream of the catalyst (TWC, NO$_x$ trap, SCR depending on the case) (see Fig. 2.6).



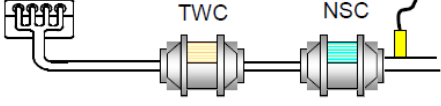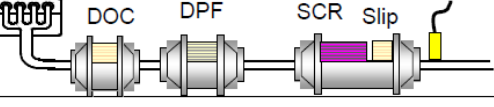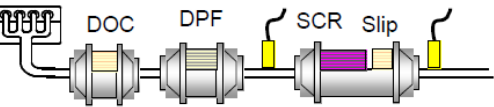Figure 2.5 Smart NO$_x$ Sensor (SNS) 120 [6]

| System Layout: typical example | Application | Explanation |
|---|---|---|
| **NSC system** <br><br> TWC    NSC | **NSC:** <br> - Passenger /Lean burn | 1) Catalyst regeneration control <br><br> 2)  Model adjustment <br><br> 3) OBD |
| **SCR System (DOC + DPF)** <br><br> DOC    DPF    SCR  Slip | **SCR:** <br> - Heavy Duty Truck (EU5) | 1) OBD of SCR system |
| **SCR System (DOC + DPF)** <br><br> DOC    DPF    SCR  Slip | **SCR:** <br> Heavy Duty Truck <br> (EU6; US2010) <br><br> **Passenger Diesel** <br> (EU6; T2bin5) | 1) OBD for the system (downstream) <br><br> 2) Urea Control (2 sensors) <br>     Modeling adjustment <br>     Feedback for Urea injection |

Figure 2.6 SNS mounting positions [6]

The operating mechanism is exposed in the Figure 2.7: a ceramic sensor made of zirconia ($ZrO_2$) electrolyte measures the oxygen concentration entering from exhaust gas through a diffusion barrier into a first cavity. The oxygen concentration inside the cavity is controlled to the constant concentration of a few ppm $NO_x$. Other components of the exhaust gas also entering the cavity as HC, CO and $H_2$ are oxidized at the pumping electrode made of Pt. From the first cavity the test gas with a few ppm $O_2$ and $NO_x$ enters a second cavity, where gaseous oxygen is totally removed by an auxiliary pump. At the measuring electrode the equilibrium of $NO \leftrightarrow N_2 + O_2$ is changed by removing oxygen generated by the reduction of NO. The measurement IP2 of this generated oxygen represents the NOx concentration of the exhaust gas [6].
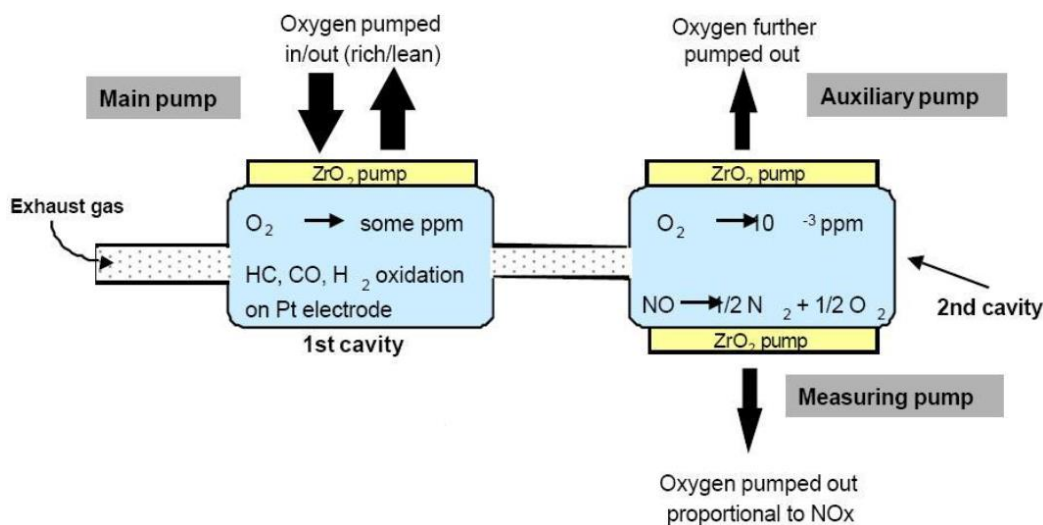


Figure 2.7 Schematic diagram of $NO_x$ sensor mechanism [6]

An electronic control unit (ECU) provides the power control for heating the sensor element to operating temperature. In an ASIC the regulation for the operation of all pumping cells to determinate $NO_x$ concentration, air/fuel ratio and binary $\lambda$ signal is realized. The ECU provides the measured gas concentrations digitally via CAN bus [6].

The SNS sensor has a very rapid response at composition changing and it is very precise at stoichiometric conditions but suffers of higher errors when the exhaust gas is in rich or lean conditions (Fig. 2.8). These characteristics make the smart NOx sensor very affordable both in steady-state, where the mixture is maintained around stoichiometric, and in transient, where the responsiveness is crucial, although larger errors are encountered since lambda oscillates more than in steady-state. Its main characteristics are reported in the following Table 2.2.

**Table 2-2 Smart NOx Sensor working characteristic**

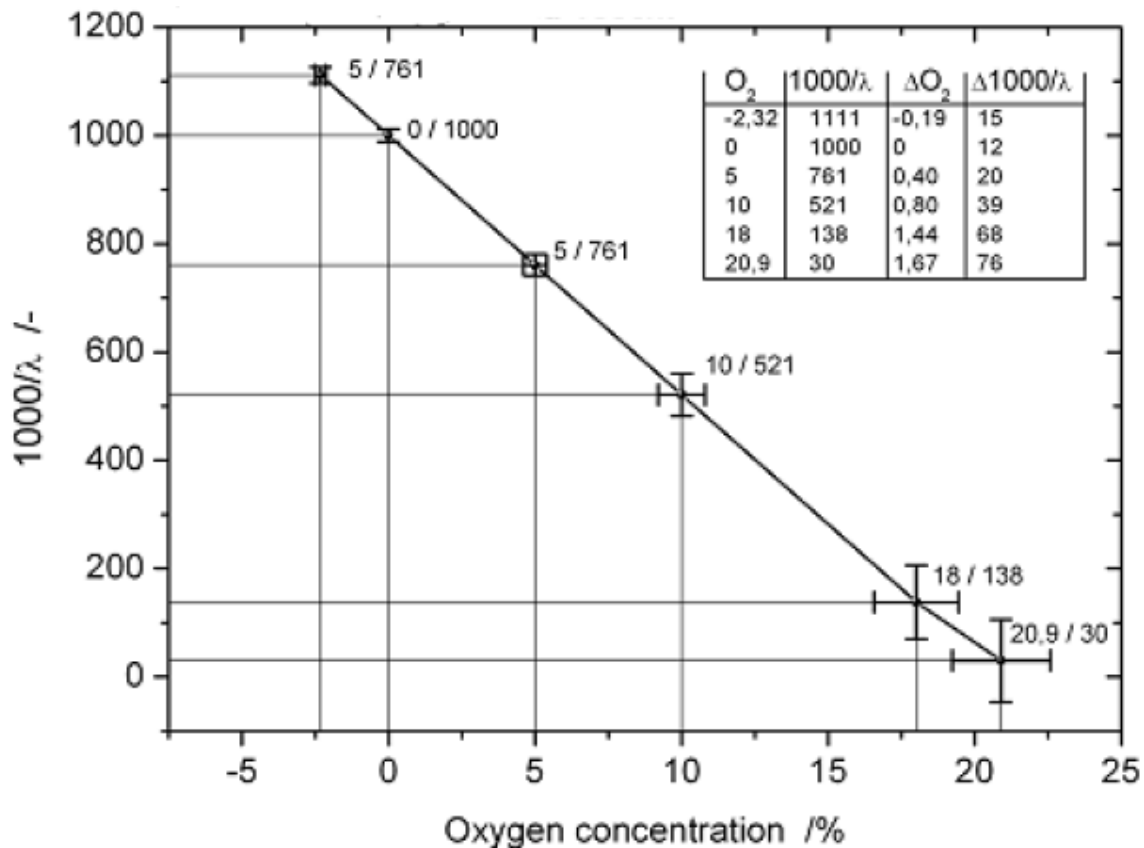| Nr | Name | Symbol | Min. | Max. | Dim. |
|----|------|--------|------|------|------|
| 1 | $NO_x$ concentration | $NO_x$ | 0 | 1500 | ppm |
| 2 | Linear Air/Fuel-ratio | $\lambda\_lin$ | 0 | 1250 | $1000/\lambda$ |
| 3 | Lambda binary | $\lambda\_rich(\lambda \leq 0.9)$ | 750 | | mV |
|   |   | $\lambda\_lean(\lambda \geq 1.1)$ | | 200 | mV |
| 4 | Lambda binary (Static-$\lambda$) | $\lambda_s$ | 0.994 | 1.010 | $\lambda$ |
| 5 | Response time $NO_x$ | $\tau_{33->66\% \, NOx}$ | | 1200 | ms |
| 6 | Response time $\lambda\_lin$ | $\tau_{33->66\% \, \lambda\_lin}$ | | 1050 | ms |
| 7 | R-to-L response ($T_{600->300 \, mV}$) | TRL | | 250 | ms |
|   | L-to-R response ($T_{300->600 \, mV}$) | TLR | | 250 | ms |

Figure 2.8 Accuracy of oxygen and 1000/λ [6].

## 2.3.2. Universal Lambda Sensor (ZFAS-U)

The Universal Lambda Sensor (Fig. 2.9) can detect stoichiometry and can also measure wide range Air Fuel ratios from rich region to lean region. While a standard oxygen sensor essentially outputs only two states-either rich or lean, the wide range air-fuel sensor can measure the degree of richness or leanness. By using those properties, it can be applied to lean burn control and several combustion controls.

This sensor is made of two zirconia ($ZrO_2$) substrate elements (Fig. 2.10), one is the $O_2$ pumping cell (Ip cell), the other is the $O_2$ detecting cell (Vs cell) heated by a ceramic heater. The Vs cell is supplied by a very small constant current, whereby $O_2$ is moved to the reference cavity of the element and fills it with $O_2$ molecules. Therefore, the Vs cell generates the galvanic potential voltage. The Ip cell controls the partial $O_2$ pressure in the detecting cavity by pumping $O_2$. As a result, Vs voltage can be kept at 450mV by controlling the pumping current Ip. Consequently, this value of the pumping current Ip corresponds to the air to fuel ratio of the exhaust gas [7].
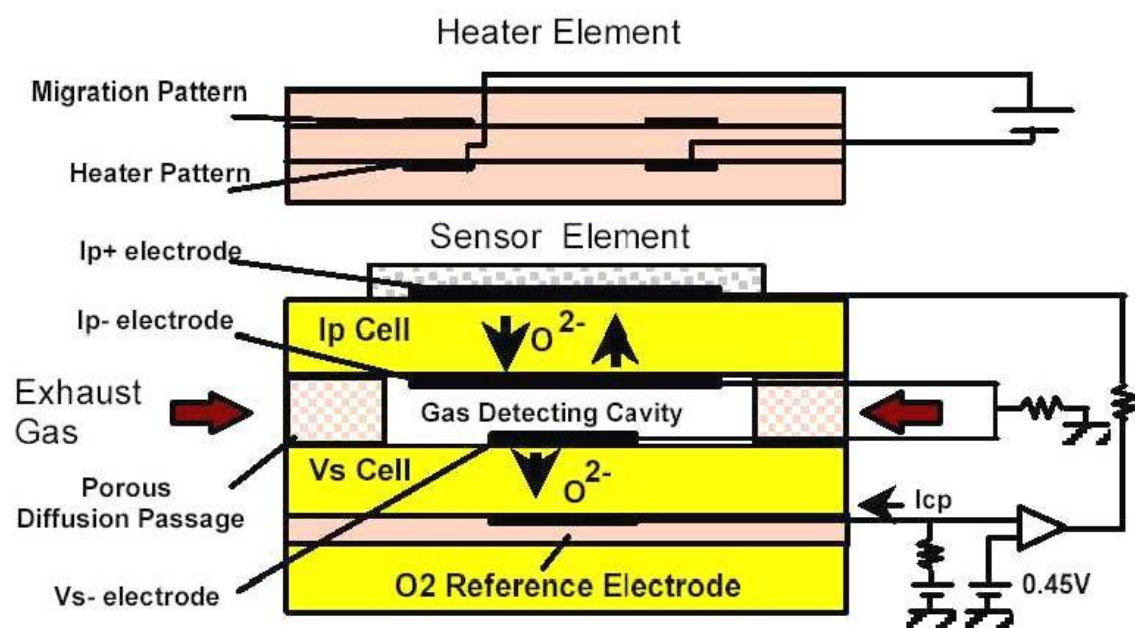
Figure 2.9 Universal Lambda Sensor ZFAS-UEGO [7]



Figure 2.10 ZFAS-UEGO Sensor structure [7]

The working characteristics of the sensor are reported in the following Table 2-3, while in the Figure 2.11 it is shown the Ip current behaviour for different A/F values.

**Table 2-3 ZFAS-UEGO characteristics [7]**

| Item | Range |
| --- | --- |
| Measurable range | $10 \leq A/F \leq Air$ |
| Exhaust temperature range | Room temperature $\rightarrow$ 850 °C |
| Hex of metal shell temp | $\leq$ 600 °C (for 400h) (Max) |
| Rubber cap temp | $\leq$ 200 °C (for 400h) (Max) |
| Lead wire temp | -40 $\rightarrow$ 240 °C |
| Connector temp | $\leq$ 120 °C (for 40h) (Max) |
| Storage temp. Range | $-40 \leq T \leq 100$ °C |
| Vibration resistance | $\leq$ 30 G (Max) |
| Tightening torque | 34.3 $\rightarrow$ 44.1 Nm (thread size: M18 x 1.5) |
| Tensile strength for Lead wire | Max. 80 N |
| Pumping current (Ip) | 0 $\rightarrow$ 0.050 mA (@ $\lambda$=1) <br> 3.859 $\rightarrow$ 5.341 mA (@ $O_2$=16%) |
| Heater resistance (Rh) | 2.8 $\rightarrow$ 3.4 Ohm (@ room temperature) |
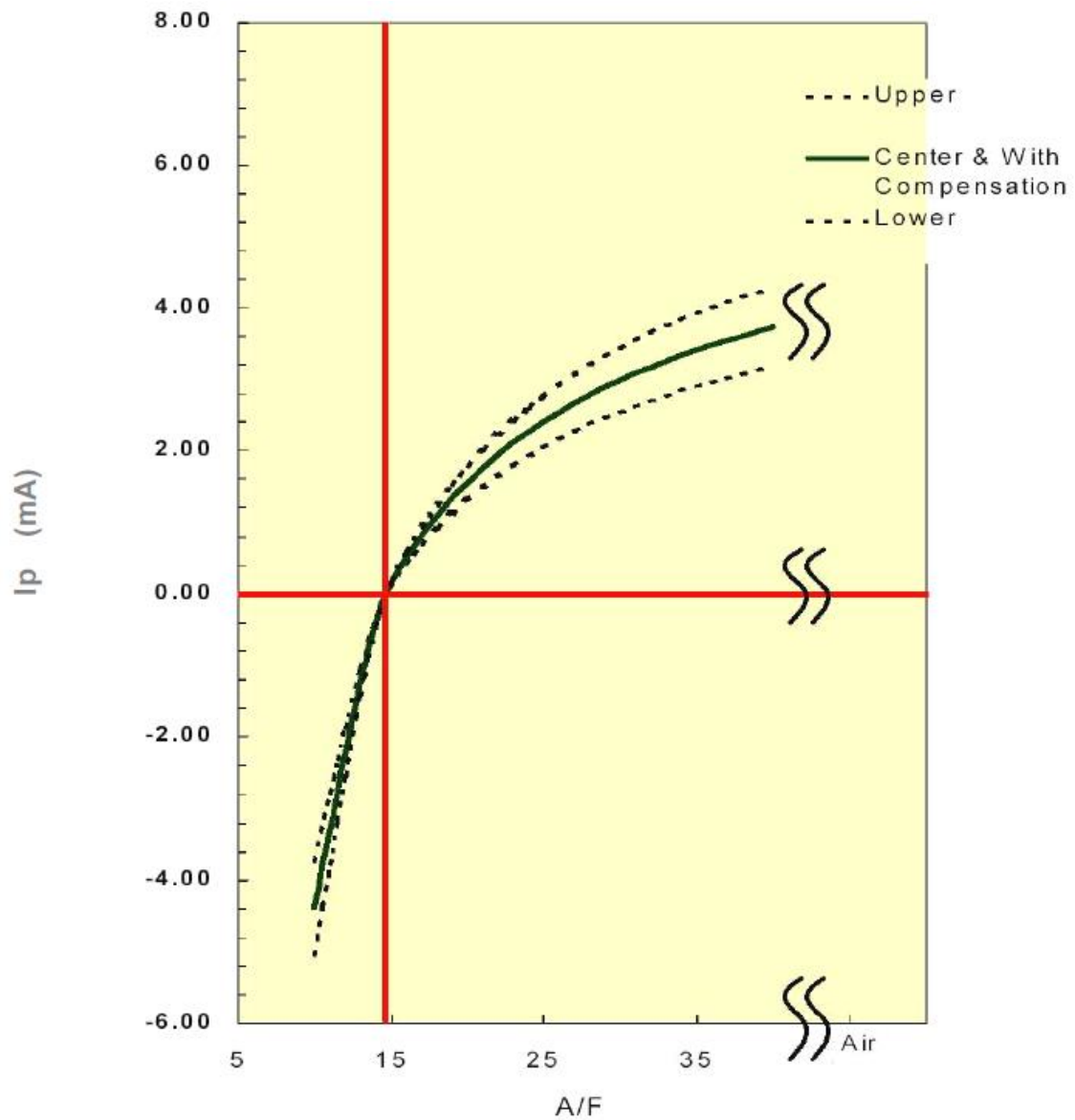
Figure 2.11 Ip current vs A/F ratio [7]

Although the very wide range of measurable A/F ratio, as for the Smart NO$_x$ Sensor, this sensor is very precise at stoichiometric but suffers of larger errors at extreme lean conditions. Furthermore, due to its characteristics, a small variation in the exhaust gas composition can affect considerably the sensed A/F value, making it oscillates a lot. For these reasons it isn't suitable in transient operations but remains affordable in steady-state conditions.

### 2.3.3. R49 relation: air to fuel ratio measurement method

The R49 regulation presents a method for the calculation of the A/F ratio through an analytical relation between the measured exhaust gases [8]. From the test bench, the concentrations of the species in the exhaust gas are obtained, hence it is possible to apply the following relation:

$$\lambda_i = \frac{\left(100 - \frac{c_{COd} \cdot 10^{-4}}{2} - c_{HCw} \cdot 10^{-4}\right) + \left(\frac{\alpha}{4} \cdot \frac{1 - \frac{2 \cdot c_{COd} \cdot 10^{-4}}{3.5 \cdot c_{CO2d}}}{1 + \frac{c_{COd} \cdot 10^{-4}}{3.5 \cdot c_{CO2d}}} - \frac{\varepsilon}{2} - \frac{\delta}{2}\right) * (c_{CO2d} + c_{COd} \cdot 10^{-4})}{4.764 * \left(1 + \frac{\alpha}{4} - \frac{\varepsilon}{2} + \gamma\right) * (c_{CO2d} + c_{COd} \cdot 10^{-4} + c_{HCw} \cdot 10^{-4})}$$

where:

$\lambda_i$      is the instantaneous lambda

$c_{CO2d}$    is the dry $CO_2$ concentration, per cent

$c_{COd}$     is the dry CO concentration, ppm

$c_{HCw}$    is the wet HC concentration, ppm

$\alpha$        is the molar hydrogen ratio (H/C)

$\beta$        is the molar carbon ratio (C/C)

$\gamma$        is the molar sulphur ratio (S/C)

$\delta$        is the molar nitrogen ratio (N/C)

$\varepsilon$        is the molar oxygen ratio (O/C).

In this case, as long as the composition of the exhaust gas is well determined by test bench sensors, the value of lambda is very affordable, since derive from simply chemical relations. The issue arises in transient conditions, when the lambda value calculated from this relation lags the current composition of the exhaust gas flow, since it is obtained in real time, when the engine runs, and the calculator needs time to give the result.

Considered the characteristics of each sensor and of the analytical method and analysed their pros and cons, the decision of what value of lambda was the most accurate for the purposes of the work has been separated for steady-state and transient conditions. In steady-state, the values coming from the R49 relation have been selected, since were for

sure the most accurate among all, eventually corrected of some point percent where the values were too much outside of the stoichiometric conditions (low load cases especially).

A different approach has been followed for the transient case, in which all the available sets of lambda values were affected by some errors. The Universal Lambda Sensor was extremely oscillating even in the regions of the WHTC in which the engine was idling, for this reason wasn't suitable. The value obtained from the R49 was desynchronized with respect of the engine conditions, as already explained, so also this set was useless. Hence, in transient conditions the Smart NOx Sensor has been chosen, but some corrections were needed since the accurate measurable range is tight and wide oscillations of A/F ratio and cut-offs are present in WHTC.

## 2.4    Three Pressure Analysis (TPA)

It is not possible to accurately calibrate all the engine aspects without having a proper calibration for the combustion process, since all of them are strictly related to the combustion itself. Therefore, in the first place a combustion analysis must be performed in order to achieve the exact experimental profile. The GT-Power Three Pressure Analysis has been the instrument used to do that.

Three pressure analysis, or TPA, is a fundamental tool available on GT-Power that is capable of extract the combustion rate, called "*burn rate*", from the experimental pressure traces. Its name, in fact, derives from the three main required data, the intake port pressure, the exhaust port pressure and the in-cylinder pressure. These measurements must be crank angle resolved since as average quantities will not be enough to impose at a location so close to the cylinder valves. In addition, TPA needs averaged temperatures on both intake and exhaust as well as a mono-cylindrical model that includes valves and ports at a minimum [1].

As previously mentioned, the available data for intake and exhaust pressure were only cycle averaged, so theoretically not suited for a proper TPA. Hence, to overcome the problem, a different configuration of the model has been used, including not only the ports but also a part of the runners of both intake and exhaust manifold (Fig. 2.12). Doing so, the model was capable of autonomously simulates the pressures oscillations close to

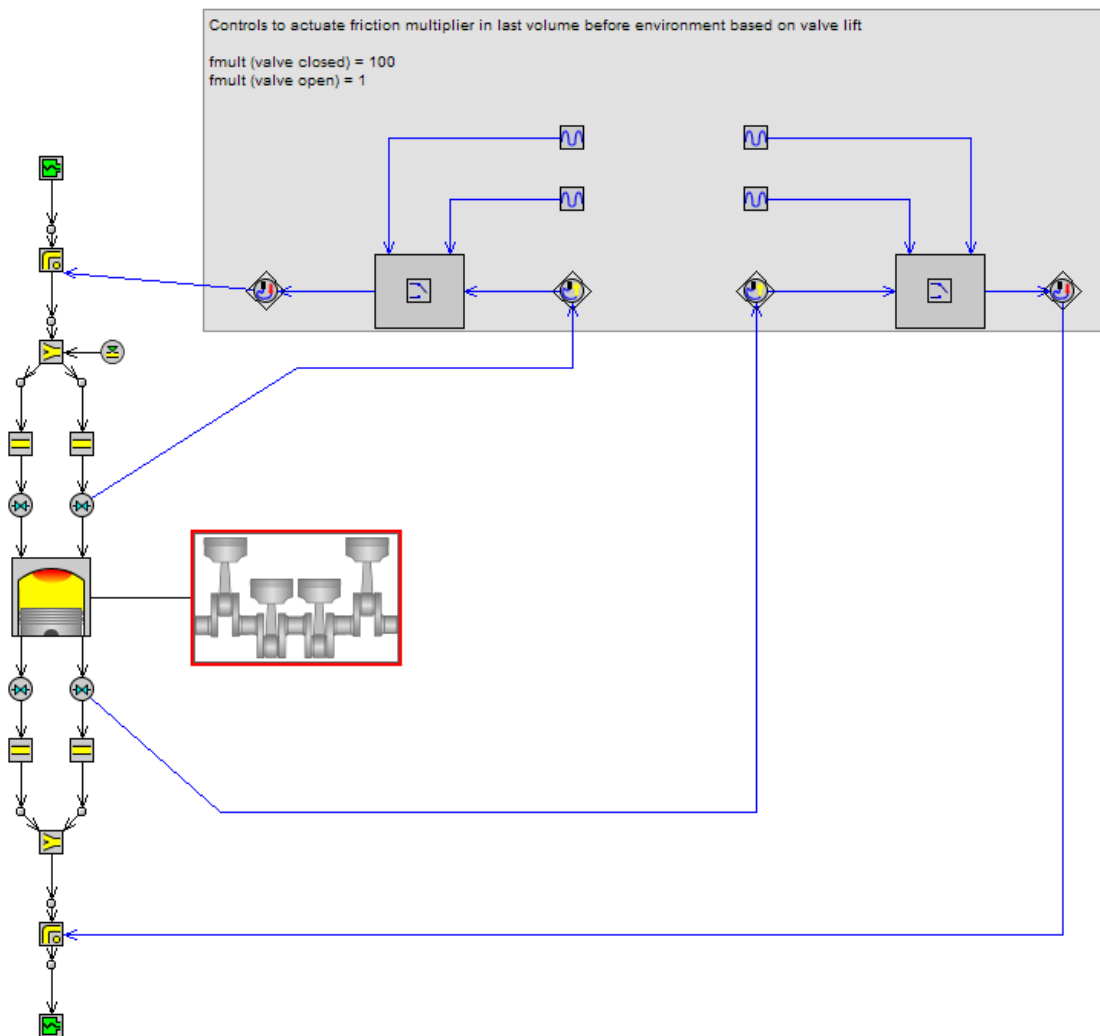the valves even though the pressures imposed at the end environments were constant over the cycle.



Figure 2.12 Monocylindrical model used for the Three Pressure Analysis

Gamma Technologies recommend at least 25 operating points spread across the engine speed range for better prediction of the burn rate for all the operating range. So, the available database was effectively enough to properly obtain a good combustion calibration for all the engine map.

Since there are possibility of some error in the cylinder pressure and other measurement data that is used as input to the TPA, GT-Power performs consistency checks to support the quality of the input data [1]. Those checks are briefly summarized in the following:

- **Reasonable IMEP.** IMEP is calculated by integrating the cylinder pressure profile and it should be greater than the BMEP which is obtained from the measurement. BMEP is equal to algebraic sum of IMEP and FMEP. If IMEP and PMEP is not reasonable, then it indicates an error in measured pressure trace data obtained from the test rig.

- **Pressure Smoothing.** Measured cylinder pressure at the test rig will have noise in the signal and this will cause error in the simulation. To avoid this, raw pressure is smoothed using a low pass filter. An RMS pressure value is reported in pressure analysis result which indicates error between raw and smoothed pressure curves. An error will be flagged if the RMS pressure is greater than 0.02 which indicates there is data loss while smoothing the curve.

- **Cumulative Burn During Compression.** During compression stroke, the apparent burn rate is calculated by integrating burn rate up to the designated start of analysis and the value should be close to zero. During this period, there should be no fuel burning, so any calculated fuel that is burned shows an indication of error in the input data and an error is flagged if the cumulative burn during compression is greater than 2% of the total fuel.

- **Fraction of Fuel Injected Late.** In direct injection models, any time before and after the injection event, if there is insufficient fuel in the cylinder, the insufficient fuel is tracked and integrated over the cycle. The amount of missing fuel is reported in pressure analysis results and this value should be always zero. If the fraction exceeds 0.02 then an error is flagged.

- **LHV Multiplier.** The Latent heating value (LHV) multiplier indicates the error in the cumulative burn rate. Ideally, the value should be 1 and if the LHV adjustment required is more than +/- 5%, an error is flagged.

- **Combustion efficiency comparison to target.** Combustion efficiency indicates the burned fuel fraction inside the cylinder. The LHV is adjusted to match the combustion efficiency with the target value. If the LHV change required is more than 5% then an error is flagged.

- **Apparent Indicated Efficiency.** During the pressure trace analysis, if the calculated indicated efficiency is greater than 45%, then it indicates an error in the input data.

- **Air Mass at IVC.** In TPA simulations, it is possible to compare the trapped air mass at IVC from the simulation to the measured air mass from the test rig. If the
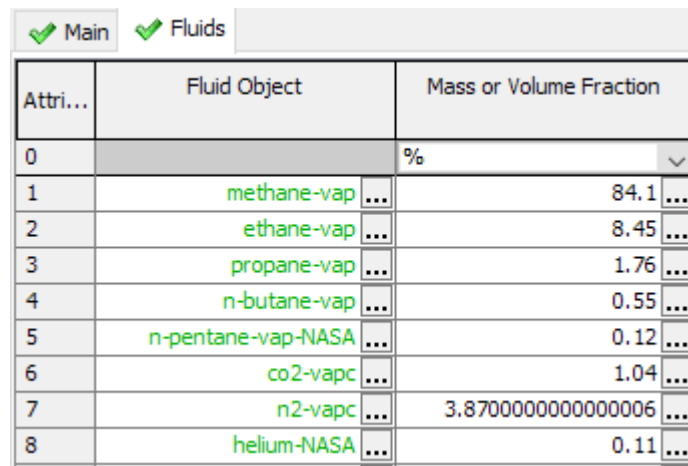
difference in the value is greater than 5% then it indicates an error in the valve timing settings.

- **Fuel Mass.** In TPA simulations, total fuel injected from the simulation is compared to the measured fuel mass from the test and if the values differ by greater than 5%, then the amount of fuel injected is incorrected.

- **Fuel Air Ratio.** In TPA simulations, simulated air-fuel ratio is compared to the measured value obtained from the test cell. If the deviation exceeds +/-5%, an error is flagged.

The advantage of the consistency checks is that they point out exactly the problems encountered during the process so that is possible to correct them directly without searching for the cause.

## 2.5   TPA Results

TPA has been performed for each experimental operating point and for everyone the analysis pointed out a flag on the LHV Multiplier, indicating an error on the cumulative burn rate. Several checks have been made on both the model setup and on the experimental data without having success. Furthermore, the value of the LHV Multiplier shown by the TPA was similar for every point, around 1.1, meaning that probably a common parameter was the one leading to bad results. After numerous checks it has been found that the fuel composition provided wasn't exactly the one used for the experimental tests on which the available data were acquired, creating a mismatch within the model. In Figure 2.13 it's shown the adopted composition which is typical for a CNG supplied from the gas network.

Figure 2.13 Adopted CNG composition

Notice that in the fuel blend are present $CO_2$ and $N_2$, generating further uncertainty on the composition. In fact, if those compounds, for example, are reduced and $CH_4$ is augmented in their place of 2%, the fuel so obtained won't even need the LHV multiplier and the TPA would be correct.

The errors were anyway limited, also considering that for the TPA a mono-cylindrical model is required while for the complete calibration have to be performed on the six-cylinder model and in the passage from one to the other the error margins can be amplified or reduced. Then, only after the implementation of the burn rates in the six-cylinders model, is possible to appreciate the total errors that will affect the general calibration and, in this case, as will be exposed in the following, were practically cancelled. An example of the obtained burn rate is reported in the following Fig. 2.14.

Furthermore, among the available pressure data from experimental tests was present a value for the pressure after the throttle valve, imposed at the inlet environment, but wasn't present a value of pressure at the cylinder exhaust, that should have been imposed to the outlet environment. In its place, it has been imposed the pressure at the turbine intake, the only one available for the exhaust manifold. In other words, the delta of pressure between intake and exhaust of the cylinder imposed in the TPA is not the correct one and the error relative to this issue is visible in the peak pressure (Fig. 2.16-18).

Three of the twenty-five corrected results are shown in the figures 2.16-17-18, in which with "Measured" (pressure) is intended the imposed one, so the experimental and with "Simulated" the pressure traces obtained after the calculation of the burn rate.
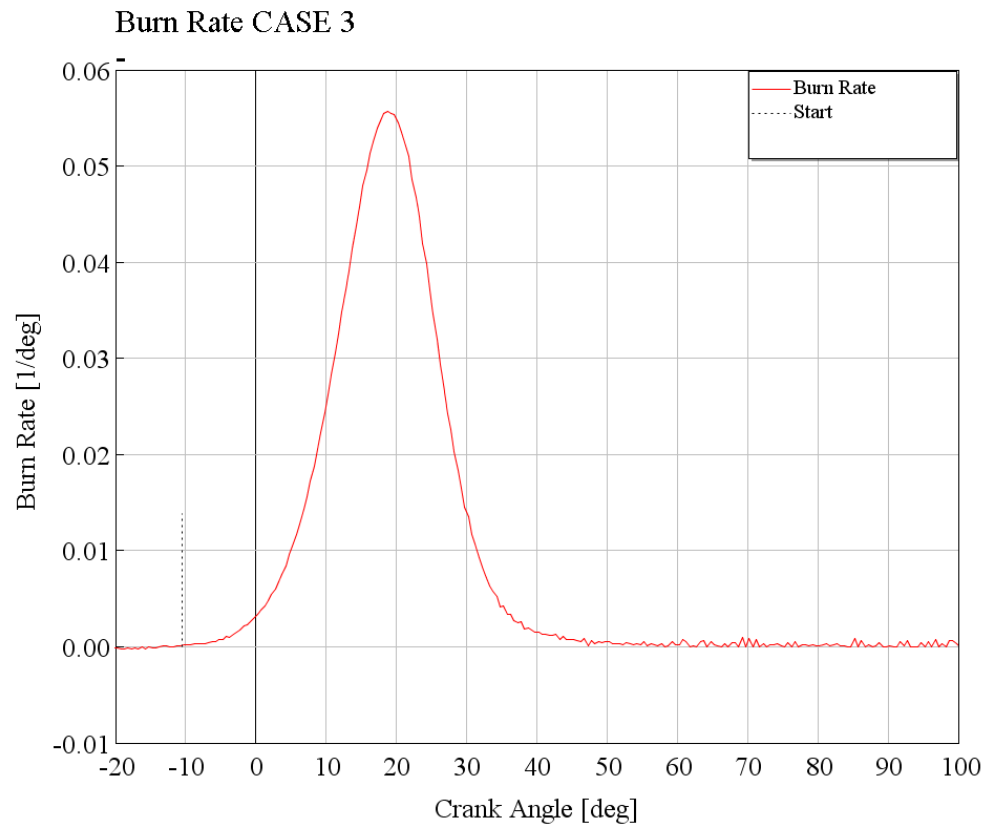
Burn Rate CASE 3



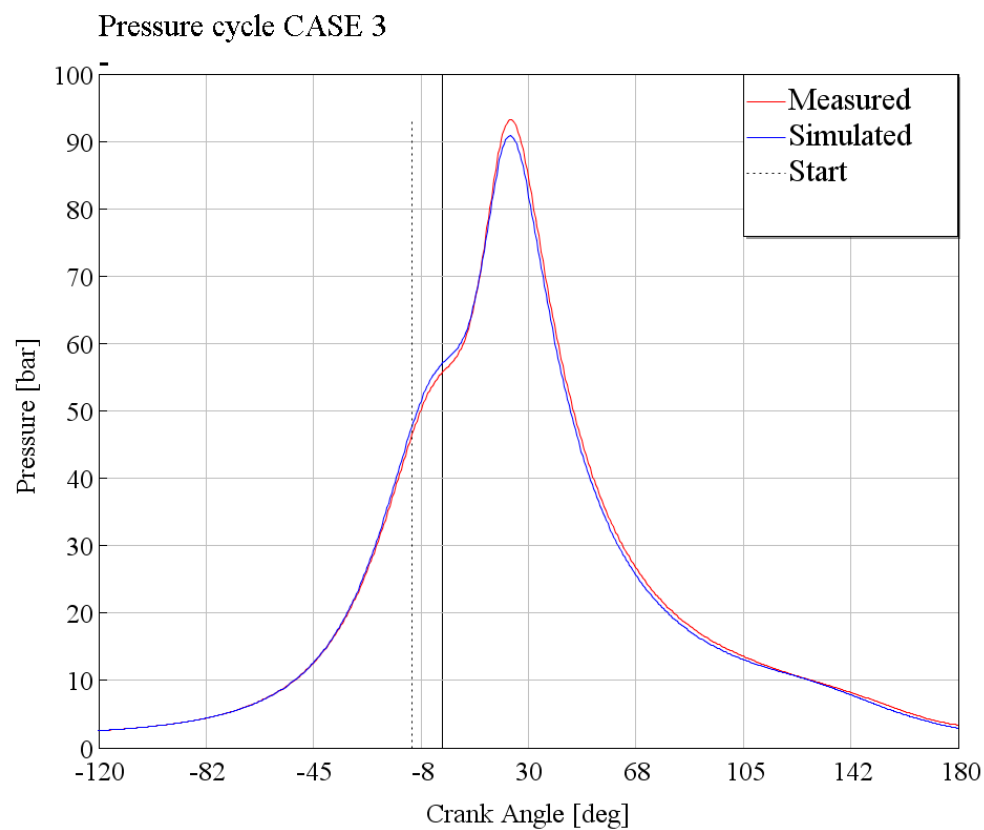Figure 2.14 Example of a Burn Rate obtained as a result from TPA (CASE 3 [1500rpm x 100%load])

Pressure cycle CASE 3



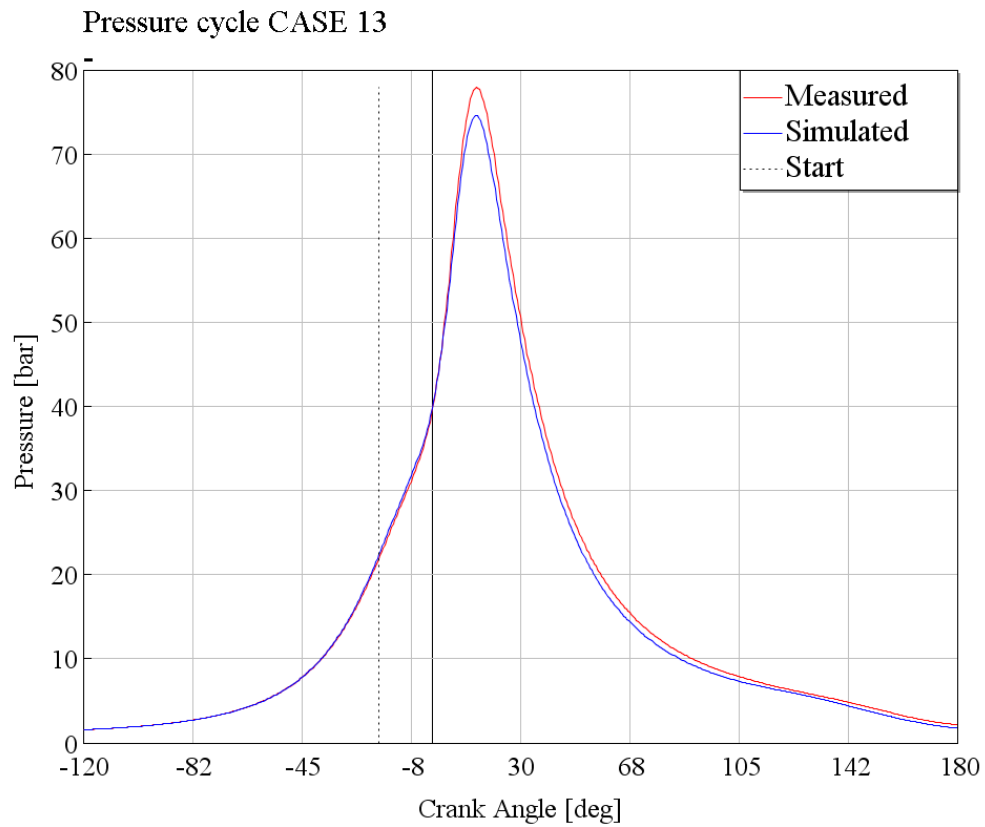Figure 2.15 TPA result of CASE 3 [1500rpm x 100%load]

Pressure cycle CASE 13



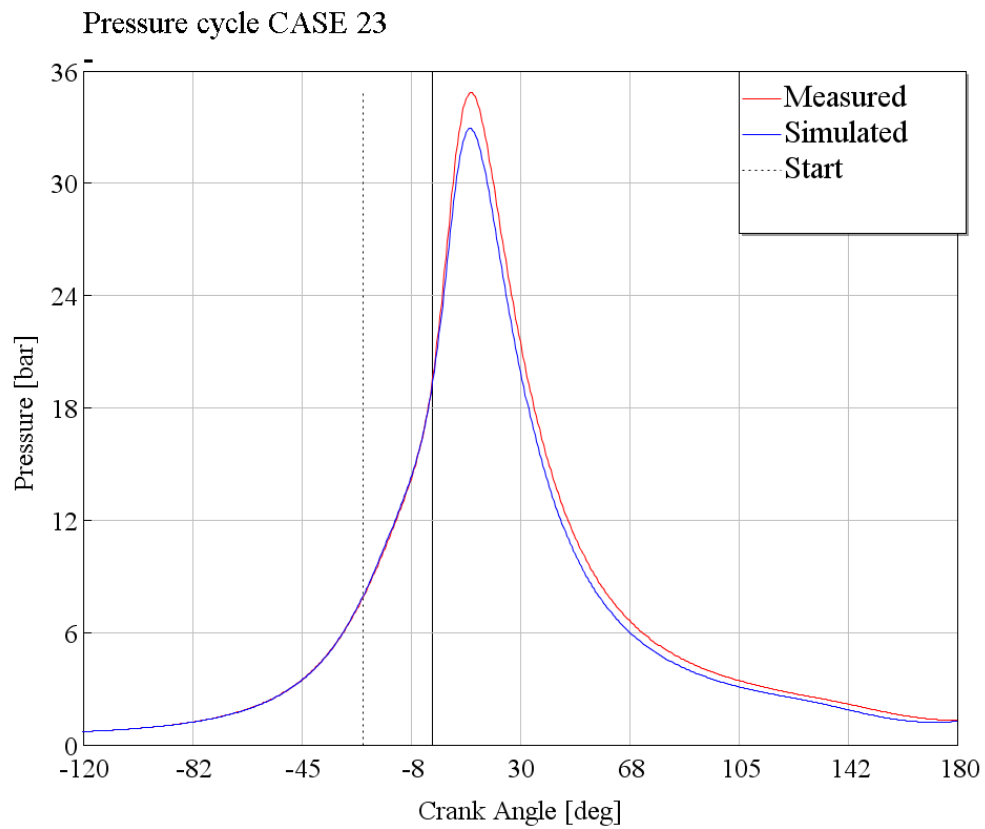Figure 2.16 TPA result of CASE 13 [1500rpm x 60%load]

Pressure cycle CASE 23



Figure 2.17 TPA result of CASE 23 [1500rpm x 20%load]

All the obtained burn rates have been then implemented in the complete model so to achieve the best combustion simulation possible. In this case the throttle controller was set so to follow the experimental values of IMEP, because at this level the frictions were still not calibrated and consequently the brake torque wasn't reached.

The pressure traces of the same cases shown before but achieved after the passage just explained are reported in the following (Fig. 2.18-20). As previously mentioned, the errors have balanced themselves and the simulation results were extremely well fitting the experimental data.

From these solid bases, the calibration process moved on, concentrating initially on the frictions coefficients and after on the heat transfer rate and thermal calibration of all the elements present in the model.
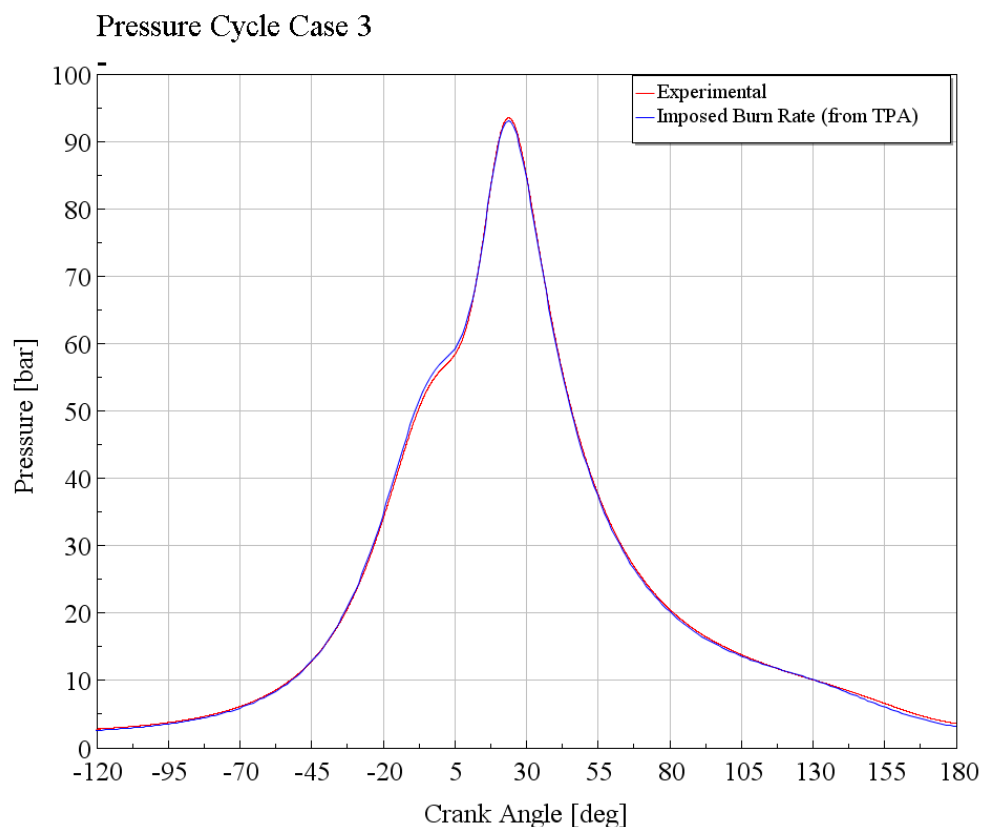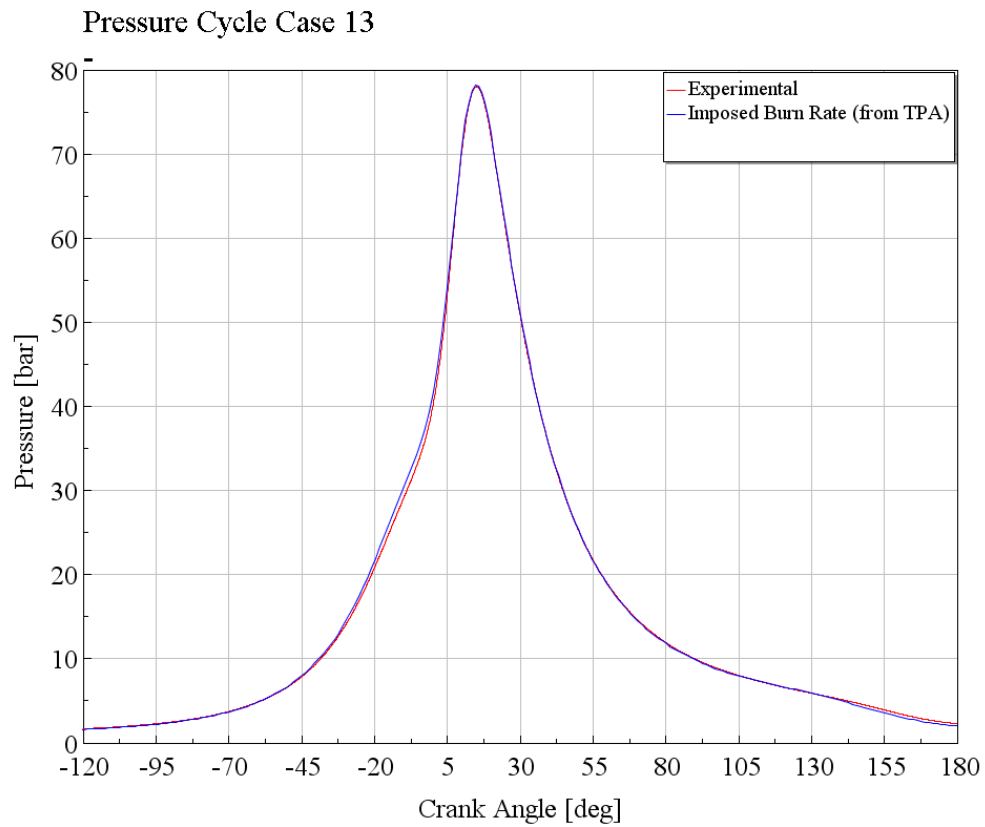


Figure 2.18 Pressure traces of CASE 3 (6-cylinder model

Pressure Cycle Case 13



Figure 2.19 Pressure traces of CASE 13 (6-cylinder model)
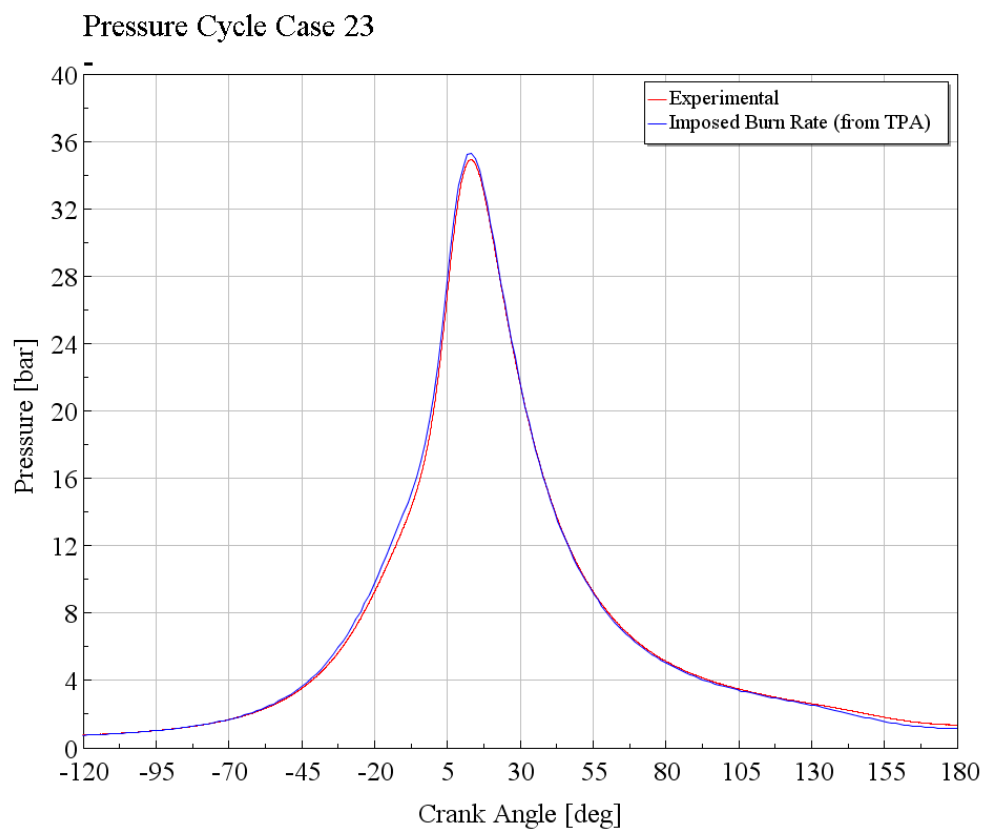
Pressure Cycle Case 23



Figure 2.20 Pressure traces of CASE 23 (6-cylinder model)

## 2.6    Friction coefficients calibration

For this task the Throttle Controller has been set up with IMEP [bar] and SPEED [rpm] respectively as target and input signal, in order to simulates the right level of the peak pressure so to be able to calibrate the FMEP [bar]. Because, in fact, the brake torque is strictly dependent on the BMEP [bar] that is in turn dependent on FMEP [bar], still not calibrated, it wasn't correct to impose it as the target.

The relations involved in this aspect, based on the Chen Flynn engine friction model, are:

- $BMEP = IMEP + FMEP$,
- $FMEP = FMEP_{const} + A \cdot P_{Cyl,max} + B \cdot c_{p,m} + C \cdot c_{p,m}^2$,

    where:

    $FMEP_{const}$ [bar] is a constant pressure term, $P_{Cyl,max}$ [bar] is the peak pressure in the cylinder and $c_{p,m}$ [m/s] is the mean piston speed; $A$, $B$ and $C$ are the calibration coefficients that have been tuned.

Nine operating points across the engine map have been considered in this phase, the cases n. 1, 3 ,5, 11, 13, 15, 21, 23, 25 in particular, since they can be associated to the main sub zones of the engine map, from low to high engine load and speed. The first values of the calibration coefficients were taken from previous similar models, as already explained for the valves, to have a starting point from which begin. These values were optimized only for the high-speed medium-load conditions as can be easily seen from the following figures (Fig. 2.21-22), while in the other conditions the errors were large, in some case over 60%. It is important to note that from low to medium engine speed the tendency is similar for increasing load whereas once reached the highest speed, the errors tendency is opposite (Fig. 2.22).

After this preliminary analysis, an automated optimization has been performed pointing at the minimum load conditions, i.e. where the FMEP have larger absolute effect; the target value was obviously the FMEP and the independent variables the four calibration coefficients shown before. The result of this optimization reduced the errors on the frictions, but the deviation between the different conditions was still too much, hence a manual calibration followed. After the analysis on the effectiveness of each parameter and several trial a maximum error under ±4.5% has been achieved, as reported in the Figures 2.23-24.
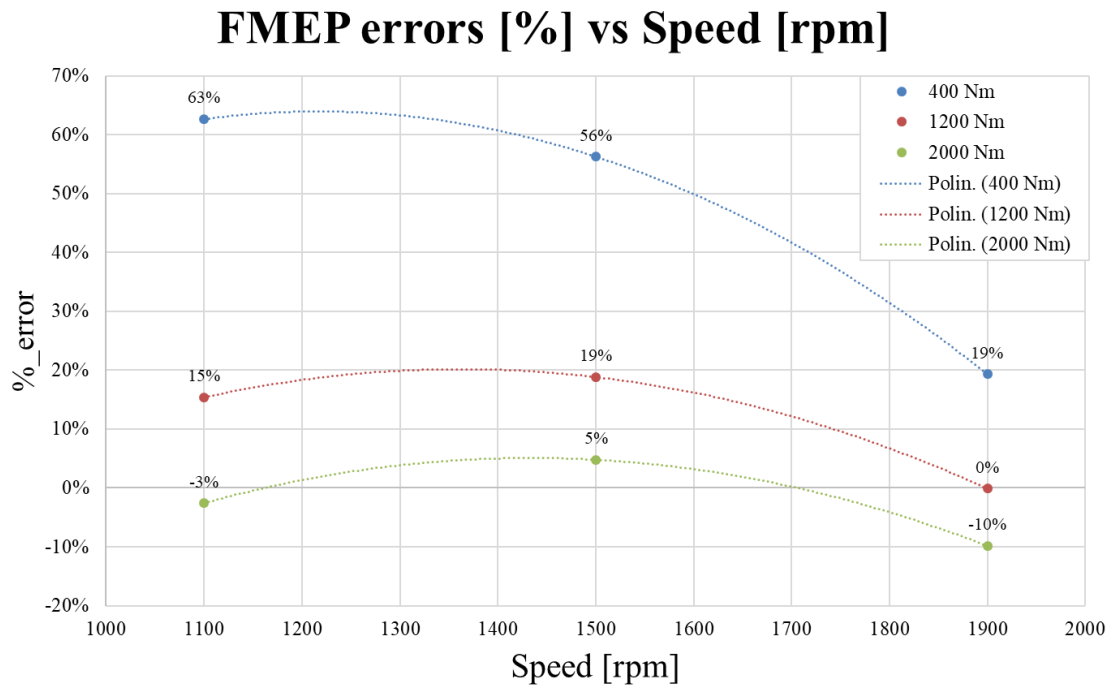
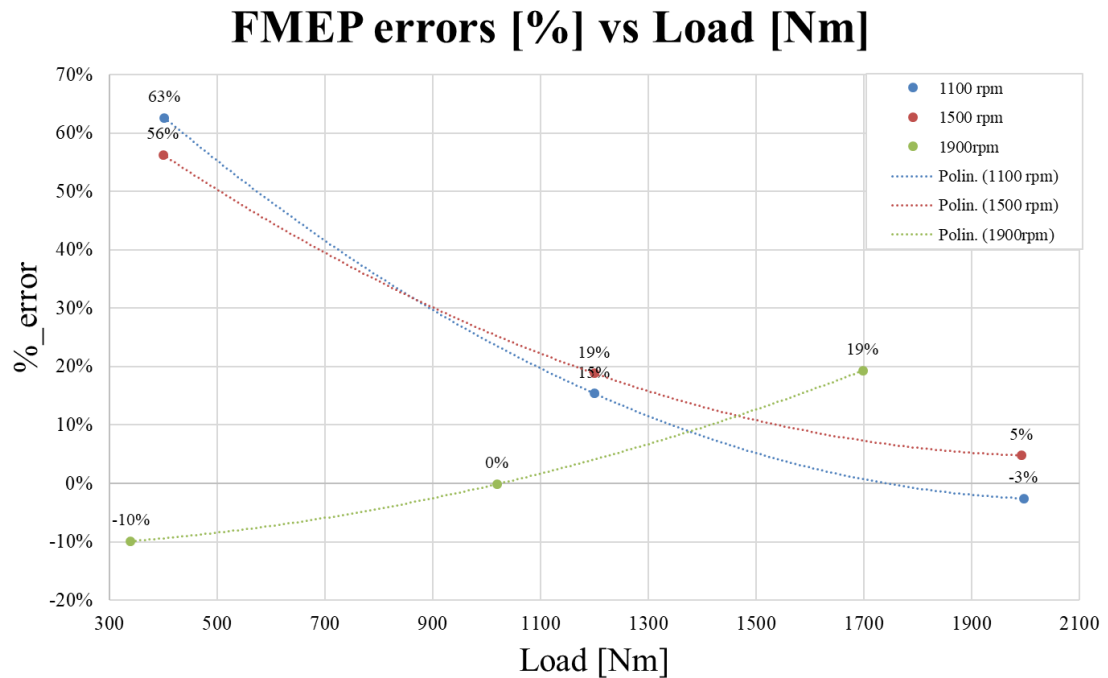Figure 2.21 FMEP percentage errors vs engine speed before calibration



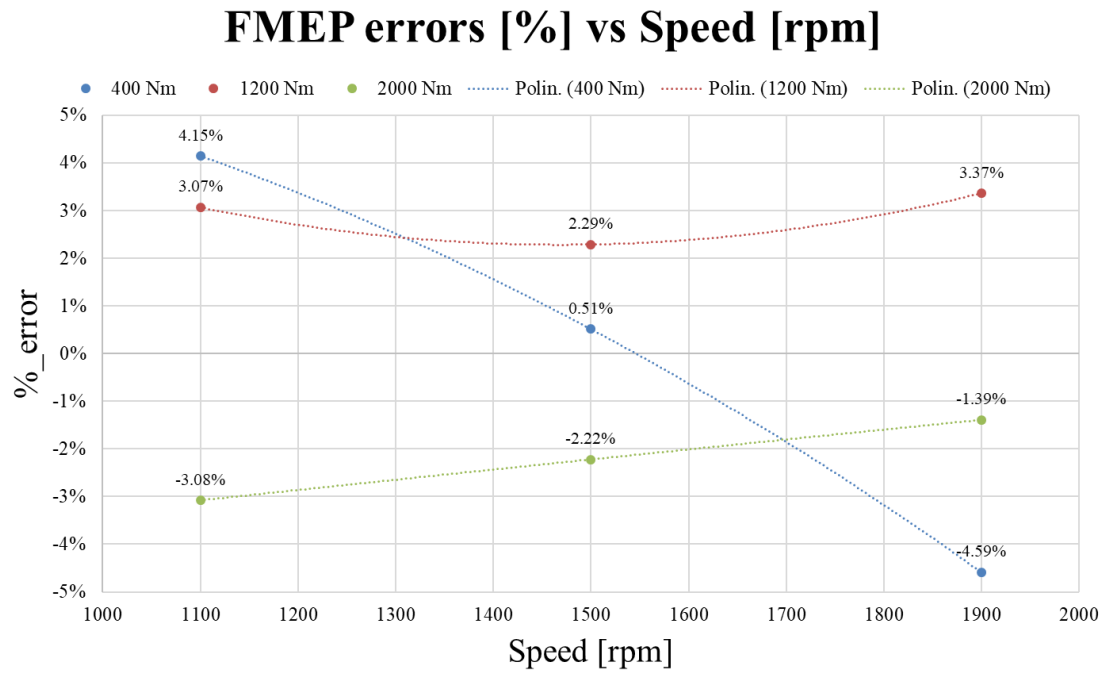Figure 2.22 FMEP percentage errors vs load before calibration

# FMEP errors [%] vs Speed [rpm]

Figure 2.23 FMEP percentage errors vs engine speed after calibration

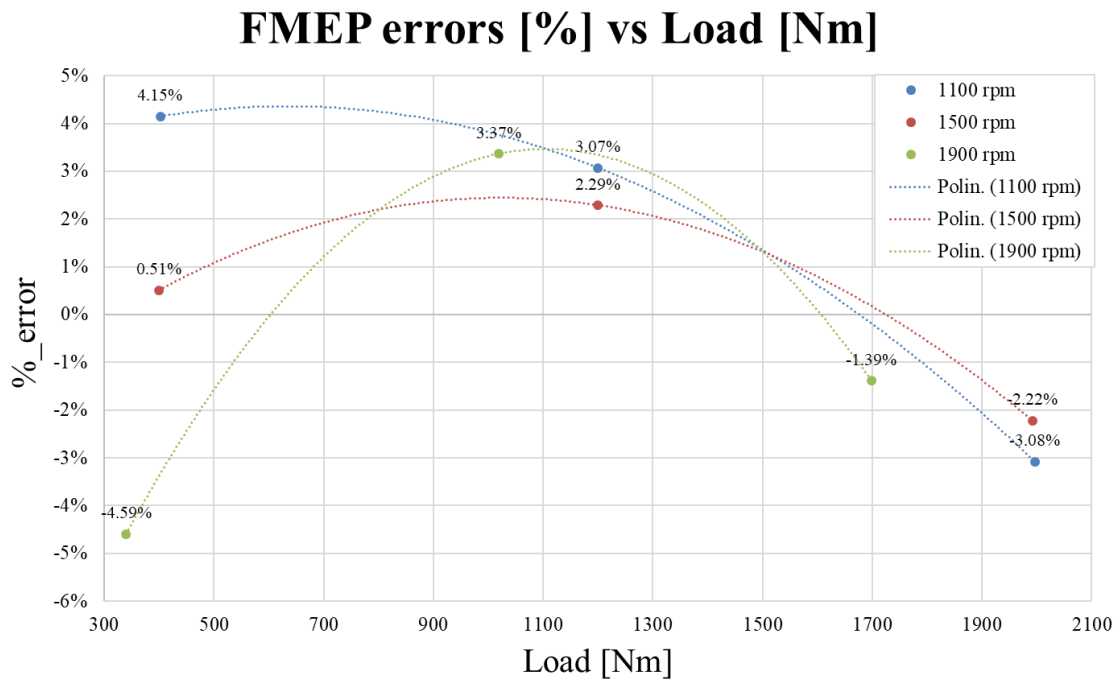# FMEP errors [%] vs Load [Nm]

Figure 2.24 FMEP percentage errors vs engine load after calibration

In the following table are reported the values of the FMEP parameters before and after the calibration process:

**Table 2-4 FMEP equation parameters before and after calibration**

|                    | $FMEP_{const}$ | $A$        | $B$       | $C$        |
|--------------------|----------------|------------|-----------|------------|
| *Before calibration* | -1.226       | 0.001399   | 0.8538    | -0.05764   |
| *After calibration*  | 0.45375      | 0.01139375 | 0.0521875 | 0.00051875 |

Once the frictions were corrected, the controller target has been changed from IMEP to Brake Torque, since it is more correct if compared to the actual one (that controls the load) and it easier to be implemented.

## 2.7 Cylinder HTR and flow temperatures calibration

This part of the work has been focused on the calibration of the temperatures, especially those concerning the cylinders, the exhaust manifold, the turbine, and the pipe that link the turbine with the aftertreatment system (ATS). These are in fact the most important of all the model temperatures, since strictly dependent on the combustion process and directly influencing the pollutant emissions, since they affect the chemical reactions both inside the combustion and in the ATS.

The parameters on which GT-Power allows a thermal calibration are very few, especially considering the pipes, where is only possible to define the initial temperature (for simulation purposes) and a tuning factor, the so called "Heat Transfer Multiplier". For the cylinder model, on the contrary, an "Heat Solver" object has to be set up, in which are defined the materials of piston, cylinder and valves, the heat transfer rates between the gas in the chamber and the walls and the initial temperatures at which the simulations start.

Materials and initial temperatures have been taken from a similar previous model, as already seen for the frictions and valves, whereas the cylinder heat transfer rates have been calibrated with a relation based on the engine speed, so taking in consideration the flow

turbulence in the chamber and the speed of the fluids in the walls. The Heat Transfer Multiplier of the pipes have been instead calibrated apart trying to match the flow experimental temperatures. The following figures (Fig. 2.25-28) show the resulting simulated temperature for each available operating point compared with the experimental temperatures taken on the previously mentioned positions of the engine.
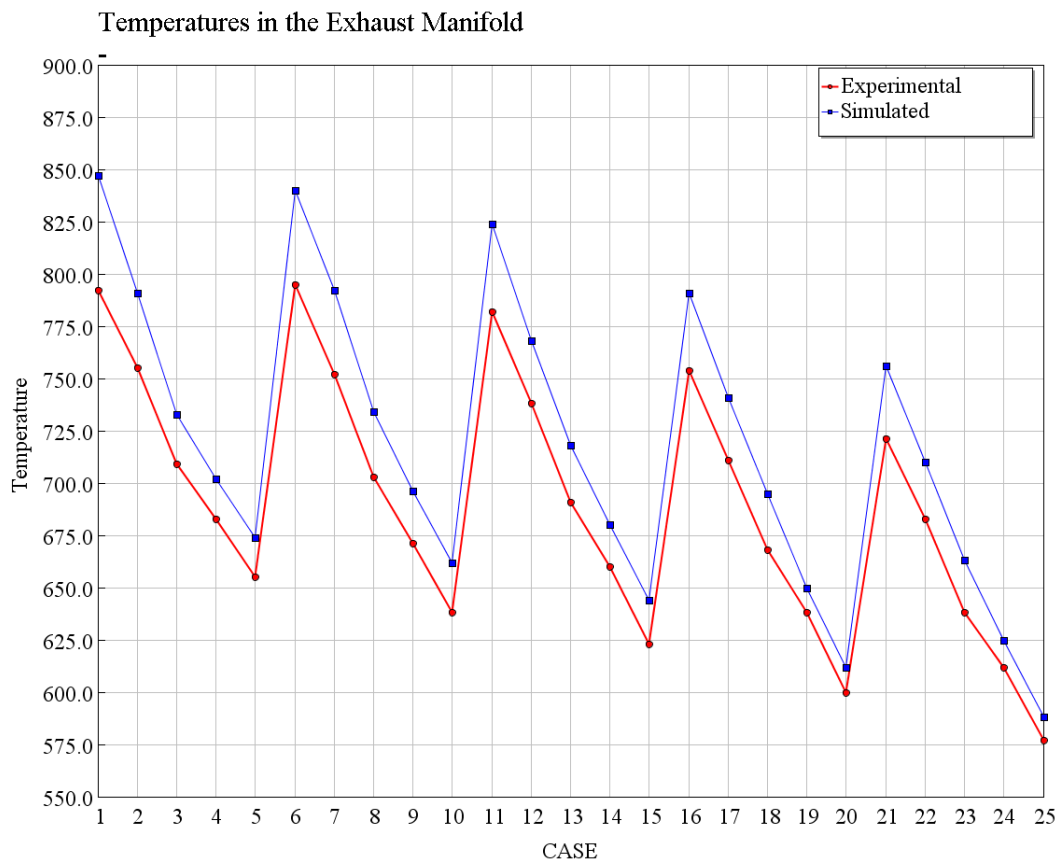


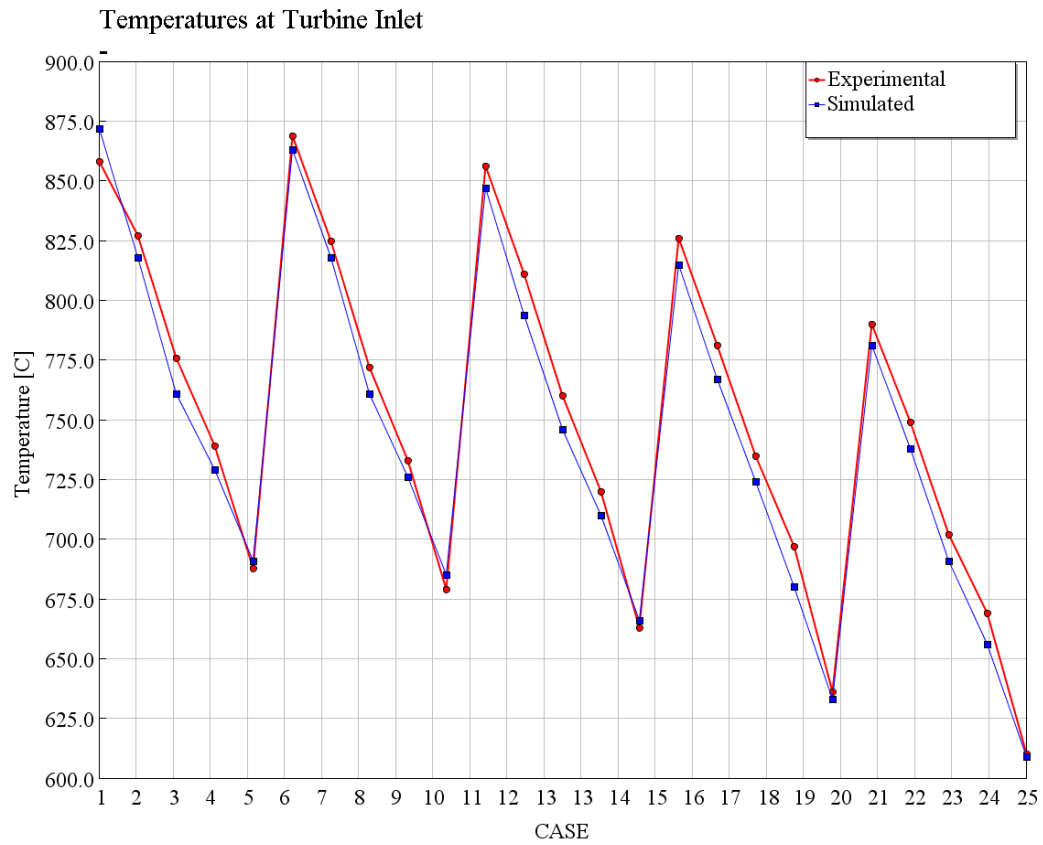Figure 2.25 Temperatures calibration results at exhaust manifold.

Temperatures at Turbine Inlet



Figure 2.26 Temperature calibration results at turbine inlet.
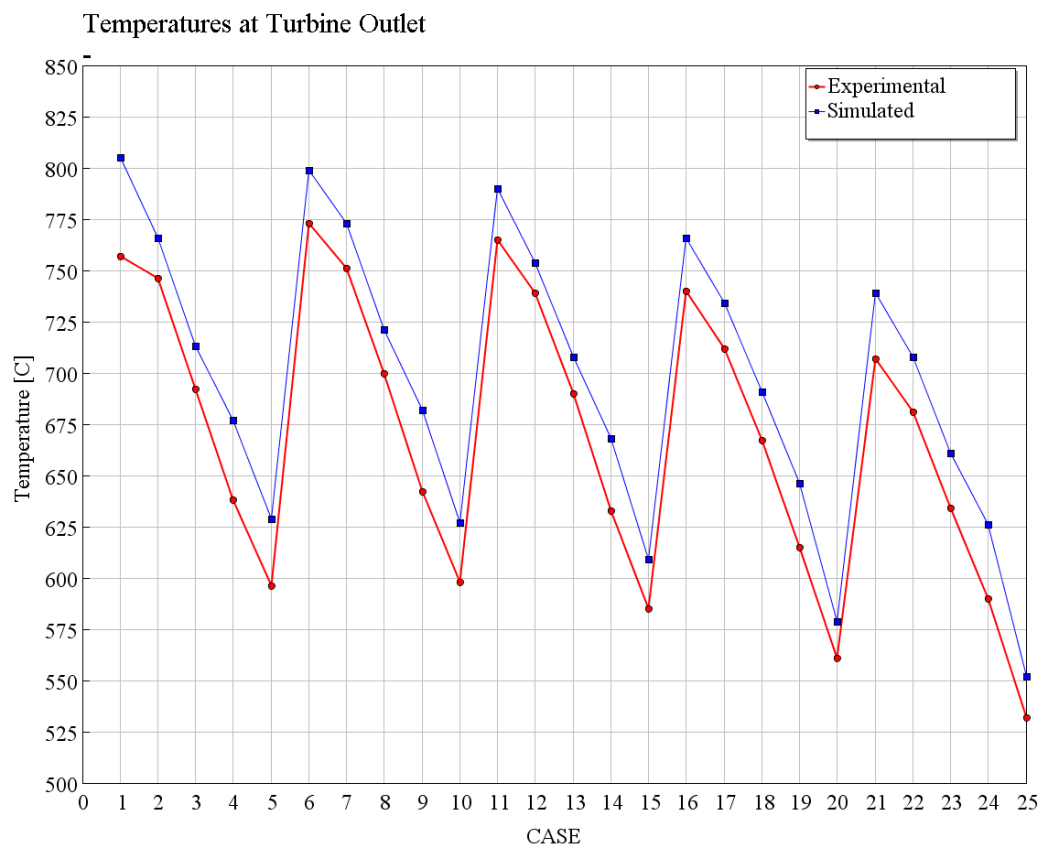
Temperatures at Turbine Outlet



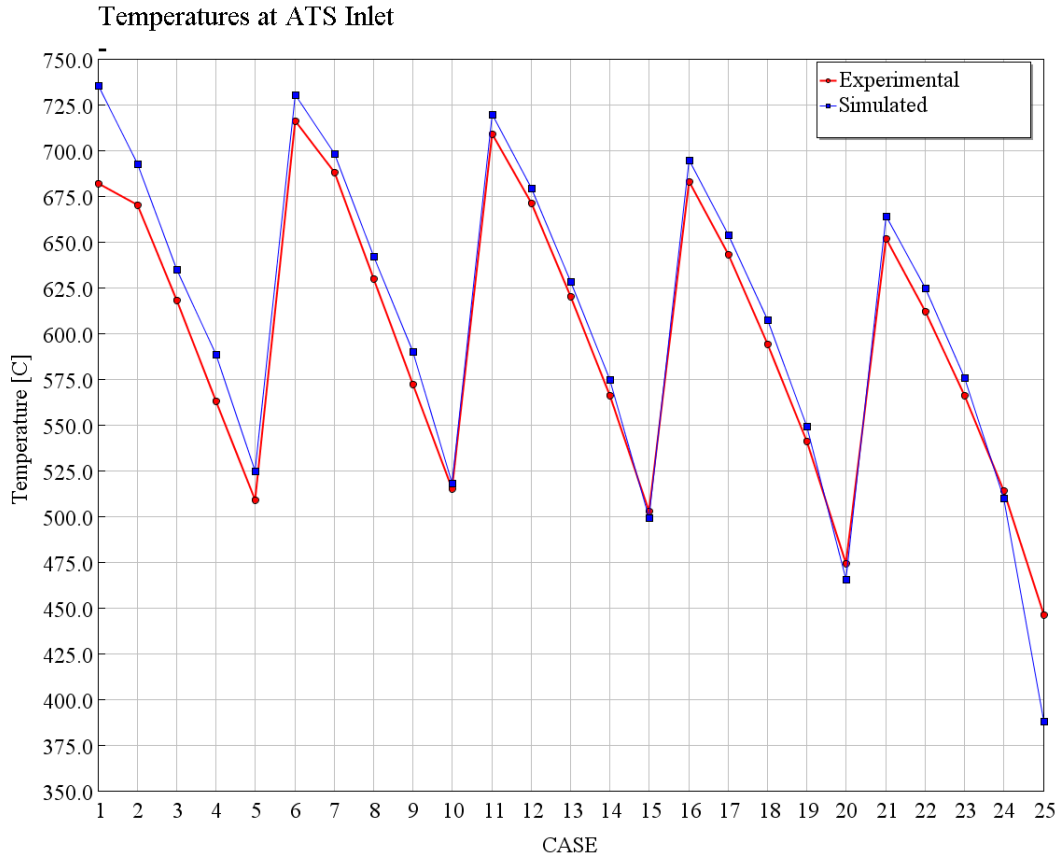Figure 2.27 Temperature calibration results at turbine outlet.

Figure 2.28 Temperature calibration results at ATS inlet.

The relation implemented on the model to obtain the good calibration shown on the previous figures has been used for both the "Head Coolant HTR" and the "Cylinder Coolant HTR", that are two of the parameters available in the heat solver object, and it is reported below:

$$HTR = 1350 \cdot (SPEED/1100)^{1/3}$$

where "*SPEED*" is the engine speed. The multiplier and the power terms have been obtained through several iteration while checking the previous graphs. Initially, in fact, with only a simple ration between engine speeds for considering the increasing velocity of the flows, the temperatures were showing a linear behaviour that wasn't compatible with the experimental data: the power of a third shown the best fitting for the engine.

The values of both the pre-multiplier of the previous relation and of the pipe's "Heat Transfer Multiplier" has been found instead by fitting as much as possible the temperatures at turbine inlet and, at the same time, containing the errors in the other accounted positions of the model.

## 2.8  Predictive combustion model: SITurb

Once the whole model has been calibrated based on the combustion obtained from the TPA, a predictive combustion model has been investigated. Among the predictive models already present in GT-Power, the "SITurb" was the most suitable, since it predicts the burn rate for homogeneous charge, spark ignited engines.

In the SITurb, the combustion model is based on the two-zone, entrainment and burn-up model, already described in 1.5, considering also the chamber geometry, spark location and timings, flow motion and fuel properties. The mass entrainment and rate into the flame front and the burn rate are governed by the following equations:

- $\dfrac{dM_e}{dt} = \rho_e A_e (S_T + S_L),$

- $\dfrac{dM_b}{dt} = \dfrac{M_e - M_b}{\tau},$

- $\tau = \dfrac{\lambda}{S_L}$

where,

$M_e$ = Entrained mass of unburned mixture

$t$ = Time

$\rho_u$ = Unburned density

$A_e$ = Entrainment surface area at the edge of flame front

$S_T$ = Turbulent flame speed

$S_L$ = Laminar flame speed

$M_b$ = Burned mass

$\tau$ = Time constant

$\lambda$ = Taylor microscale length.

The first equation states that the unburned mass of mixture is entrained into the flame front with a rate that is proportional to the sum of laminar flame speed and turbulent flame speed. The second equation indicates that the burn rate is proportional to the amount of

unburned mixture behind the flame front, divided by a time constant which is calculated as the ratio between the Taylor microscale length and the laminar flame speed.
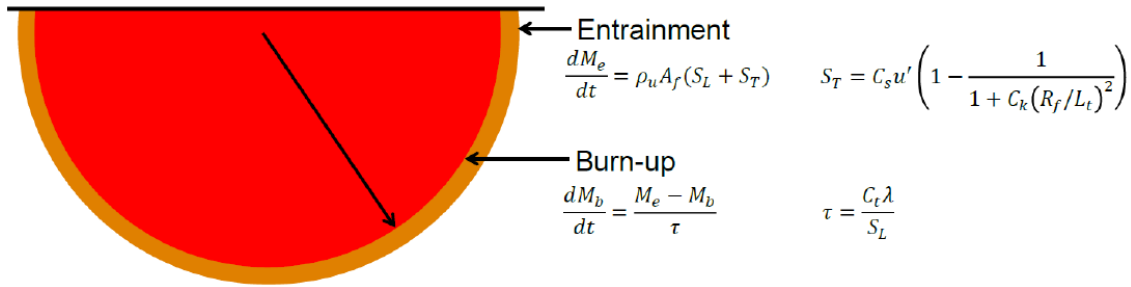


Figure 2.29 SITurb model description [2]

### 2.8.1. Laminar flame speed calibration

GT-Power provides several laminar speeds on the dedicated window of the SITurb model, corresponding to the type of fuel with which the engine is operated, including methane. Unfortunately, the experimental data provided for the calibration of the model were obtained through tests in which the engine worked with natural gas, hence with a mixture of different gases and not methane only. So, it has been necessary to calculate a new custom laminar speed and to impose it into the model, in order to have the best correspondence possible to the actual operating conditions.

The software calculates the laminar speed by using the two following equations [3]:

$$S_L = S_{L0} \left( \frac{T_u}{T_{ref}} \right)^\alpha \left( \frac{p_u}{p_{ref}} \right)^\beta f(Dilution) \tag{2.1}$$

$$f(Dilution) = 1.0 - 0.75 \cdot DEM(1.0 - (1.0 - 0.75 \cdot DEM \cdot Dilution)^7) \tag{2.2}$$

where,

$T_u$, $p_u$ = Unburned gas temperature and pressure respectively

$T_{ref}$, $p_{ref}$ = Ambient conditions (reference) temperature and pressure respectively

in which:

$$S_{L0} = B_m + B_\Phi (\Phi - \Phi_m)^2 \tag{2.3}$$

$$\alpha = a_2\Phi^2 - a_1\Phi + a_0 \tag{2.4}$$

$$\beta = -b_2\Phi^2 + b_1\Phi - b_0 \tag{2.5}$$

where,

$\alpha, \beta$ = constant determined using a second order polynomial in the range of 0.7 to 1.2 equivalent ratio to best fit the cubic laminar burning velocity function described in the publication [4]

$B_m$ = Maximum Laminar Speed

$B_\Phi$ = Laminar Speed Roll-off Value

$\Phi$ = Equivalence Ratio

$\Phi_m$ = Equivalence Ratio at Maximum laminar speed.

**Table 2-5 Coefficients proposed by Liao et al. [4] for a Chinese Natural Gas**

| Fuel | $a_2$ | $a_1$ | $a_0$ | $b_2$ | $b_1$ | $b_0$ |
|---|---|---|---|---|---|---|
| Natural Gas | 5.7500 | 12.150 | 7.9800 | 0.9250 | 2.0000 | 1.4730 |

The value of $S_{L0}$ has been calculated through the following relation, that considers the percentages of the main alkane compounds present into the CNG [5]:

$$S_{L0}(\phi, \chi_1, \chi_2) = \left(1 + \nu_1\chi_1^{\tau_1}\right)\left(1 + \nu_2\chi_2^{\tau_2}\right)W\phi^\eta e^{-\xi(\phi-\sigma-\Omega_1\chi_1-\Omega_2\chi_2)^2} \tag{2.6}$$

where,

$\chi_1, \chi_2$ = fraction of ethane and propane in the CNG mixture,

and

**Table 2-6 Coefficients proposed by Distaso et al. [5]**

| Fuel | $W\ [cm/s]$ | $\eta$ | $\xi$ | $\sigma$ | $\nu$ | $\tau$ | $\Omega$ |
|---|---|---|---|---|---|---|---|
| $CH_4/\ C_2H_6$ | 38.638 | -0.15 | 6.2706 | 1.1 | 0.2103 | 0.545 | -0.0191 |
| $CH_4/\ C_3H_8$ | | | | | 0.2129 | 0.8312 | -0.0439 |

Obtained the value of $S_{L0}$ from (2.6), all the parameters needed by GT-Power ($B_m$, $B_\Phi$ and $\Phi_m$) have been calculated by inverting the equation (2.3) and then implemented into the laminar speed window of the SITurb model (Fig. 2.30).

Figure 2.30 Custom CNG Laminar Speed implementation

## 2.8.2. Turbulent flame speed calibration

The calibration of the parameters for the turbulent speed of the SITurb model upon different engines is performed through four multipliers present in its template on GT-Power; the goal is to find a single combination of these multipliers that allows the best possible match of the combustion profile for a wide range of operating points of the engine map. The four multipliers are:

- **Dilution Multiplier**. It is used to scale the dilution effect (residuals + EGR) on the laminar flame speed. Increasing the value, the dilution effect is increased hence reducing the burn rate and vice versa, Fig. 2.31.

- **Flame Kernel Growth Multiplier**. It is a parameter that affect the development of the flame kernel and it is used to scale the calculated value of flame kernel growth. It affects the ignition delay so, if increased, the delay decreases, if decreased the delay increases, Fig.2.32.

- **Turbulent Flame Speed Multiplier**. It is used to scale the calculated turbulent flame speed and, as for the previous, increases or decreases the burn rate in accordance with its increasing or decreasing. It is the most influent of the parameters, as is possible to see in Fig. 2.33.

- **Taylor Length Scale Multiplier**. This is used to scale the calculated value of the "Taylor microscale length" of turbulence that, as reported in the previous equation, influences the time constant of fuel/air mixture entrained into the flame zone. This multiplier mostly influences the tail part of the combustion (burn rate) and

its influence strongly depend on the combination of the previous, but it is usually relatively insensitive compared to the others, Fig. 2.34.

GT-Power provides an automated process for the calibration of predictive combustion models based on the already mentioned Three Pressure Analysis. The process is performed in a very simple way: the software searches for a combination of the four multipliers that could match as much as possible the burn rate obtained from the TPA, using as combustion constraints the information implemented on the SITurb combustion model. Gamma Technologies call this process "Measured + Predicted" and it can be implemented in the combustion object of the cylinder combined with the use of the Advanced Optimizer tool, set up with a sweep between the multipliers. They also recommend limits for the multipliers, reported below:

**Table 2-7 Multipliers limits [1]**

|  | Minimum | Maximum |
|---|---|---|
| Dilution Exponent Multiplier | 0.5 | 3.0 |
| Flame Kernel Growth Multiplier | 0.5 | 3.0 |
| Turbulent Flame Speed Multiplier | 0.5 | 3.0 |
| Taylor Length Scale Multiplier | 0.5 | 3.0 |

The following figures report the multipliers sweeps made on one of the twenty-five available operating points, in order to show the influence of each parameter on the burn rate. The data implemented on the SITurb model were specific for this engine (natural gas), while the multipliers were set to "default" (=def) if not accounted for the sweep.
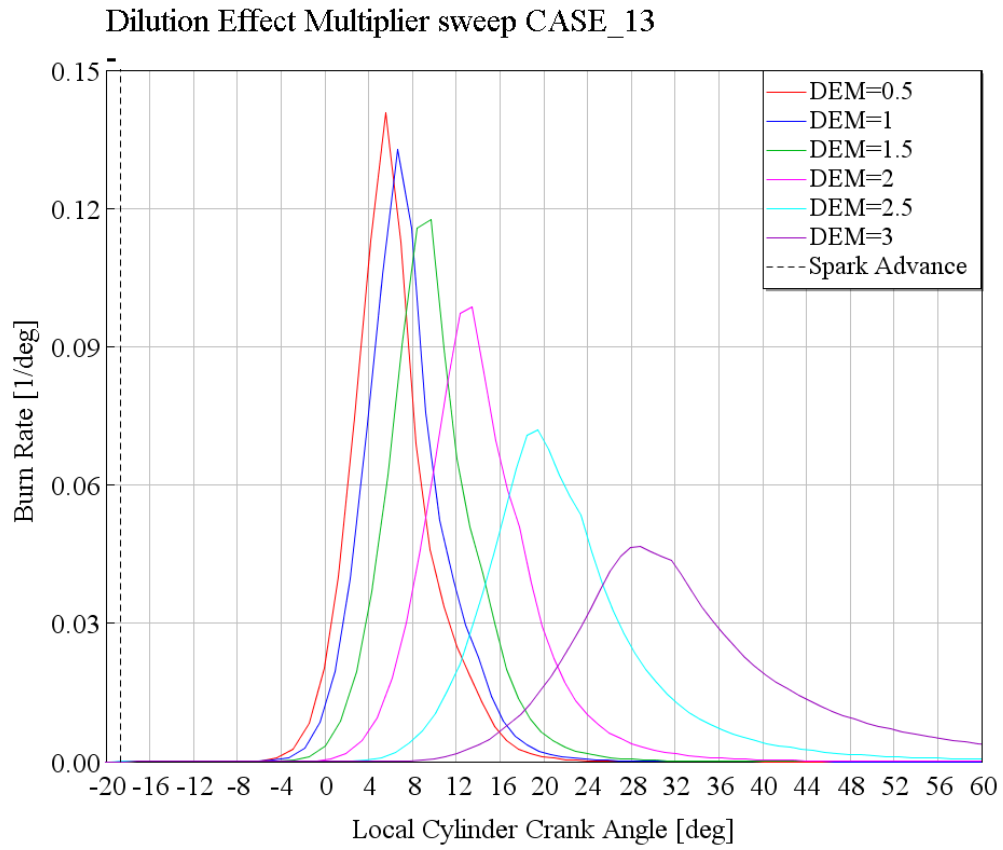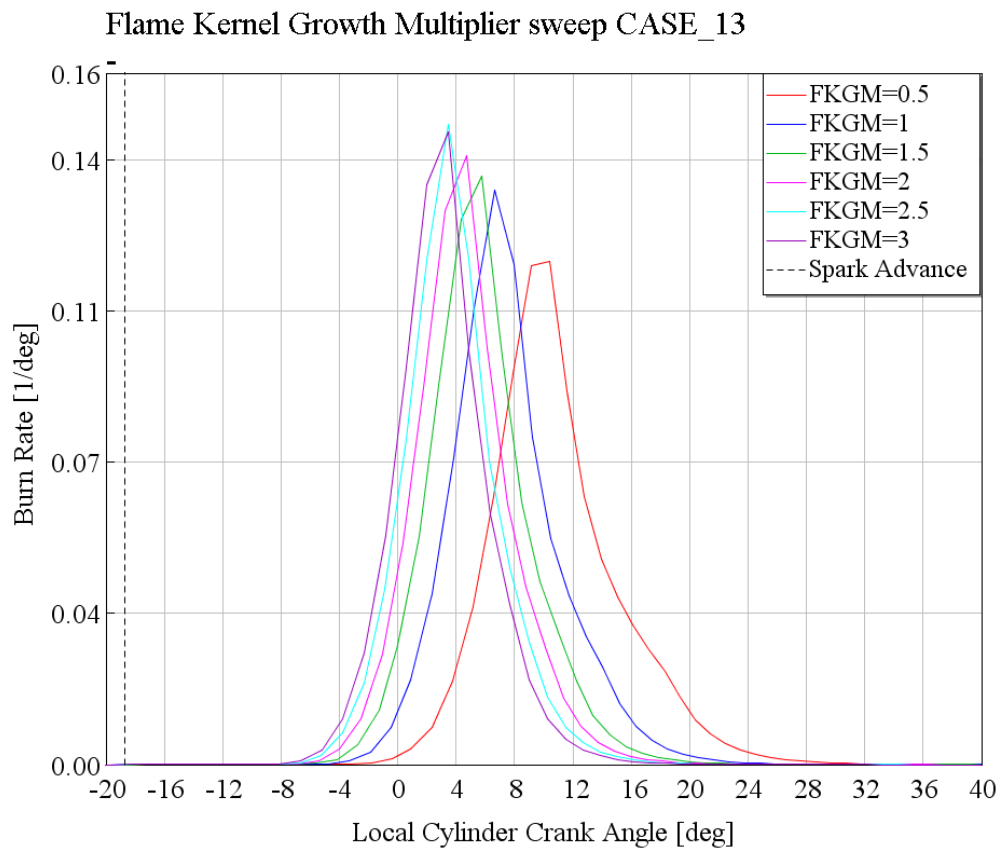
Dilution Effect Multiplier sweep CASE_13



Figure 2.31 Burn Rate DEM sweep

Flame Kernel Growth Multiplier sweep CASE_13



Figure 2.32 Burn Rate FKGM sweep

Turbulent Flame Speed Multiplier sweep CASE_13



Figure 2.33 Burn Rate TFSM sweep

Taylor Length Scale Multiplier sweep CASE_13
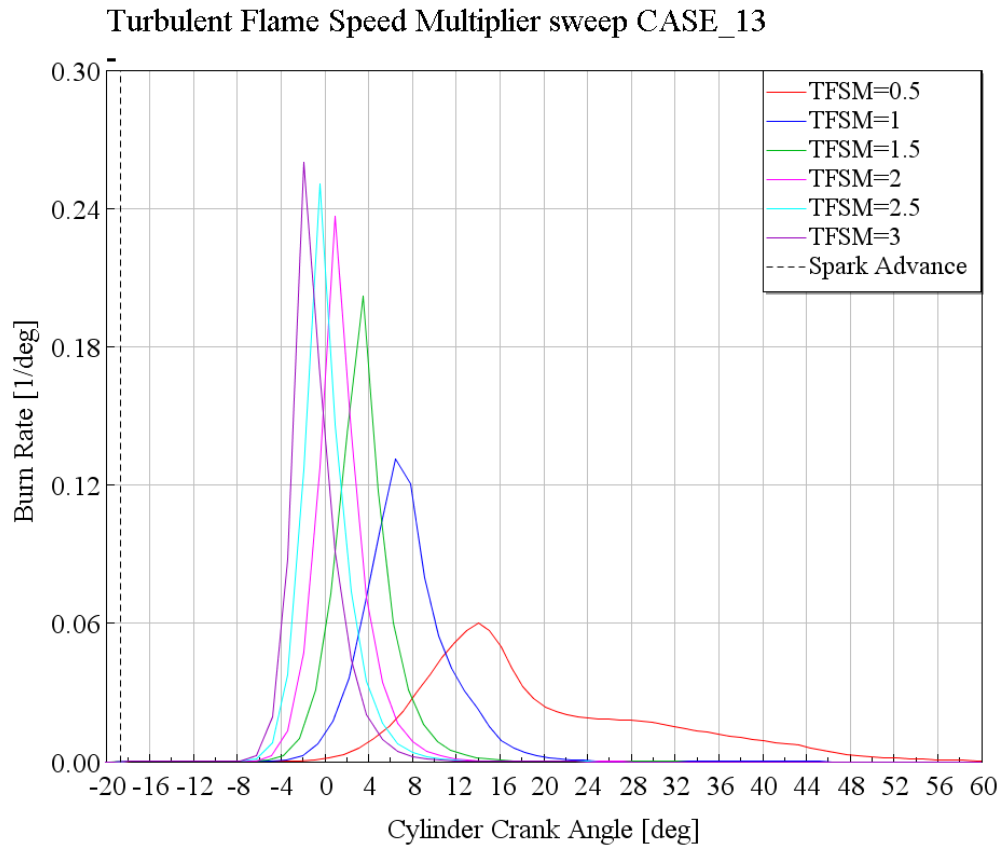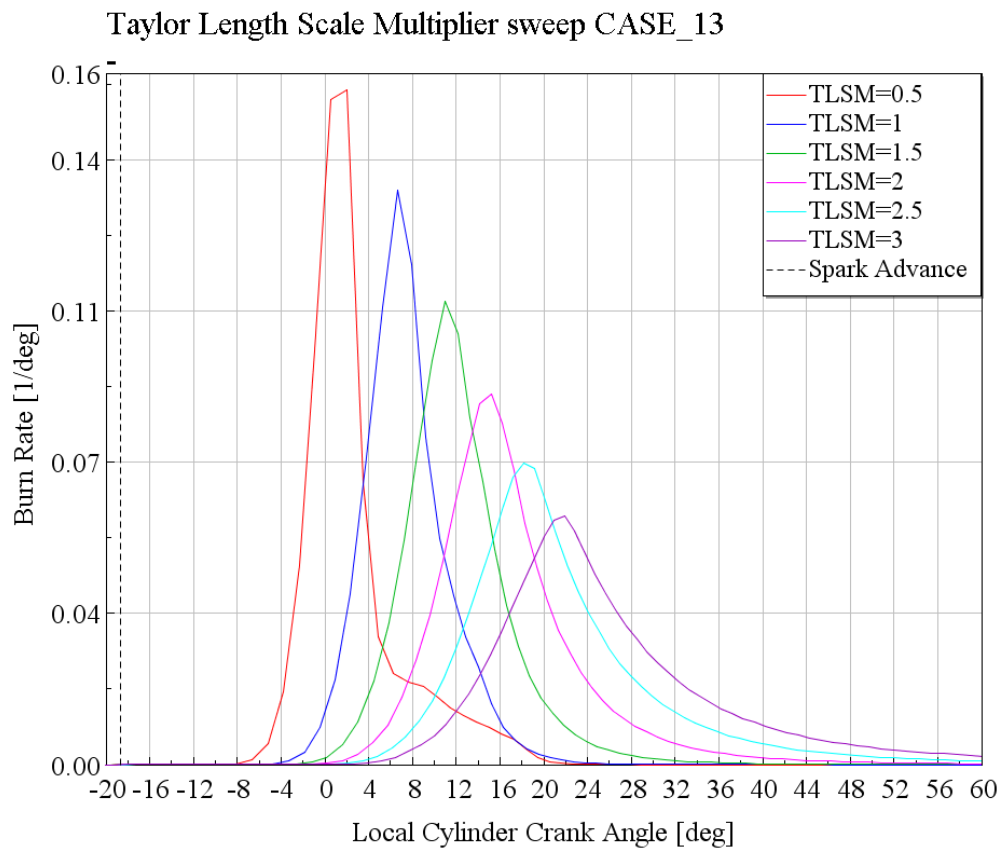


Figure 2.34 Burn Rate TLSM sweep

### 2.8.3. Predictive combustion model results

The automated process just exposed, used for fitting the combustion curve, has been run lots of times and for different points among the engine map but without having success in any of them. The SITurb model, in fact, has shown some important limits for this specific engine, and in particular when CNG fuel is used, for which it hasn't never been able to reach a good matching of the burn rate curves between measured (experimental) and simulated.

The major issue has been identified on the very beginning of the flame development, i.e. at the kernel growth. As it is possible to notice in the figures from 2.31 to 2.34, every curve lags the Spark Advance (indicated with the dashed line), of about 16 degrees, in whatever situation; of course, those curves are not representing a calibration process result, but the hint is anyway clearly visible.

Three graphs, referred to the already presented cases 3, 13 and 23, that could expose the problem in a better way, are reported in the following Figures 2.35, 2.36 and 2.37. In each figure are present four burn rate curves: one is the burn rate obtained from the TPA, hence the closest to the actual combustion for that specific case; a second curve is the best fitting curve achieved with the automated process for that specific case while the last two are the burn rates obtained when a set of multipliers found optimizing a different case is used into the simulation of the first.
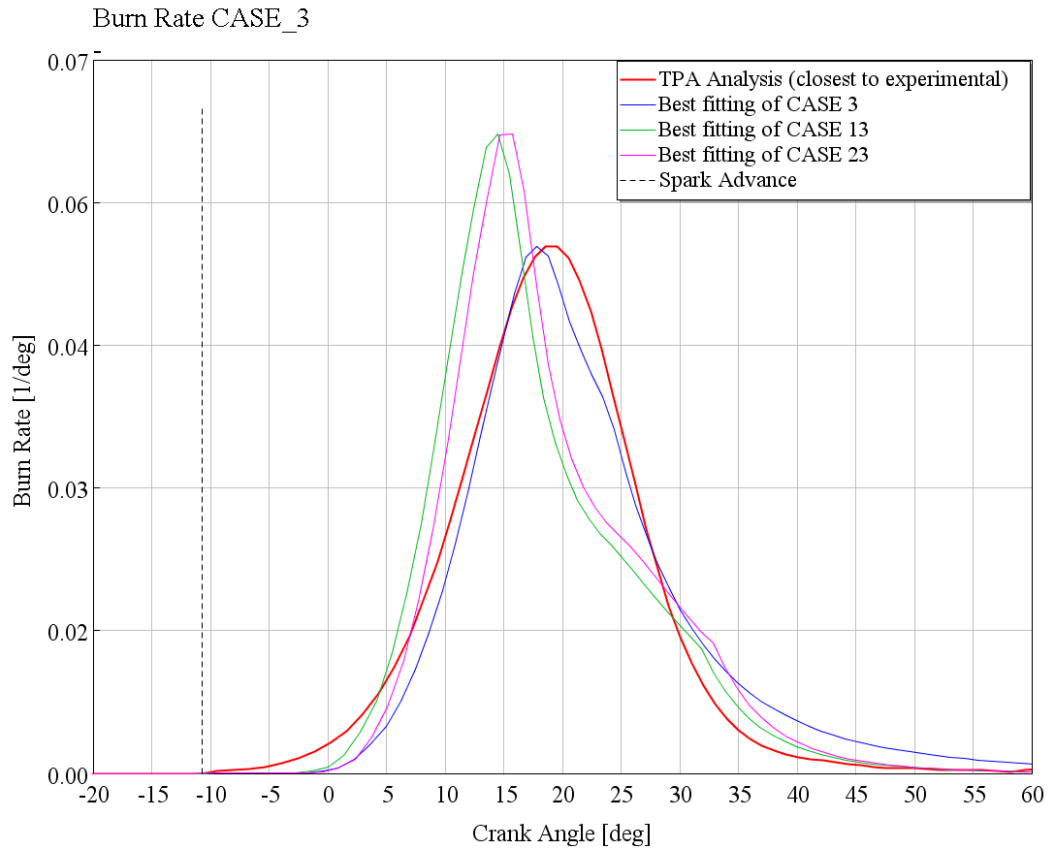
Burn Rate CASE_3



Figure 2.35 Predicted Burn Rates, CASE 3

Burn Rate CASE_13



Figure 2.36 Predicted Burn Rates, CASE 13
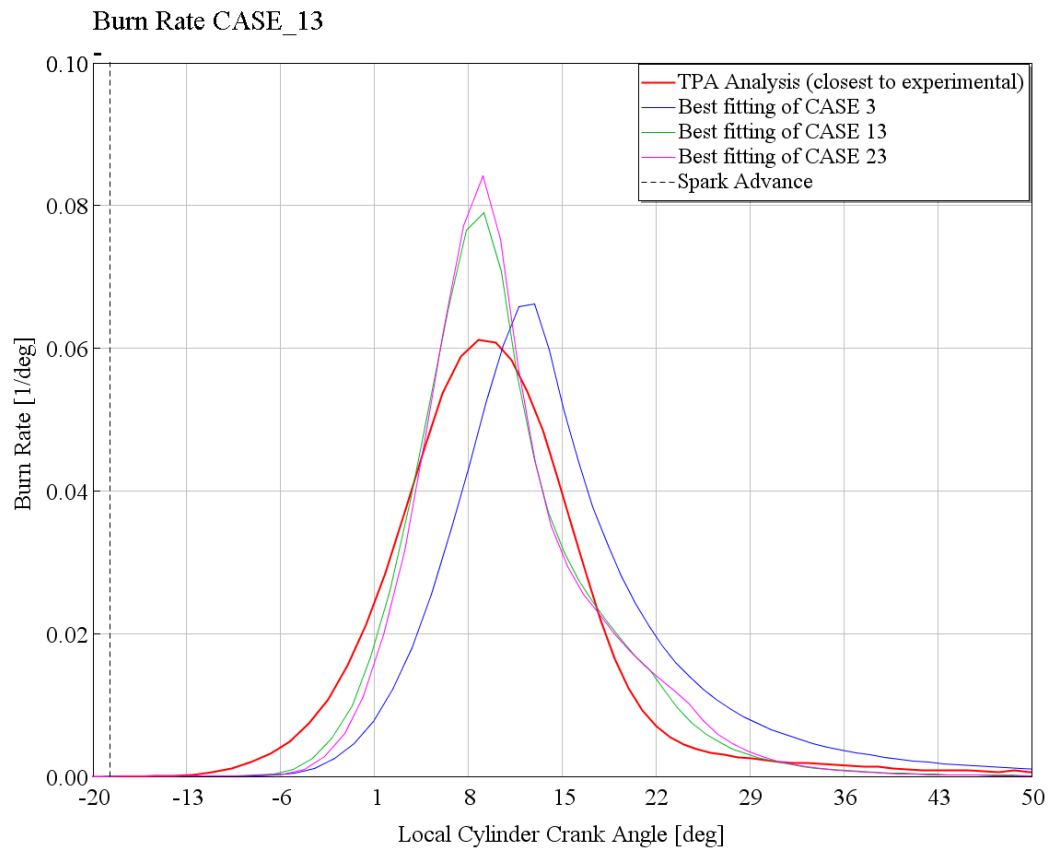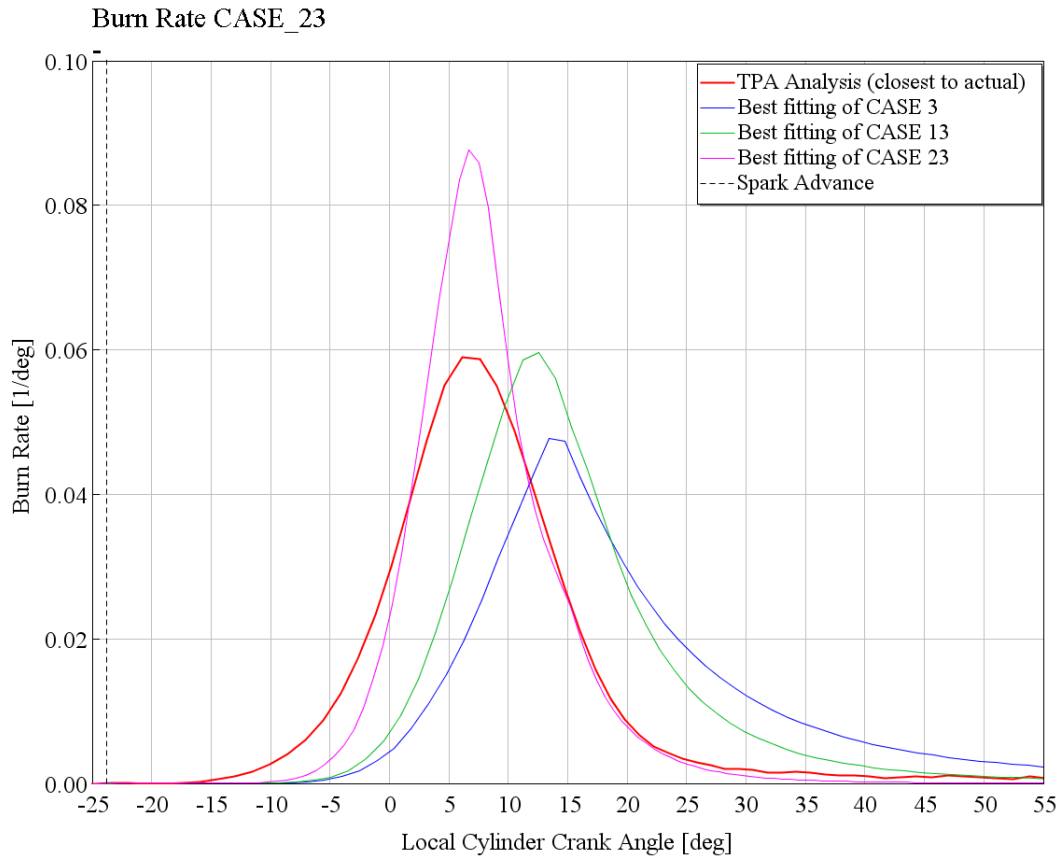
Burn Rate CASE_23



Figure 2.37 Predicted Burn Rates, CASE 23

Since the combination of the multipliers should be unique for the whole engine map, also the burn rates should be well fitted in each case with only one set, but this is not happening. On the contrary, taking as example the CASE 3 (high load), the more the load decreases, the more is the lag when its set of multipliers is used in cases at lower loads, CASEs 13 and 23 (medium and low load) and vice versa. The multipliers combinations obtained from the automated process are reported in the following Tables 2-8.9.10:

| Table 2-8 SITurb multipliers CASE 3 | | Table 2-9 SITurb multipliers CASE 13 | | Table 2-10 SITurb multipliers CASE 23 | |
|---|---|---|---|---|---|
| **CASE 3** | | **CASE 13** | | **CASE 23** | |
| **TFSM** | 0.703 | **TFSM** | 0.625 | **TFSM** | 0.751 |
| **TLSM** | 2.075 | **TLSM** | 0.625 | **TLSM** | 1.632 |
| **FKGM** | 4.120 | **FKGM** | 2.748 | **FKGM** | 2.496 |
| **DEM** | 1.6726 | **DEM** | 1.750 | **DEM** | 0.544 |

Analysing more closely all the graphs it is clear how both in the burn rate and in pressure traces (Fig. 2.38-40) the main issue is the simulation of the early stages of the flame development, i.e. immediately after the spark, performed by the SITurb model. In none of the cases the burn rate follows the kernel growth but is very steep afterwards: the model in fact start the combustion with a low energy release and tends to balance the accumulated delay with respect to the TPA trace by increasing the burn rate when the flame is already well developed. In then reaches a peak that is over the correct profile and creates an error that is impossible to be contained. Several trials have been performed, also manually, in order to achieve better results but no one has achieved the objective. With the possibility to tweak only the four explained parameters, there isn't any combination that can overcome this problem. This issue arises only because of the CNG fuel, for which the turbulent flame speed isn't well modelled, since with gasoline the start of the combustion is well reproduced. Only by changing the "spark size" value, that takes into account the length of the spark, and hence isn't a calibration parameter but a geometrical one, it is possible to improve the results, although this method is completely incorrect from a logical point of view. Spark-plug length is a design characteristic, independent from the combustion development.
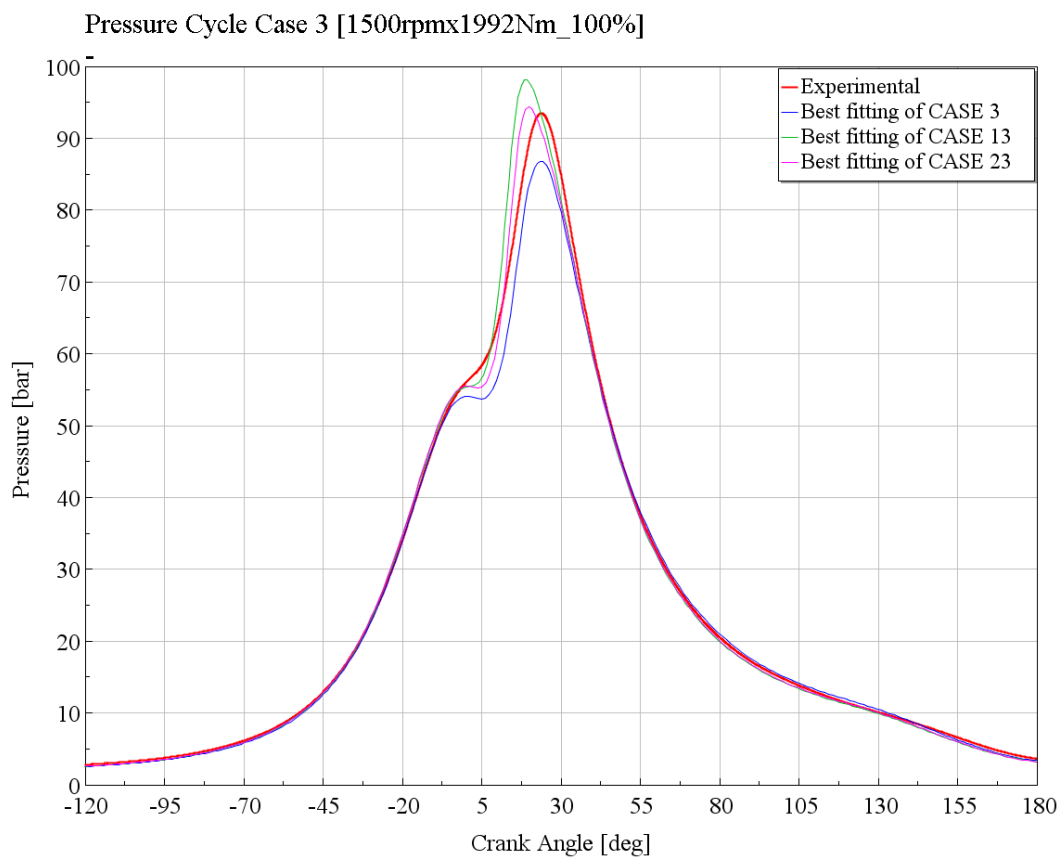


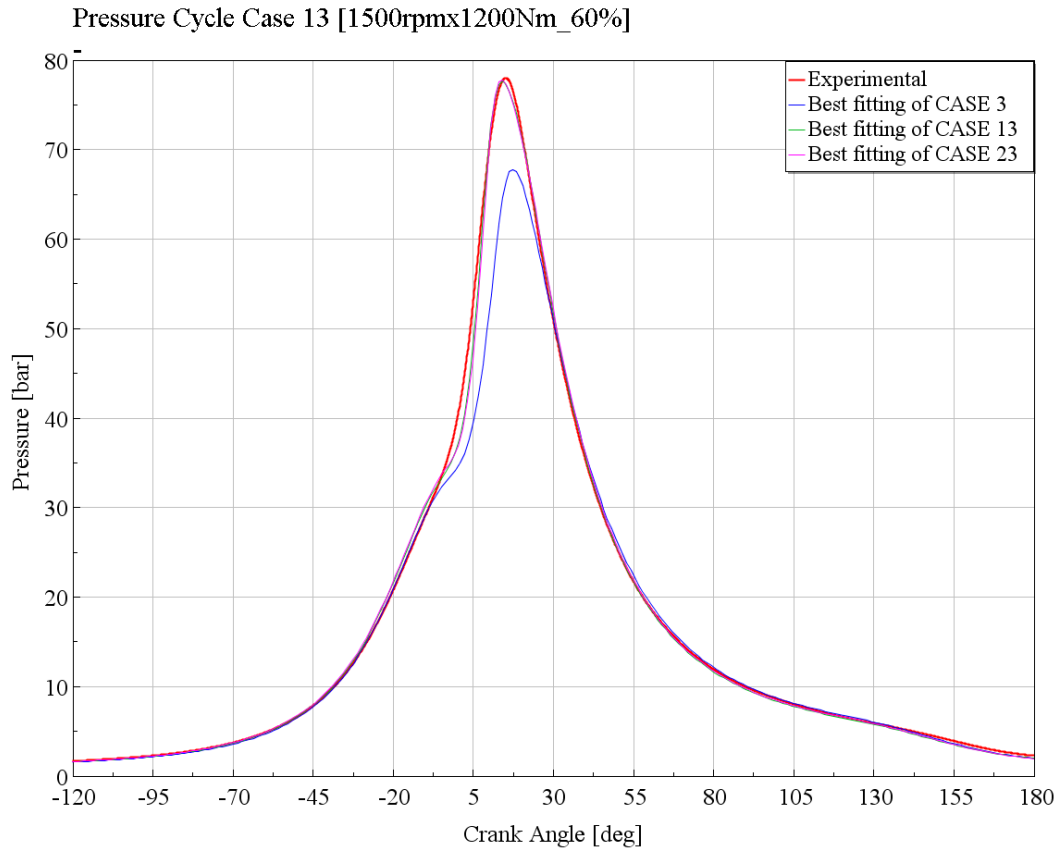Figure 2.38 Predicted pressure traces, CASE 3

Pressure Cycle Case 13 [1500rpmx1200Nm_60%]



Figure 2.39 Predicted pressure traces, CASE 13
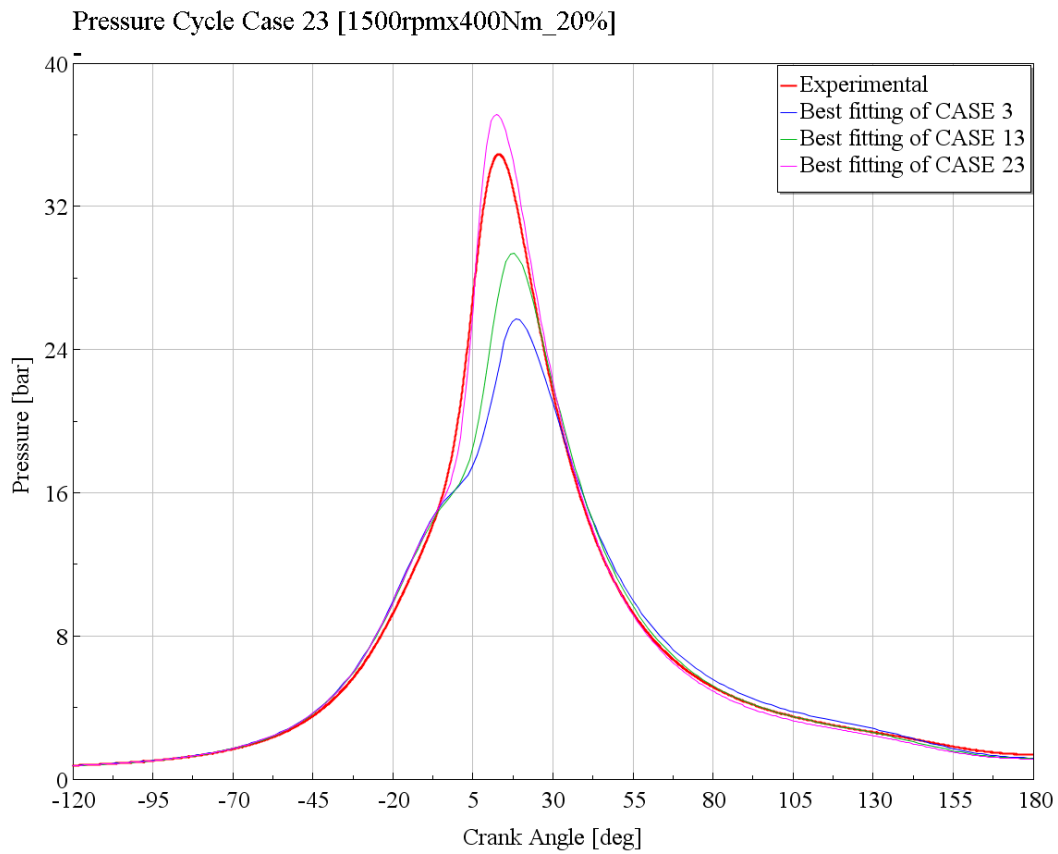
Pressure Cycle Case 23 [1500rpmx400Nm_20%]



Figure 2.40 Predicted pressure traces, CASE 23

For the reasons just exposed, the Predictive SITurb model has been put aside in favour of a semi-empirical combustion model with which it has been possible to predict the emissions at engine out, that was the main objective of the work. Unfortunately the combustion isn't anymore predicted, so excluding all the features of that type of model.

It is important to notice that GT-Power can be connected to external softwares, like Matlab, Simulink and others, to perform external routines which can overcome problems like the one encountered in this model. For example, it is possible to set up a complete custom combustion model through external compilators, using Fortran language, and then link the compiled files to the GT-Power model. Thanks to that, the software avoids the internal simulation of the combustion replacing it with the external routine. It is anyway a very time costing process, impossible to be completed in the time used for this thesis project and, moreover, was not the main purpose of the work.

## 2.9   Semi-Empirical combustion model

To overcome the issue arose with SITurb combustion model it has been chosen to exploit the TPAs performed previously so to create a map of burn rates that could simulate the engine behaviour in all the conditions. GT-Power, in fact, allows to impose multiple combustion profiles (and hence burn rates) linked to both engine speed and load and automatically make an interpolation in between two imposed burn rates. Doing so, it is possible to achieve the aim that with the predictive method was not possible but, in this case, the model is much more rigid, being constrained to the burn rate profiles imposed by the user. A model built with these characteristics is not capable of correctly simulates the engine behaviour when combustion related parameters are changed and cannot substitute the test bench, but it is anyway useful to predict the emissions.

The Table 2-11 reports how the implementation in GT-Power has been performed. Because of the software do not allows empty cells in the table, some corrections for the cases at 1900 rpm and those below the 1100 rpm have been applied. In particular, since the rows were corresponding to different level of torque with respect of the actual engine capabilities, burn rates of other cases, more correcting representing the curve for those cells, have been inserted.

**Table 2-11 Combustion profiles map**

| Speed[rpm] | 700 | 900 | 1100 | 1300 | 1500 | 1620 | 1900 |
|---|---|---|---|---|---|---|---|
| **Torque[Nm]** | | | | | | | |
| **2000** | Burn rate CASE 15 | Burn rate CASE 10 | Burn rate CASE 5 | Burn rate CASE 4 | Burn rate CASE 3 | Burn rate CASE 2 | Burn rate CASE 1 |
| **1600** | Burn rate CASE 15 | Burn rate CASE 10 | Burn rate CASE 10 | Burn rate CASE 9 | Burn rate CASE 8 | Burn rate CASE 7 | Burn rate CASE 6 |
| **1200** | Burn rate CASE 15 | Burn rate CASE 15 | Burn rate CASE 15 | Burn rate CASE 14 | Burn rate CASE 13 | Burn rate CASE 12 | Burn rate CASE 12 |
| **800** | Burn rate CASE 20 | Burn rate CASE 20 | Burn rate CASE 20 | Burn rate CASE 19 | Burn rate CASE 18 | Burn rate CASE 17 | Burn rate CASE 17 |
| **400** | Burn rate CASE 25 | Burn rate CASE 25 | Burn rate CASE 25 | Burn rate CASE 24 | Burn rate CASE 23 | Burn rate CASE 22 | Burn rate CASE 22 |

The following Figures 2.41,42, instead, explain how the software make the interpolation between two curves. In the studied case, the selected interpolation method is the *Unconstrained* one.
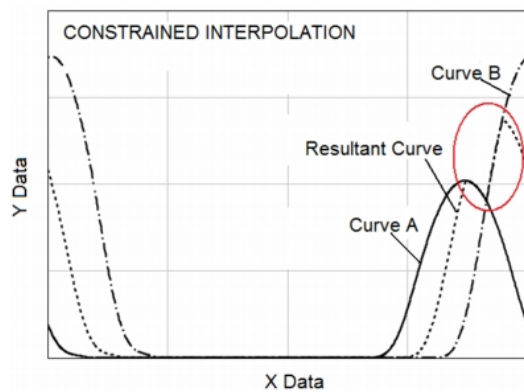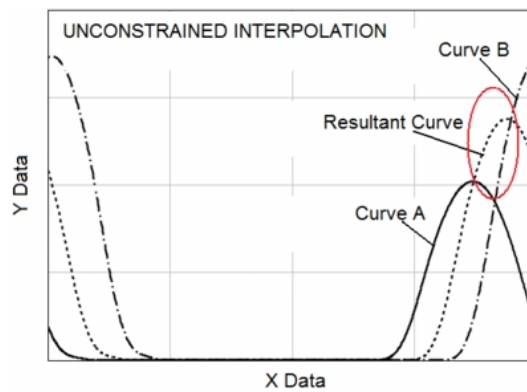


Figure 2.41 Constrained interpolation [9]                    Figure 2.42 Unconstrained interpolation [9]

## 2.10  Emissions calibration

In GT-Power emissions are modelled through well-known chemical relation, taken from the literature. For each emission compound, HC, $NO_x$ and CO it is possible to select a model from the library of the software, like already done for the combustion. In every model, there are multipliers and parameters that could be modified in order to proper calibrate the emission model related to the specific engine.

In this work, only $NO_x$ and CO have been considered, each one with its specific model implemented inside the combustion model, as shown in the Figure 2.43:



Figure 2.43 Emission models implementation

### 2.10.1.  NOx calibration model

$NO_x$ have been modelled through the "*EngCylNOx*" object that is capable of predict the formation of NO during combustion. $NO_2$ is in fact a very little fraction of NOx, almost zero if compared to NO and hence can be neglected.

The results of that object are very sensitive to the equivalence ratio (availability of oxygen) and temperature. Therefore, trapped cylinder mass (i.e. engine airflow, EGR fraction, trapping ratio), fuel-to-air ratio, and combustion rate all must be reasonable values before any reasonable NO prediction can be expected. Hence, it is always necessary that the simulated values for those results compare well before trying to calibrate the NO emissions [10].

The NO calculation is based on the extended Zeldovich mechanism of which the involved chemical reactions are reported below [10]:

- N$_2$ oxidation:             $O + N_2 \leftrightarrows NO + N$
- N oxidation:                $N + O_2 \leftrightarrows NO + O$
- OH reduction:               $N + OH \leftrightarrows NO + H$

Each reaction above has a reaction rate that is implemented in the software as follows:

- N$_2$ oxidation rate:        $k1 = F_1 * 7.60 * 10^{10} * e^{-3800*A_1/T_b}$
- N oxidation rate:           $k2 = F_2 * 6.40 * 10^6 * T_b * e^{-3800*A_2/T_b}$
- OH reduction rate:          $k3 = F_3 * 4.10 * 10^{10}$

where:

$F_1$ = N$_2$ Oxidation Rate Multiplier

$F_2$ = N Oxidation Rate Multiplier

$F_3$ = OH Reduction Rate Multiplier

$A_1$ = N$_2$ Oxidation Activation Temperature Multiplier

$A_2$ = N Oxidation Activation Temperature Multiplier

$T_b$ = Burned Sub-zone Temperature (K).

The listed reaction rates are the forward ones, where $F_1$, $F_2$, and $F_3$ are the calibration multiplier that, together with another "high-level" multiplier called *"NO$_x$ multiplier"*, the user can tweak in order to achieve the best simulated result. While the formers act directly on the reaction, and hence on the Zeldovich mechanism, the latter is a simple method to scale the simulated emissions.

Since Zeldovich mechanism is largely proven to be accurate for a lot of different engines, the NO calibration for this work has been done acting only on the high-level scalar multiplier, so to do not destabilize the mechanism itself. **The value found for the NO$_x$ multiplier that has given good results was 0.85**, so reducing the emission amount calculated by the Zeldovich mechanism, in coherence with the fuel type.

## 2.10.2. CO calibration model

Similarly to what just exposed for the NO$_x$, also the emissions of CO are modelled by GT-Power through known relation found in the literature. The implemented model has been the "*EngCylCO*" which replace the equilibrium in-cylinder carbon monoxide (CO) model with a kinetic CO model [11].

The levels of CO observed in spark-ignition engine exhaust gases are lower than the maximum values measured within the combustion chamber but are significantly higher than equilibrium values for the exhaust conditions. Thus the processes which govern CO exhaust levels are kinetically controlled. In premixed hydrocarbon-air flames, the CO concentration increases rapidly in the flame zone to a maximum value, which is larger than the equilibrium value for adiabatic combustion of the fuel-air mixture. CO formation is one of the principal reaction steps in the hydrocarbon combustion mechanism, which may be summarized by [12]:

$$RH \rightarrow R \rightarrow RO_2 \rightarrow RCHO \rightarrow RCO \rightarrow CO$$
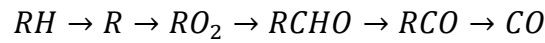
where R stands for the hydrocarbon radical.

The CO formed in the combustion process via this path is then oxidized to CO$_2$ at a slower rate. Calculation is based on the following mechanism and was developed for homogenous combustion:

CO oxidation: $\qquad CO + OH \leftrightarrows CO_2 + H$

with a reaction rate of:

Reaction rate: $\qquad K_{forward} = A * 6.67 * 10^7 * e^{T/_{B*1102}}$

where:

*A* = Pre-exponent Multiplier

*B* = Activation Temperature Multiplier

that can be modified in order to calibrate the emissions.

As already done for the NO$_x$, also in this case the calibration has been concentrated only on the "A" multiplier but, contrary to the previous, the results were not completely acceptable, so further inspections will be needed.

## 2.11 References

[1]     GT-Suite v2016, *Engine Performance Application manual*, Gamma Technologies.

[2]     Robert Wang, (2014)., *Predictive Combustion Modelling*, Gamma Technologies.

[3]     GT-Suite v2016, *"Help" panel of Laminar Speed in GT-Power software*, Gamma Technologies.

[4]     S.Y. Liao, D.M. Jiang, Q. Cheng (2004), *Determination of laminar burning velocities for natural gas*, Fuel, v.83, i.9, p.1247-1250.

[5]     R. Amirante, E. Distaso, P. Tamburrano, R.D. Reitz (2017), *Analytical Correlation for Modelling the Laminar Flame Speed of Natural Gas Surrogate Mixtures*, Energy Procedia, 126, p. 850 – 857.

[6]     Goettler, H and Lemire, B.,(2011) *Specification Smart NO$_x$ Sensor "120"*, Continental Corporation.

[7]     Doc No. NTK-50-050310-SC (Mar 2005), *User's guide and product description of NTK ZFAS-U and ZFAS-U controller*, NGK SPARK PLUG Europe GMBH.

[8]     Addendum 48: Regulation No.49 Revision 5 (May 2011), *Uniform provisions concerning the measures to be taken against the emission of gaseous and particulate pollutants from compression-ignition engines for use in vehicles, and the emission of gaseous pollutants from positive-ignition engines fuelled with natural gas or liquefied petroleum gas for use in vehicles*, pag. 296.

[9]     GT-Suite v2016, *"Help" panel of RLTDependenceProfXYZ - RLT Dependent Variable*, Gamma Technologies.

[10]   GT-Suite v2016, *"Help" panel of EngCylNOx - NOx Model for Combustion*, Gamma Technologies.

[11]   GT-Suite v2016, *"Help" panel of EngCylCO – In-cylinder Kinetic CO Model*, Gamma Technologies.

[12]   Heywood, J. B. (1988). "*Internal combustion engine fundamentals*", Cap. 11.3. (Vol. 930). New York: Mcgraw-hill.

# 3. Steady-state results

The simulation results for the steady-state conditions obtained after the engine calibration exposed in the previous chapter will be reported in the following.

First, the amount of air and fuel that flow in the engine that are related to the chosen lambda. Since lambda is imposed on the injectors, the ration between air and fuel is always respected but, the absolute amount of them is not. The calibration has given very good results on this aspect with errors inside an adequate range between numerical and experimental, as shown in the Figures 3.1 and 3.2, in which the maximum error is around 10% and generally below, especially for the air flow rate. The percentage deviation is higher at lower loads both because of higher experimental uncertainty and because of with lower values the percentage is increased for the same absolute errors. Also the quality of the fuel is impacting on this aspect: as previously said, with a better CNG blend (higher percentage of $CH_4$ in place of $N_2$ and $CO_2$), the fuel amount will be corrected. Furthermore, with the engine model controlled by IMEP, and not by torque, results are even better.

Then, FMEP has given optimal simulated results as well, with engine controlled by torque (Fig. 3.3), meaning that the frictions have been correctly validated. All the results are anyway reported with engine controlled by IMEP since slightly less affected by errors.

For what concern the temperature calibration, below are reported the graphs of the most important for the engine behaviour and exhaust prediction: the temperature at turbine inlet and outlet (defining the enthalpy exploited by the turbine) and immediately before the ATS system (Fig. 3.4-6). The last one is of importance for the heating and the correct working of the three-way catalyst. Also in this case, the errors are largely below the 5% showing that the simulation has been well performed.

Finally, the predictive results for the emission of $NO_x$, CO and $CO_2$ are shown in Figures 3.7-8-9. As it is possible to observe, the errors are larger than in the previous graphs, especially for the CO. The reasons must be ascribed to simulation models used in the software and the calibration possibilities that they give to the user. The predictive models are in fact based on mathematical relations based on homogeneous combustion for spark ignition engines, fuelled with gasoline. CNG engines, even though are spark ignited as

the gasoline ones, have a different combustion behaviour, as already exposed in the SITurb paragraph, and the kinematic relations on which is based the CO prediction have too low flexibility on this aspect which don't permits a calibration in each operating condition. Furthermore, it is not possible to directly act on the equations since are contained in the models but only some parameters can be changed. Thus, they can't never perfectly reproduce the actual engine emissions. Often have been encountered limits on finding a unique value of those parameters that could limits the errors among the whole engine map; if the low loads were optimized, then errors were increased for high loads and vice versa. The reported results are obtained with value optimized for the part of the engine map more used in the transient WHTC cycle, so to minimize the errors for the transient conditions. In any case, CO predicted results aren't correct, although error on $CO_2$ are relatively low, meaning that will be probably needed the implementation of an external routine to satisfy that task.
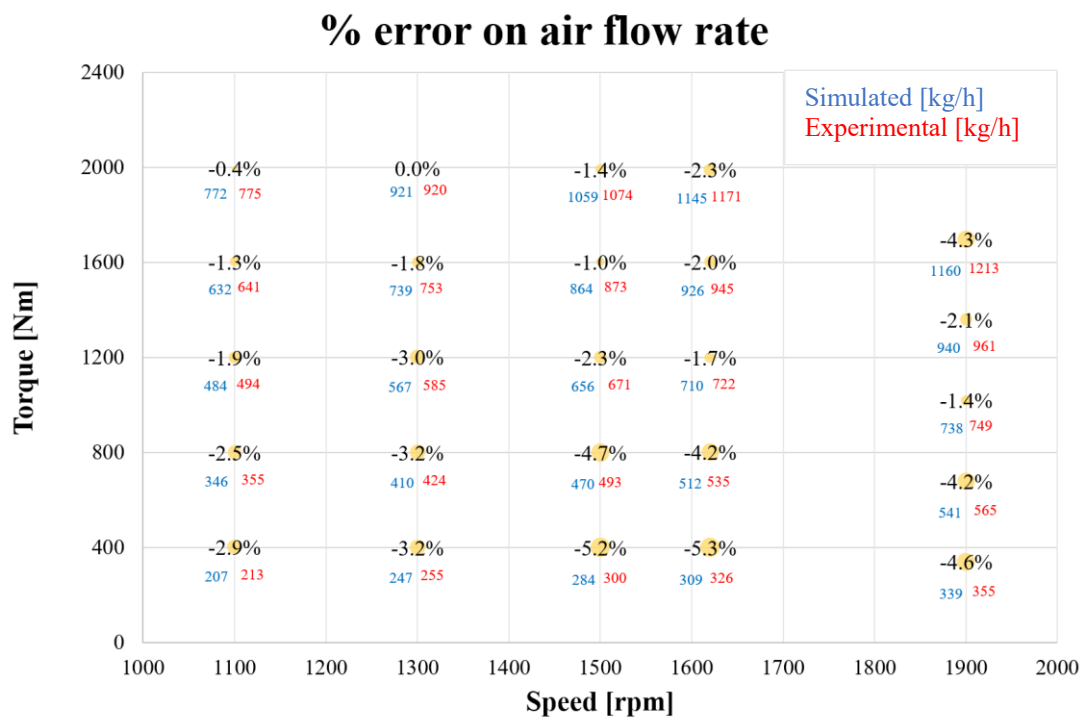


Figure 3.1 Air flow rate % error between simulated and experimental results
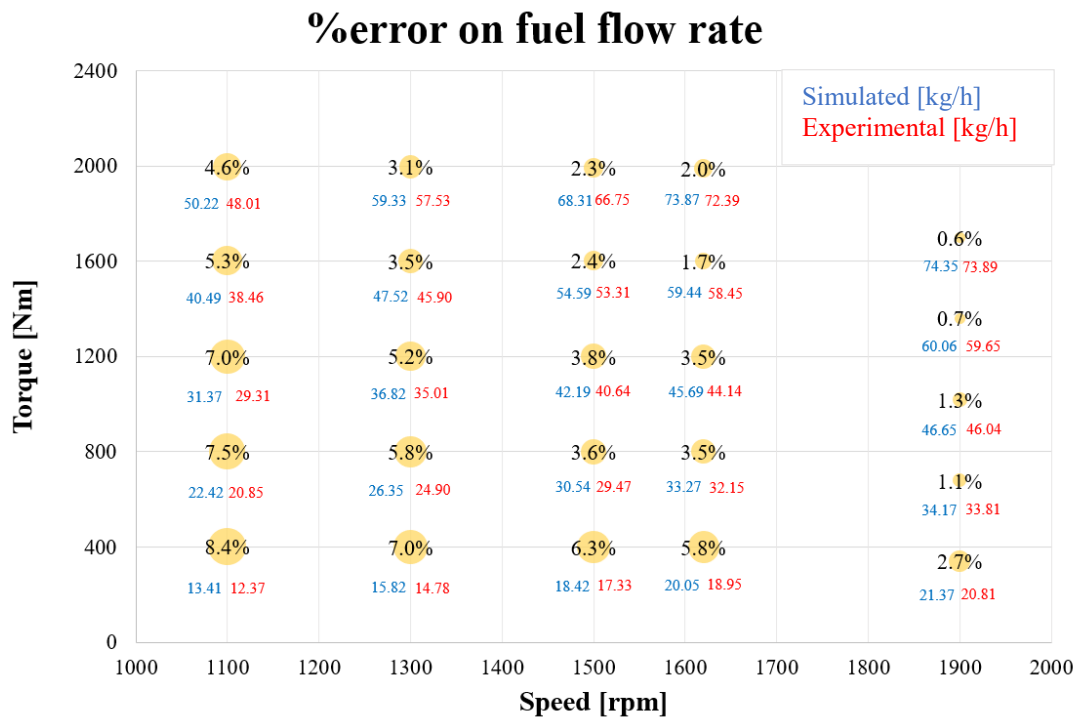
## %error on fuel flow rate



Figure 3.2 Fuel flow rate % error between simulated and experimental results
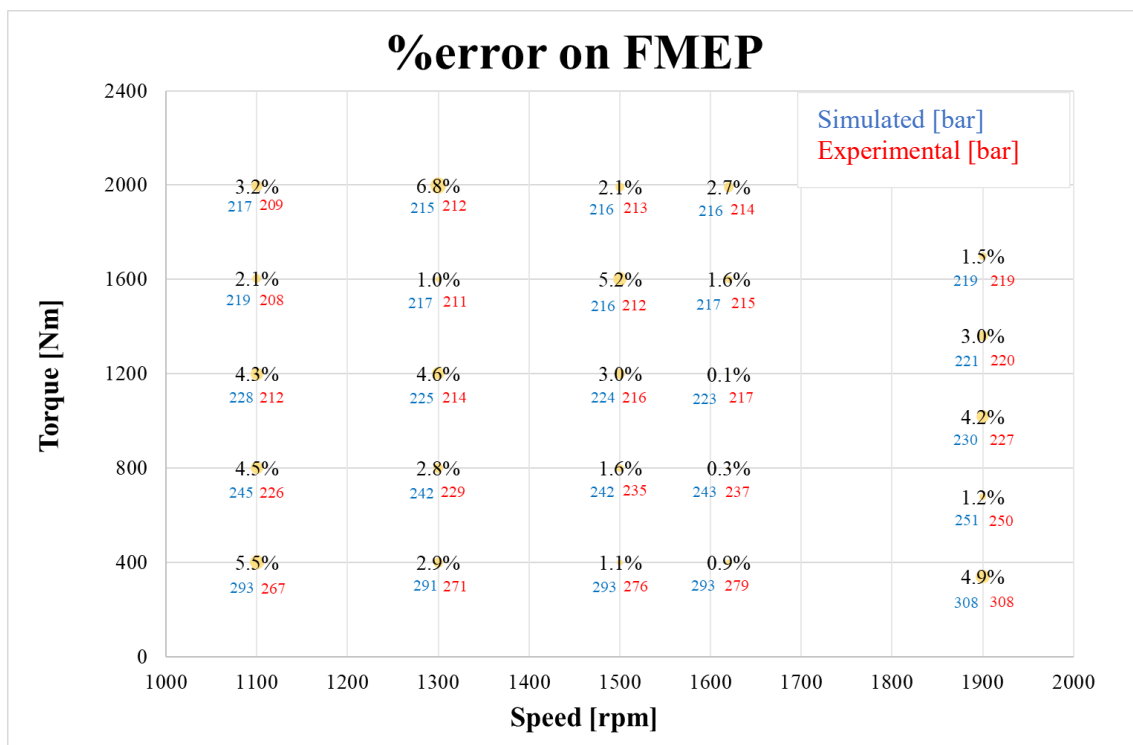
## %error on FMEP



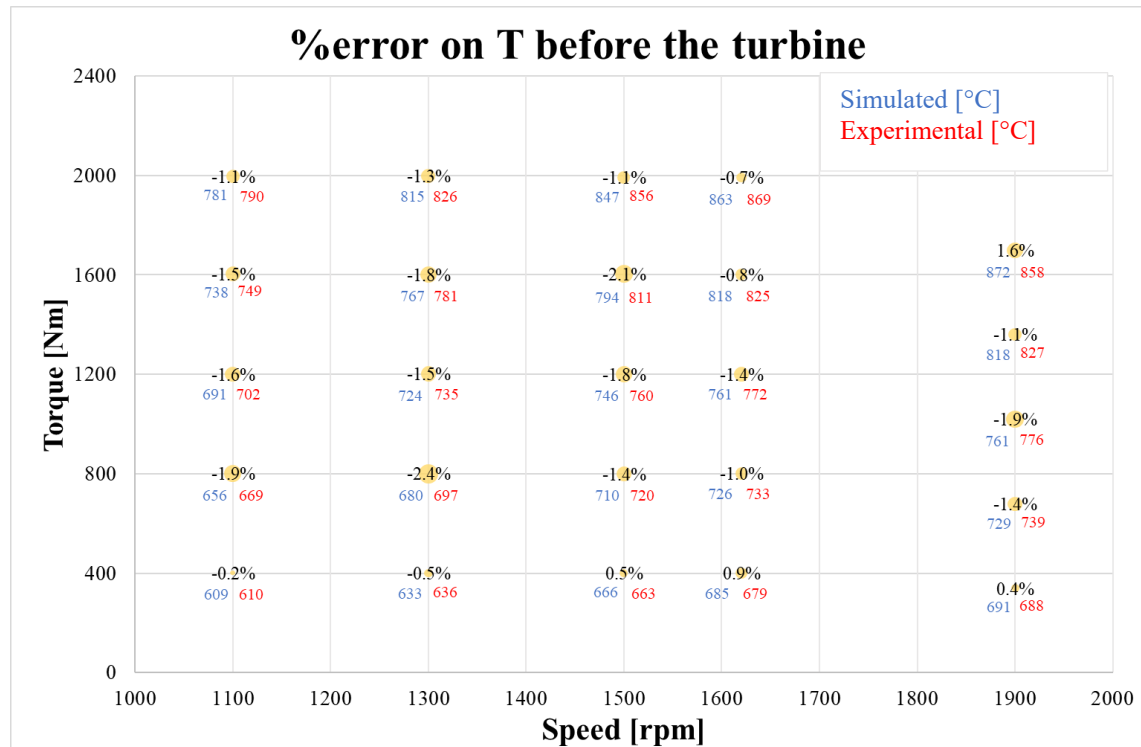Figure 3.3 FMEP % error between simulated and experimental results

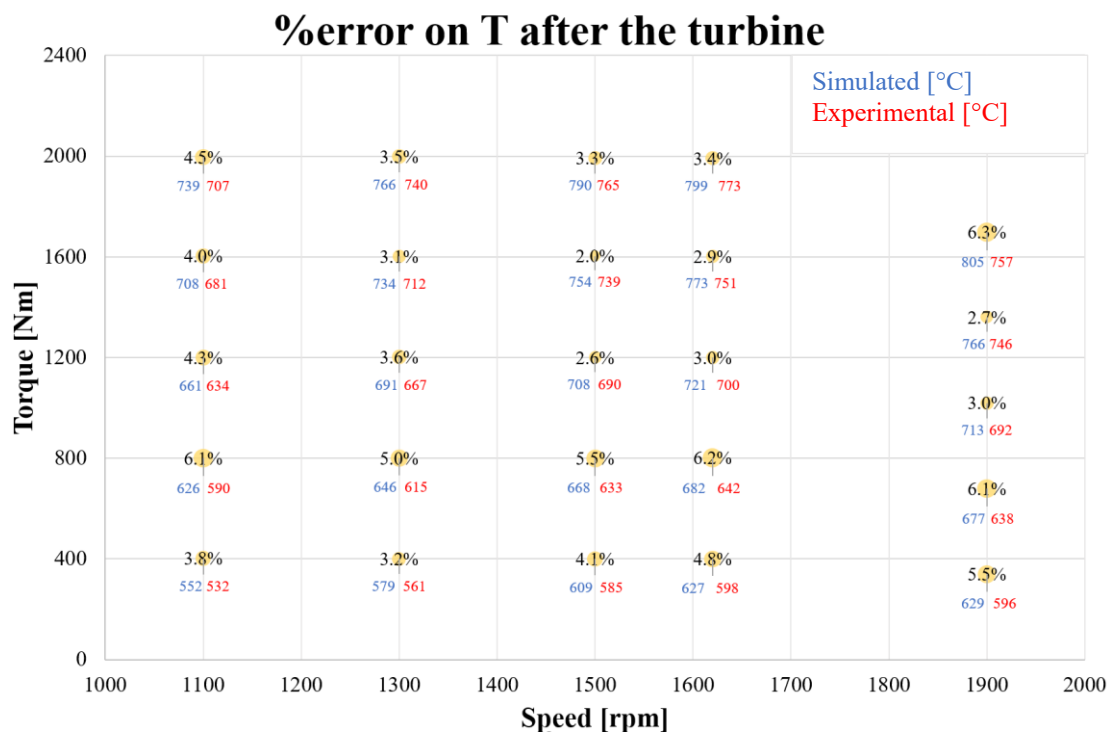Figure 3.4 Temperature % error at turbine inlet between simulated and experimental



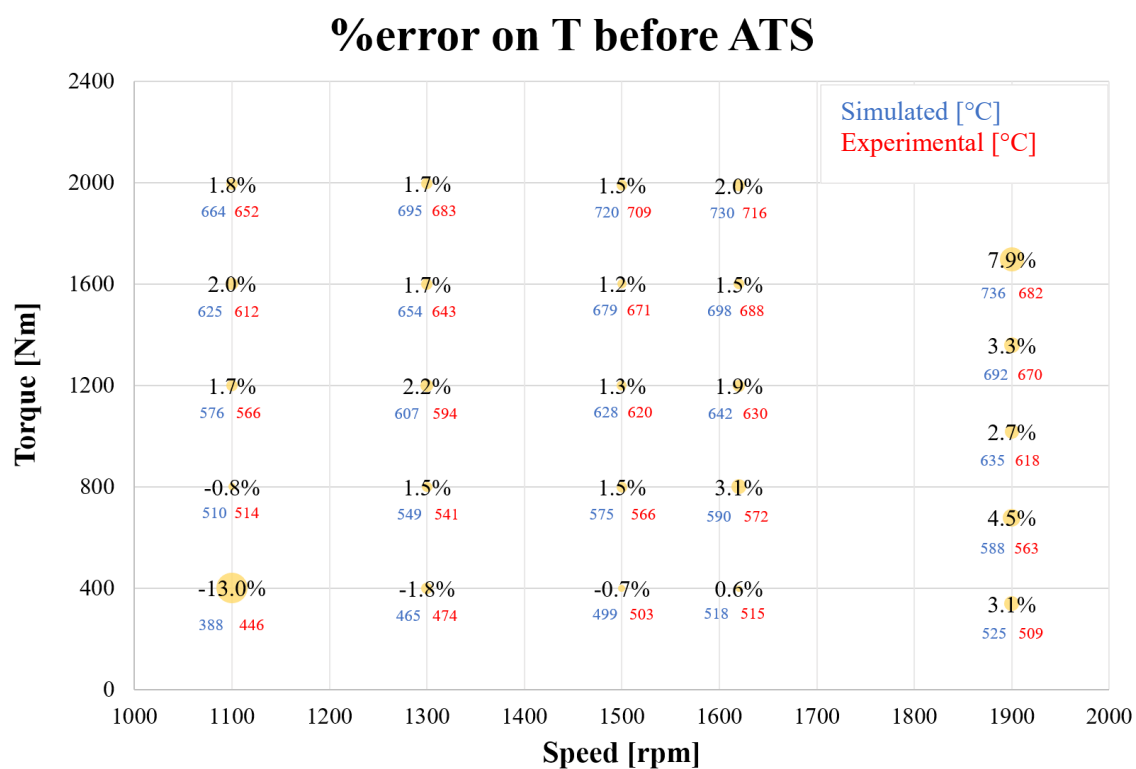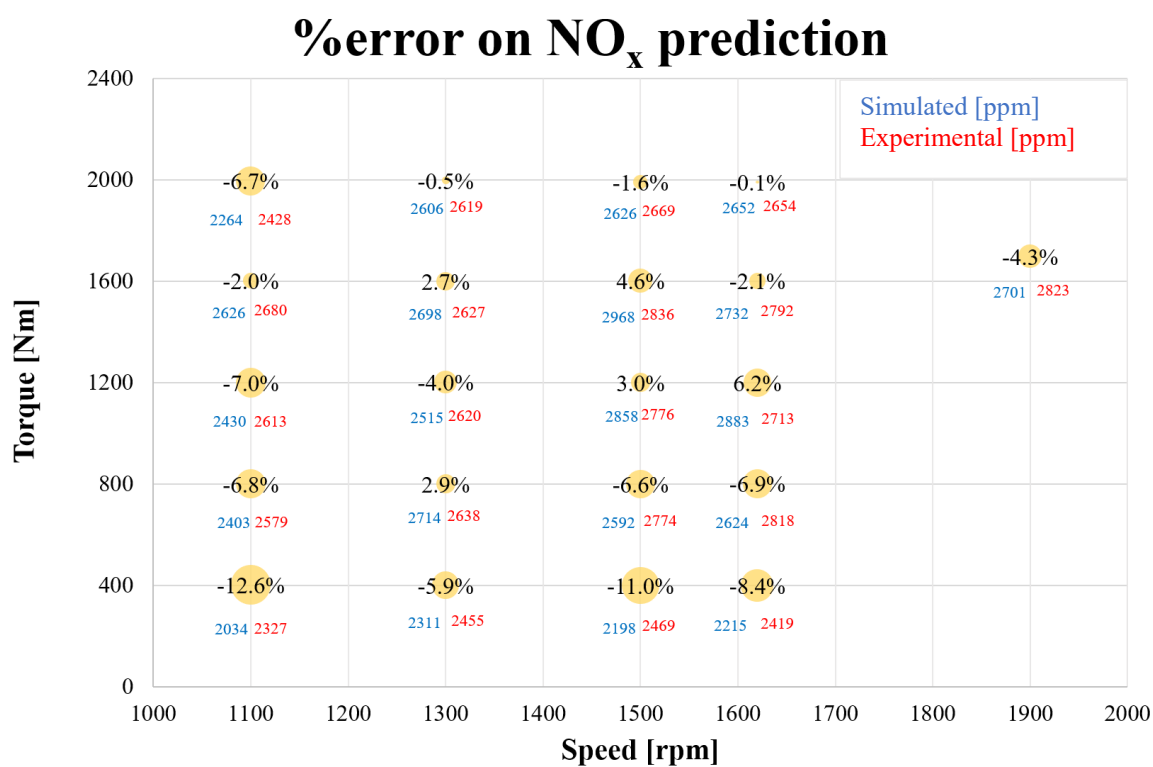Figure 3.5 Temperature % error at turbine outlet between simulated and experimental

## %error on T before ATS



Figure 3.6 Temperature % error at ATS inlet between simulated and experimental

## %error on NO$_x$ prediction



Figure 3.7 % errors on NO$_x$ between predicted emissions and experimental results

## %error on CO prediction
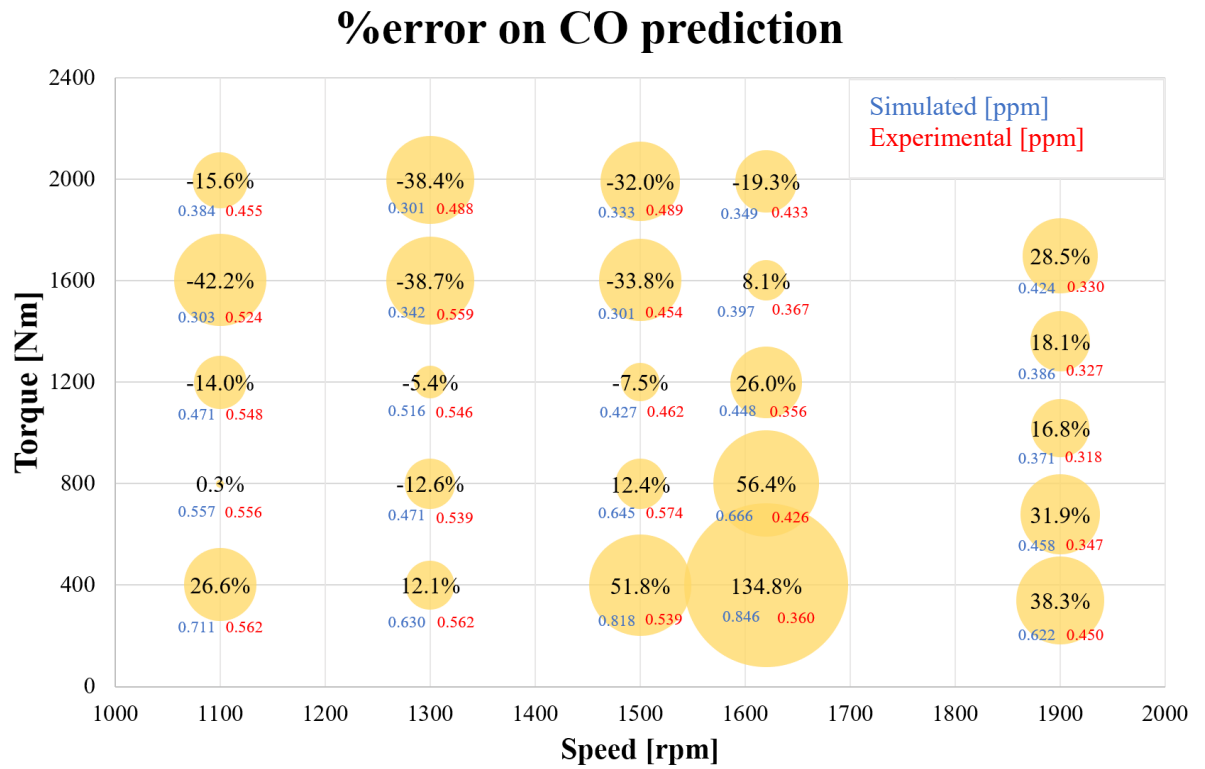


Figure 3.8 % errors on CO between predicted emissions and experimental results

## %error on CO₂ prediction
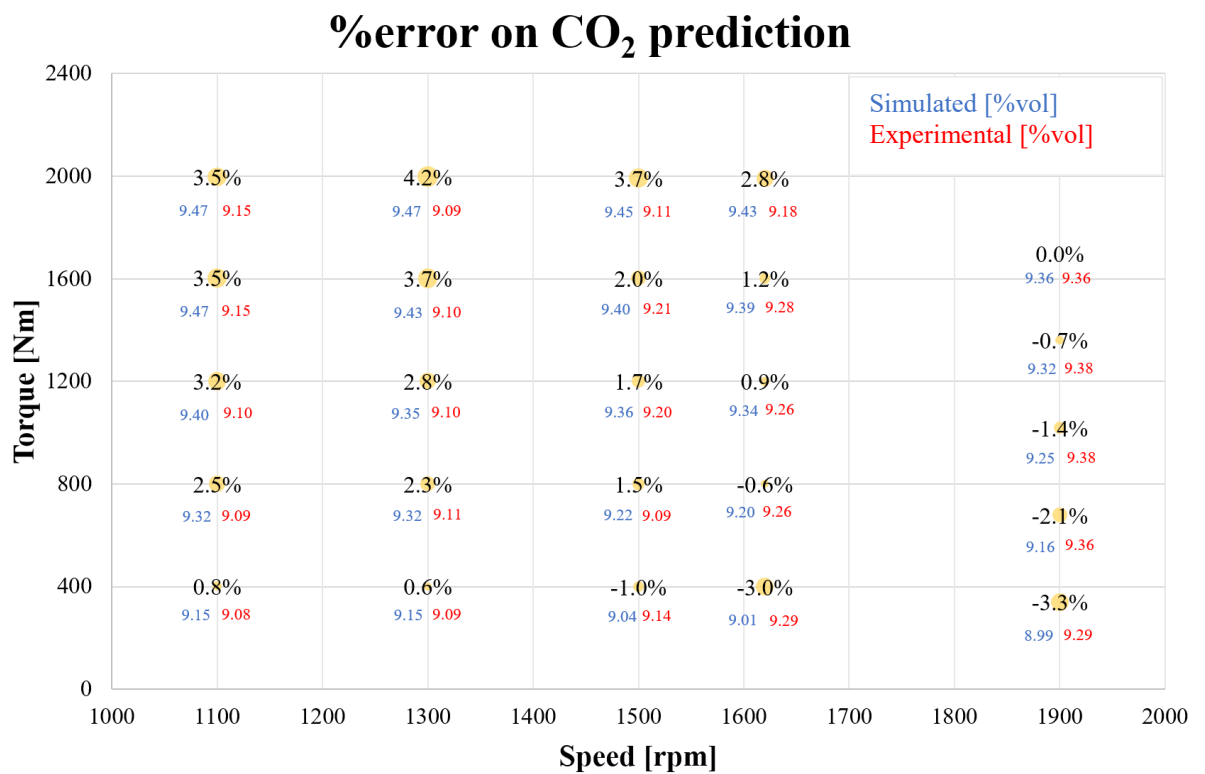


Figure 3.9 % errors on $CO_2$ between predicted emissions and experimental results

# 4. WHTC implementation

## 4.1    World Harmonized Transient Cycle definition

The World Harmonized Transient Cycle is a transient engine dynamometer schedule defined by the global technical regulation (GTR) No. 4 developed by the UN ECE GRPE group. The GTR is covering a world-wide harmonized heavy-duty certification (WHDC) procedure for engine exhaust emissions. The regulation is based on the world-wide pattern of real heavy commercial vehicle use.

The WHTC is a transient test of 1800 s duration, with several motoring segments. Normalized engine speed and torque values over the WHTC cycle are schematically shown below (Fig. 4.1).
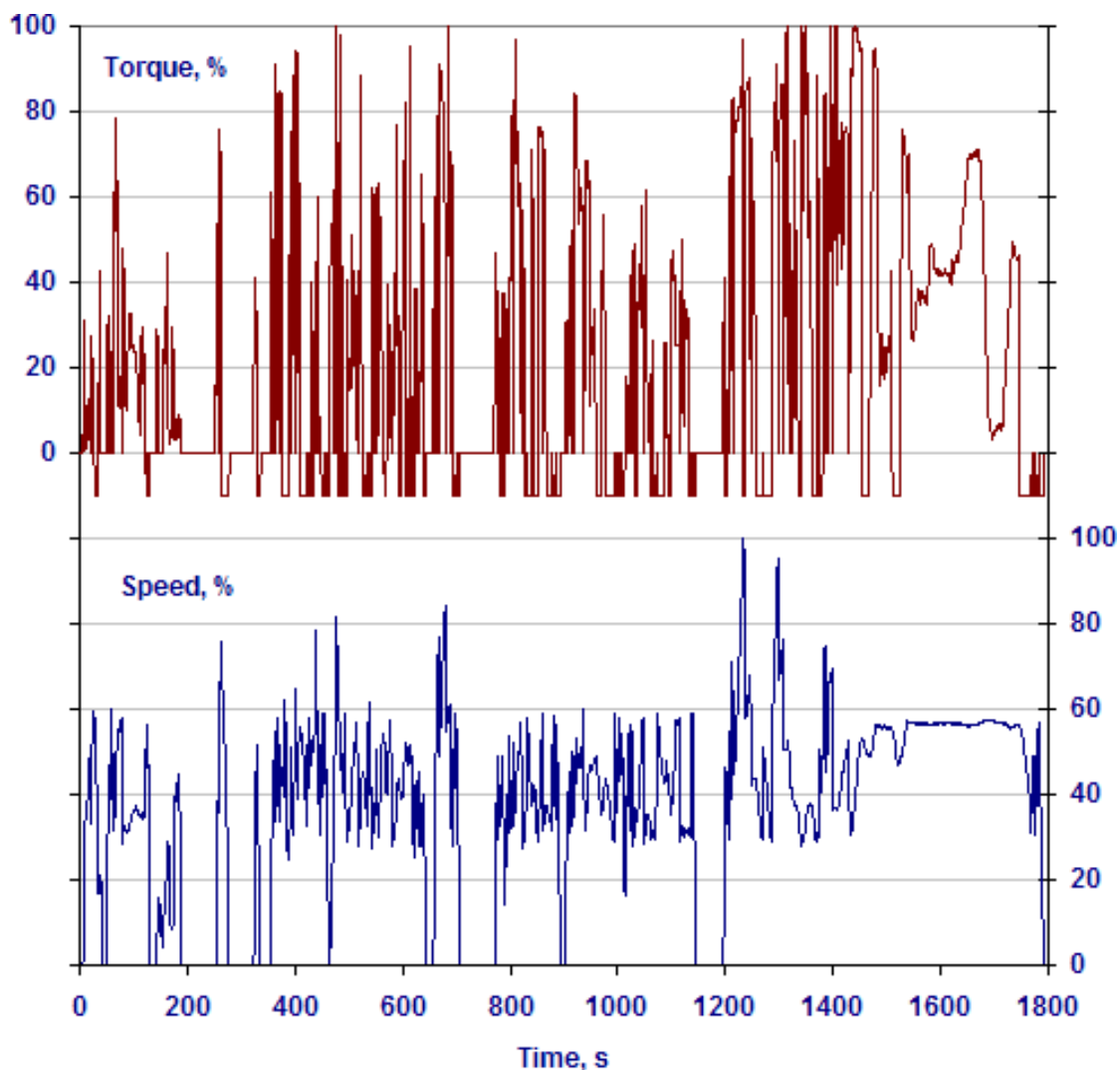


Figure 4.1 Normalized torque and speed profile of the WHTC

The homologation procedure comprehends two representative test cycles, a transient test cycle (WHTC) with both cold and hot start requirements and a hot start steady-state test cycle (WHSC), both created covering typical driving conditions in the EU, USA, Japan and Australia. WHTC testing requirements were adopted for the first time by the Euro VI emission regulation for heavy-duty engines.

## 4.2    Model modification to perform the WHTC

To perform the WHTC simulation, some modifications were needed. The engine model has been basically maintained as it was for the steady-state simulations but, in place of constant speed and torque, the transient profiles have been. Thanks to the automatic interpolation of the burn rate made by GT-Power in the combustion rate map already explained, the simulation of the transient cycle has been possible simply by imposing the boost pressure and spark advance profiles linked to the time of the cycle. The modifications are reported in the following Figures 4.2.

| Parameter | Unit | Description | Case 1 |
|---|---|---|---|
| Case On/Off | | Check Box to Turn Case On | ☑ |
| Case Label | | Unique Text for Plot Legends | WHTC |
| CASE | | | WHTC ... |
| SPEED | RPM | | WHTC_speed ... |
| brake_torque | N-m | Target Signal | WHTC_torque ... |
| Boost | | Target | boost_profile... ... |
| inlet | mm | | 72.25 ... |
| outlet | mm | Hole Diameter | 67 ... |
| throttle_angle | | Throttle Angle | 85 ... |
| Minimum-Throttle | | Minimum Output (angle or diameter) | 0 ... |
| WG | mm | Maximum Wastegate Diameter | 45 ... |
| time | s | Maximum Simulation Duration (Time) | 1805 |

Figure 4.2 Speed, torque and boost pressure profiles implementation

Further modifications have been needed for the Heat Transfer Rate relation that was now depending on transient values. Also in this case, in the HTR relation it has been implemented the speed profile instead of a constant speed (Fig. 4.3 and 4.4).

| Parameter | Unit | Description | Case 1 |
|---|---|---|---|
| **Case On/Off** | | **Check Box to Turn Case On** | ☑ |
| **Case Label** | | **Unique Text for Plot Legends** | WHTC |
| CylinderCoolantlHTR | W/(m^2-K) ∨ | Cylinder Coolant Heat Transfer Coeff… | HTR_coolant … |
| HeadCoolantHTR | W/(m^2-K) ∨ | Head Coolant Heat Transfer Coefficie… | HTR_coolant … |
| CylinderOilHTR | W/(m^2-K) ∨ | Cylinder Oil Heat Transfer Coefficient | 400 … |
| PistonOilHTR | W/(m^2-K) ∨ | Piston Oil HTC (Zone 1 for Custom FE… | 1500 … |
| HTC_Port | W/(m^2-K) ∨ | External Convection Coefficient | HTR_port … |
| HTM | | Heat Transfer Multiplier | 4.5 … |

Figure 4.3 HTR transient profiles implementation

| | Attribute | Unit | Object Value |
|---|---|---|---|
| | Input RLT Variable (X) | | avgrpm:engine … |
| | Initialization for First RLT Period | | |
| ◉ | Initial X Input | | 1500 … |
| ○ | Initial Y Output | | |
| | Dependence Object | | HTR_coolant_function … |

Figure 4.4 Speed profile implementation in the HTR relation

Finally, since the injectors model weren't capable of automatically distinguish when a cut-off or a motored section of the cycle was encountered, it has been necessary to add a further control on them, implementing a logical relation that takes into account cut-offs and motored sections of the WHTC as function of the time. The relation considers both the engine speed and the accelerator pedal travel: when the accelerator travel is zero and the engine speed is over the idle, it is obviously a situation of cut-off; on the contrary, when the speed is near idle and the pedal travel is null, is an idle condition hence lambda have to be putted to stoichiometric.

As already exposed, the injectors were controlling the lambda value and hence, to be able to simulate a cut-off, it should have been necessary to impose a value of infinite. Since it was not compatible with the software it has been decided that change the controller parameter from lambda to its inverse, phi, and put it at zero when a cut-off or a motored section was encountered. The added controller and its logical relation are shown in the following Fig. 4.5-7.
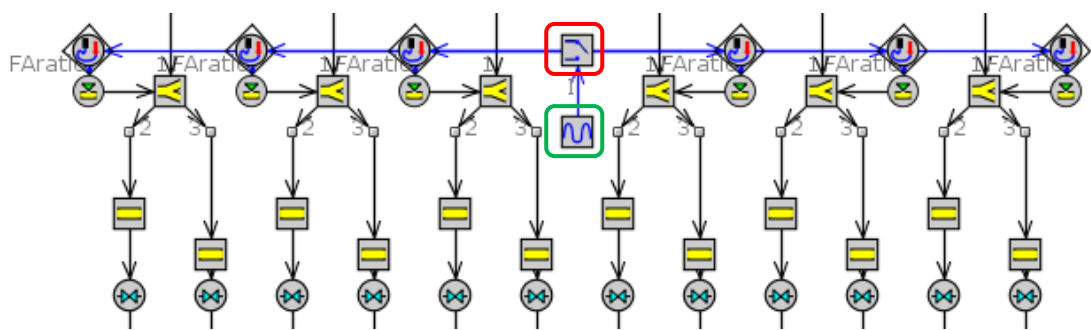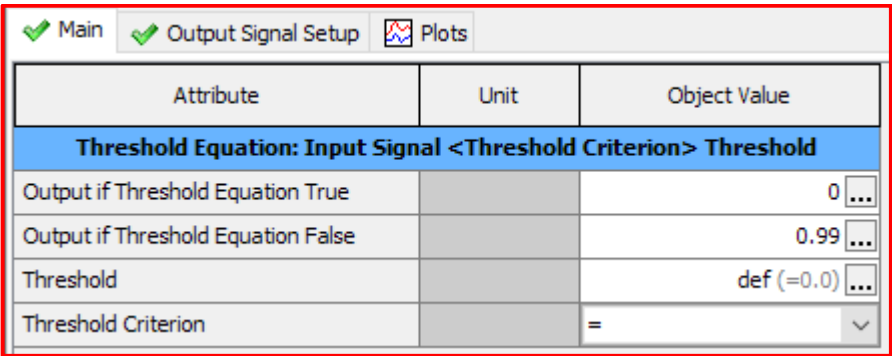
Figure 4.5 Phi controller implementation



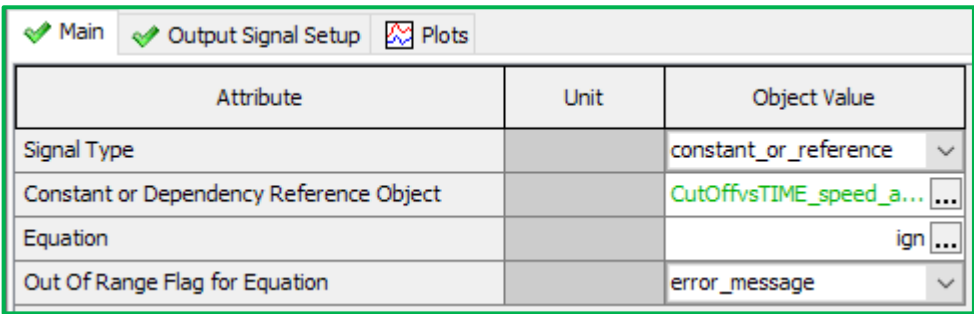Figure 4.6 Logical switch acting on phi



Figure 4.7 Logical relation imposing cut-off through phi

A further little modification on the Throttle controller has been necessary. It appeared in fact that the controller was too slow in its operations, behaviour that in steady-state for obvious reasons never appeared. To overcome the issue, it has been increased the aggressiveness factor of the proportional gain and little reduced the one of integral gain. Doing so, the model was much faster and able to follow the rapid changes of torque and speed imposed by the WHTC.

# 5. Transient cycle results

In this chapter will be exposed the results of the transient simulation over the WHTC. Because of the length of the cycle, about 1800 seconds, and the very oscillating profile, the graphs that show instantaneous results will report only a fraction of the cycle. This section has been chosen in order to have one of the most significative part of the cycle including steep accelerations, cut-offs, motored and idle sections. The cumulated graphs, instead, report the entire cycle, since the line are much more readable.

First are shown the torque result, to well expose the grade of calibration reached in this cycle and understand the error margin that cannot be overcome because of the not perfect match of the torque (Fig. 5.1). Engine speed it has been imposed while the torque was a target of the model contains some errors but, considered relatively to the entire cycle, they are anyway acceptable also considered the highly dynamic of the cycle itself.

For what concerns the air and fuel flow rates (Fig. 5.2-3), the simulation results follow what already seen for the torque, where a general good prediction is achieved even if the point-to-point deviation are larger, always caused by the strong oscillating nature of the WHTC.

Finally are reported the predicted emissions of, in the order, $NO_x$, CO, and $CO_2$ both instantaneous (Fig. 5.4-6) and cumulated (5.8-10). The calibration performed for the steady-state has given good results also when exploited in the WHTC. As it is possible to see, even with some errors in the peaks due to the transient nature of the cycle, $NO_x$ and $CO_2$ are substantially well predicted, confirmed by the cumulated results where the final deviations are small. It must be considered also that even the combustion, simulated in each timestep, is a source of error since it is calculated through an interpolation based on the burn rate profiles table already explained in the paragraph 2.9. Completely different situation for the CO where the simulated values are very far from the experimental data. This is a direct consequence of the problems already encountered in the steady-state, where the point-to-point deviations in the engine map were too large to find common calibrating parameters able to give more reliable results. This behaviour is for sure dictated by the method that has been used to achieve a combustion profile map without the possibility of exploit the predictive combustion model. It is in fact not present for $NO_x$ and $CO_2$, where also the steady-state simulations were good.

It has been included also the instantaneous transient graph of the predicted $O_2$, for the time interval of 600-900 seconds (Fig.5.7). The oxygen, like the $NO_x$ and the $CO_2$, follows the experimental trace within a little amount of error. The cumulated, however, it is not comparable because the highly nervous profile of the WHTC as well as the large number of cut-offs affect the oxygen sensor that, in extreme conditions, isn't capable of correctly sense the oxygen giving highly uncorrected values. For that reason, the predicted cumulated value results to be largely different from the experimental.
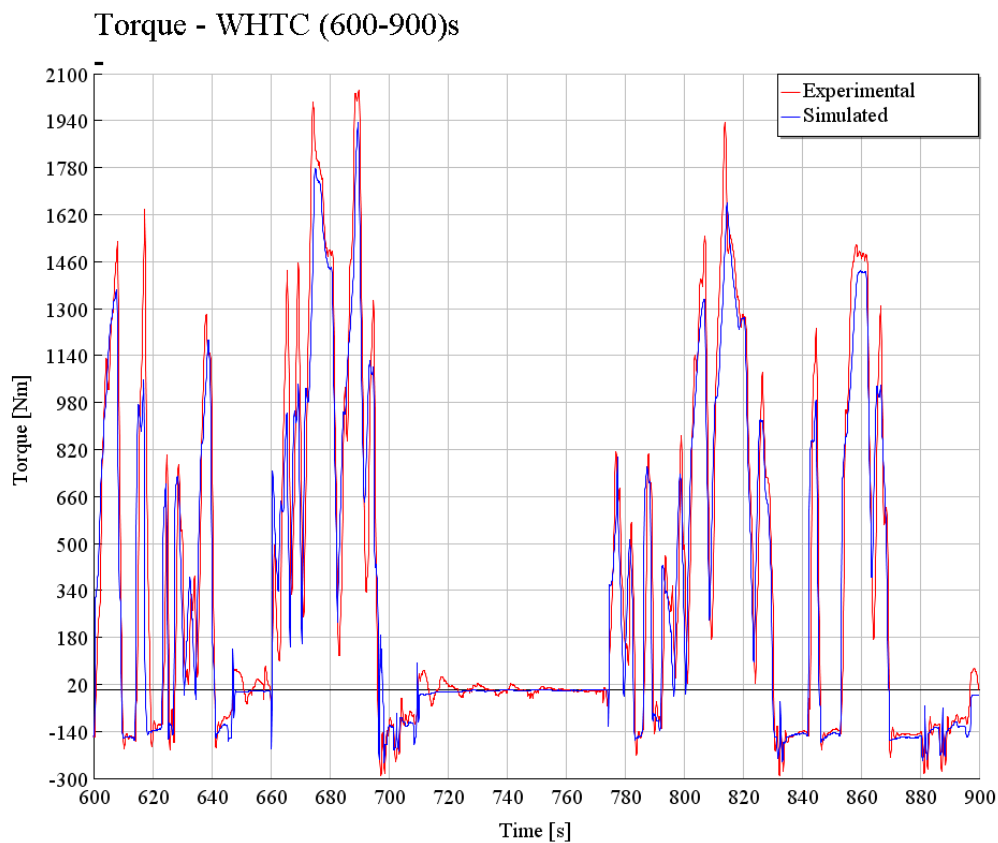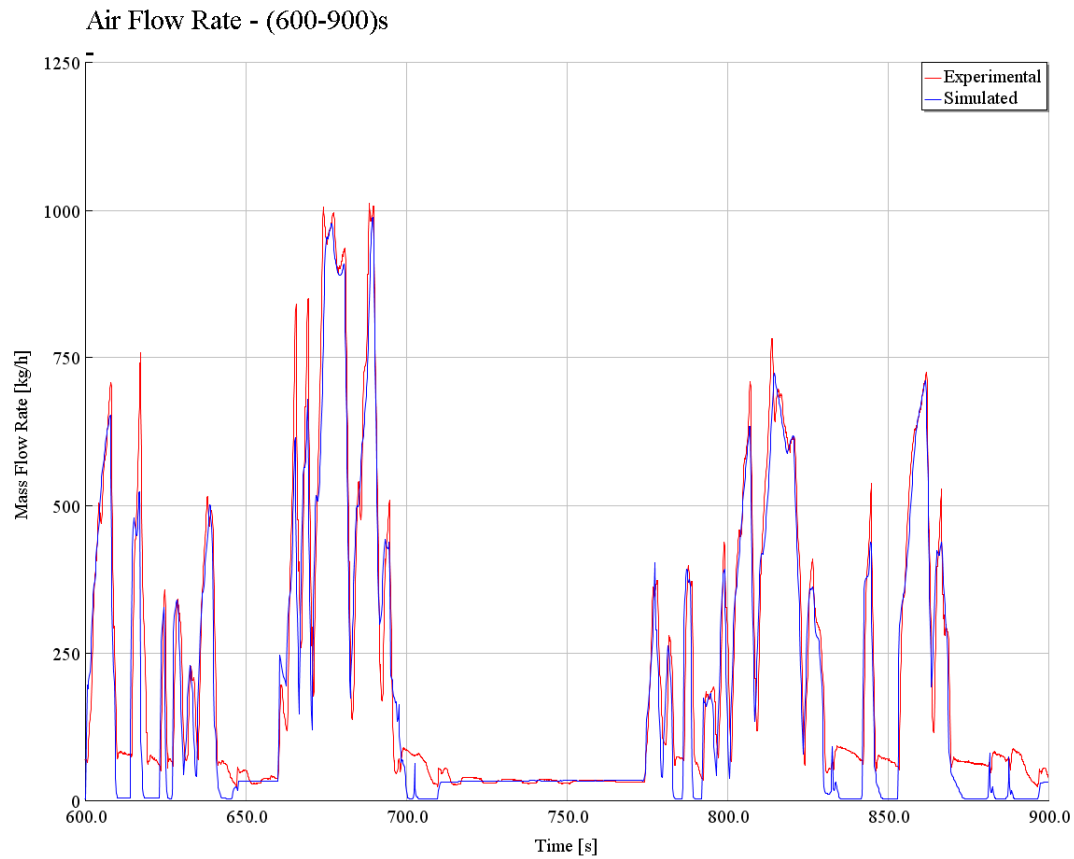


Figure 5.1 WHTC torque profiles

Air Flow Rate - (600-900)s



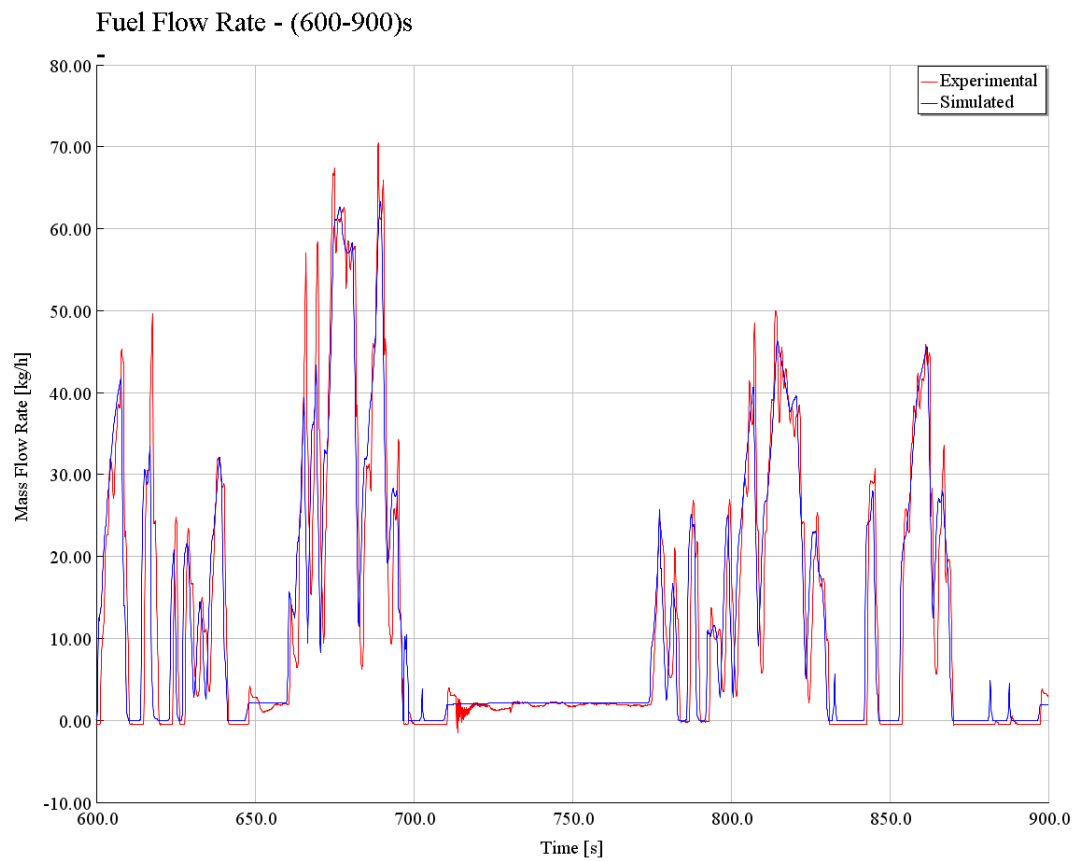Figure 5.2 WHTC Air flow rate profiles

Fuel Flow Rate - (600-900)s



Figure 5.3 WHTC Fuel flow rate profiles

Normalized NOx Concentration at ATS inlet
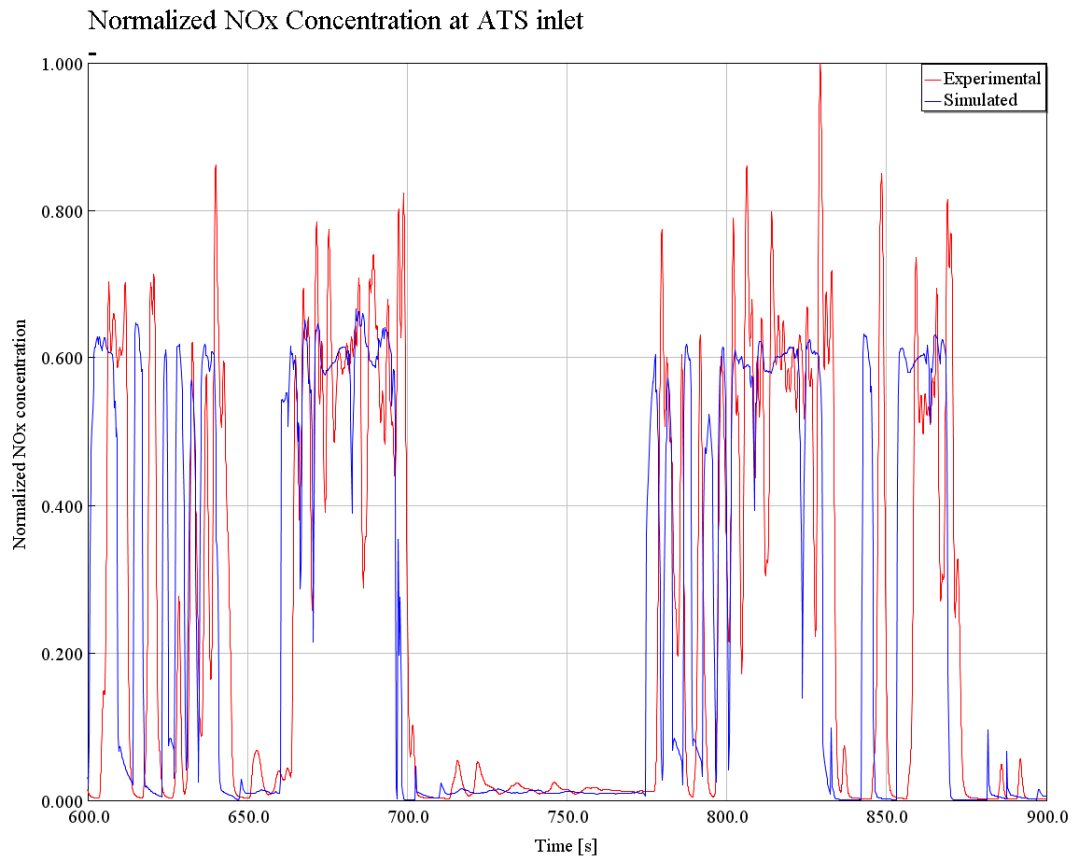


Figure 5.4 Predicted NOx (instantaneous)

Normalized CO concentration at ATS inlet
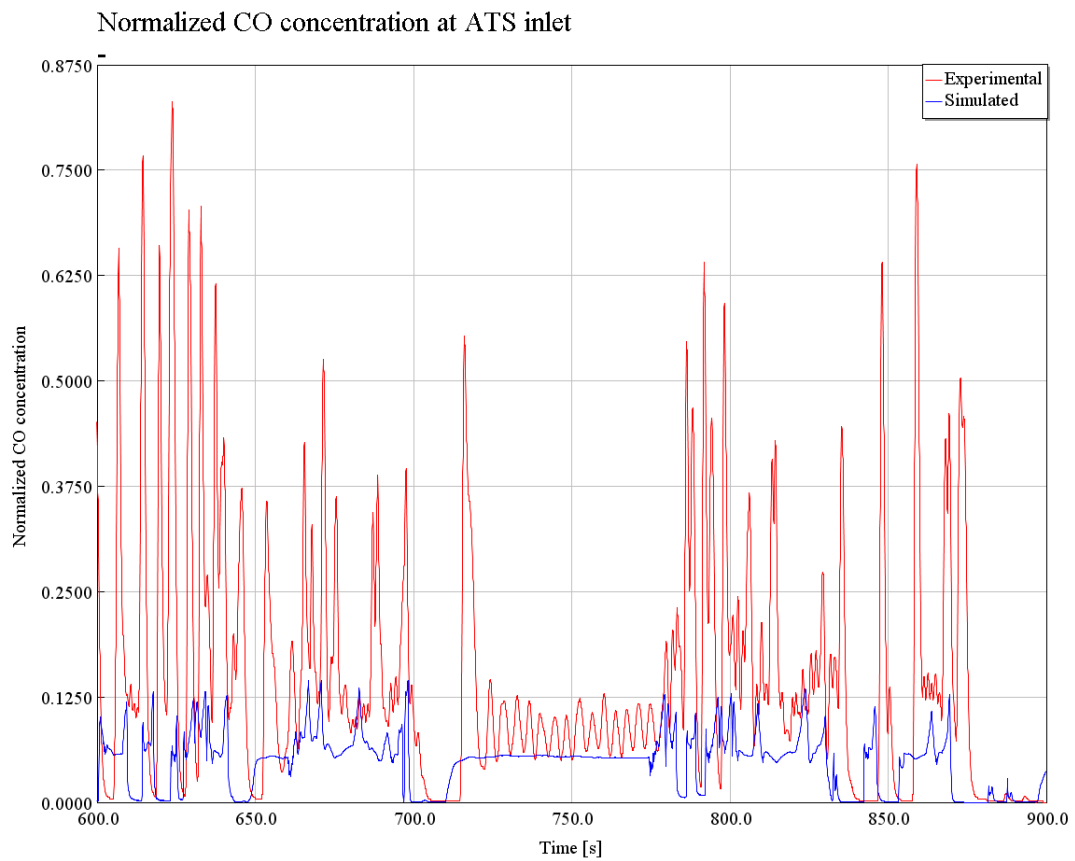


Figure 5.5 Predicted CO (instantaneous)

Normalized CO2 concentration at ATS inlet
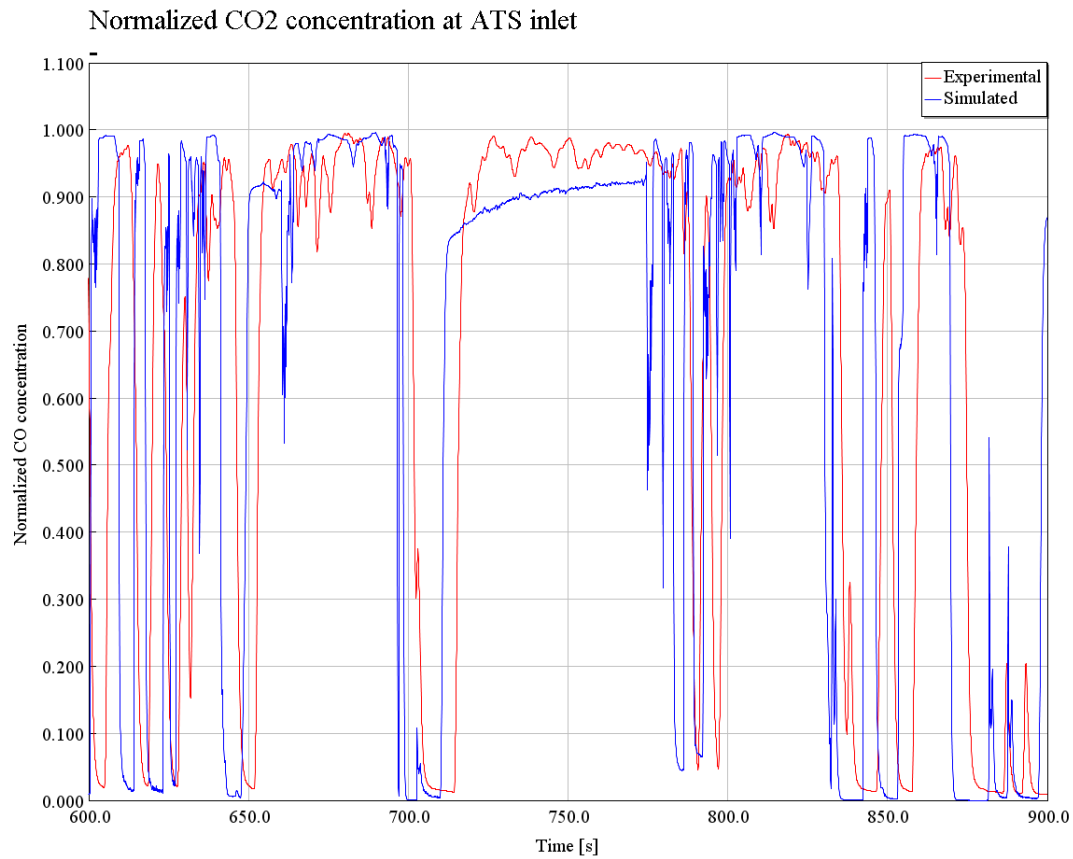


Figure 5.6 Predicted $CO_2$ (instantaneous)

Normalized O2 concentration at ATS inlet
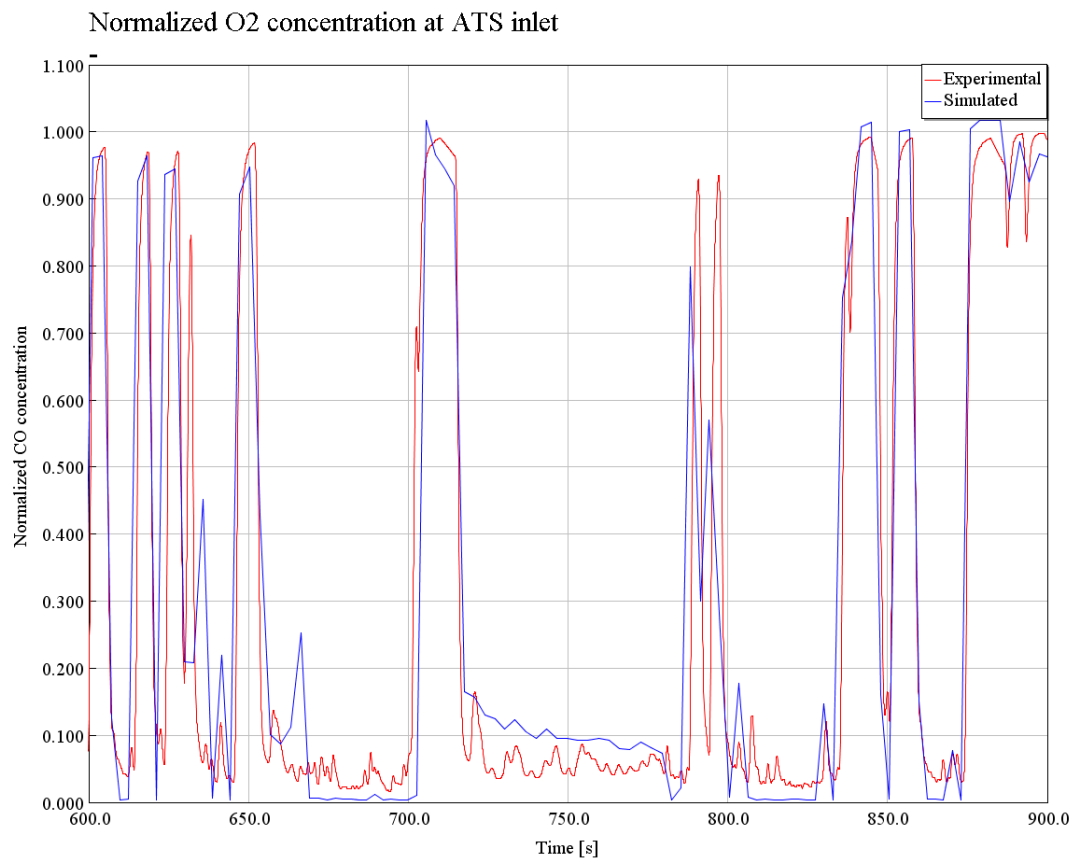


Figure 5.7 Predicted $O_2$ (instantaneous)

Normalized Cumulated NOx emissions at ATS inlet
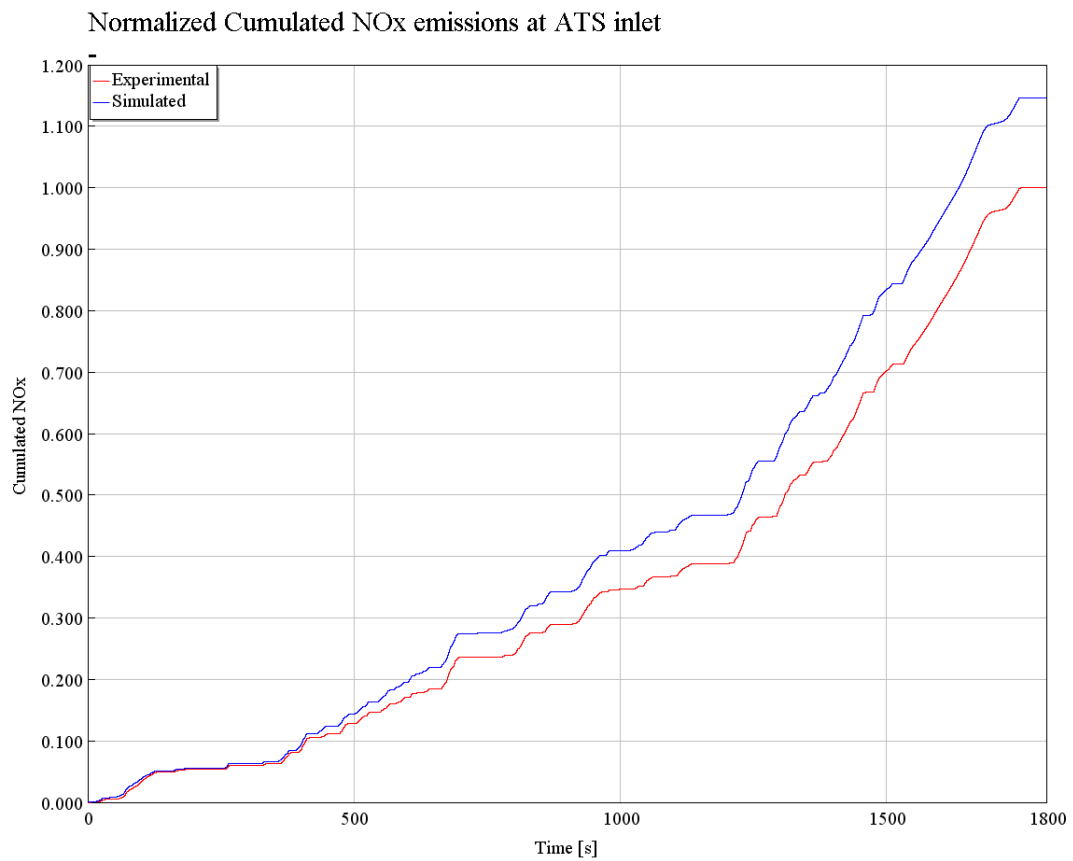


Figure 5.8 Predicted NOx (cumulated)

Normalized Cumulated CO emissions at ATS inlet
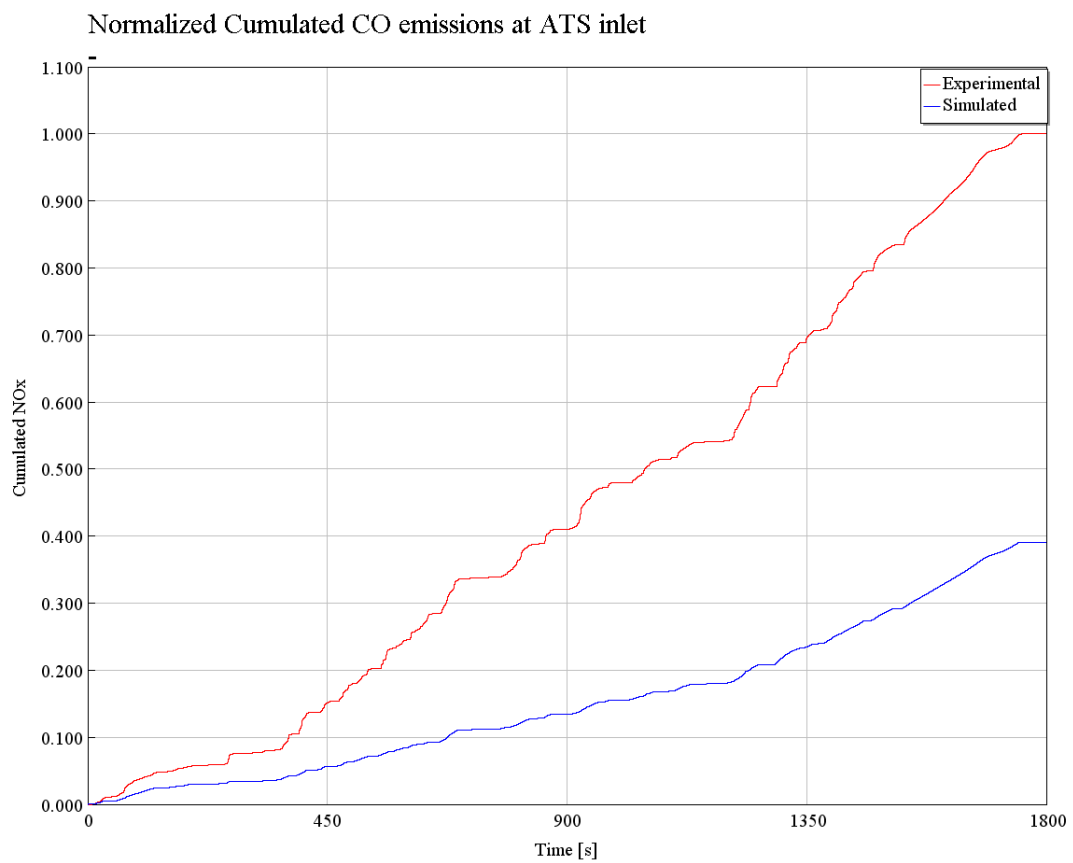


Figure 5.9 Predicted CO (cumulated)

Normalized Cumulated CO2 emissions at ATS inlet
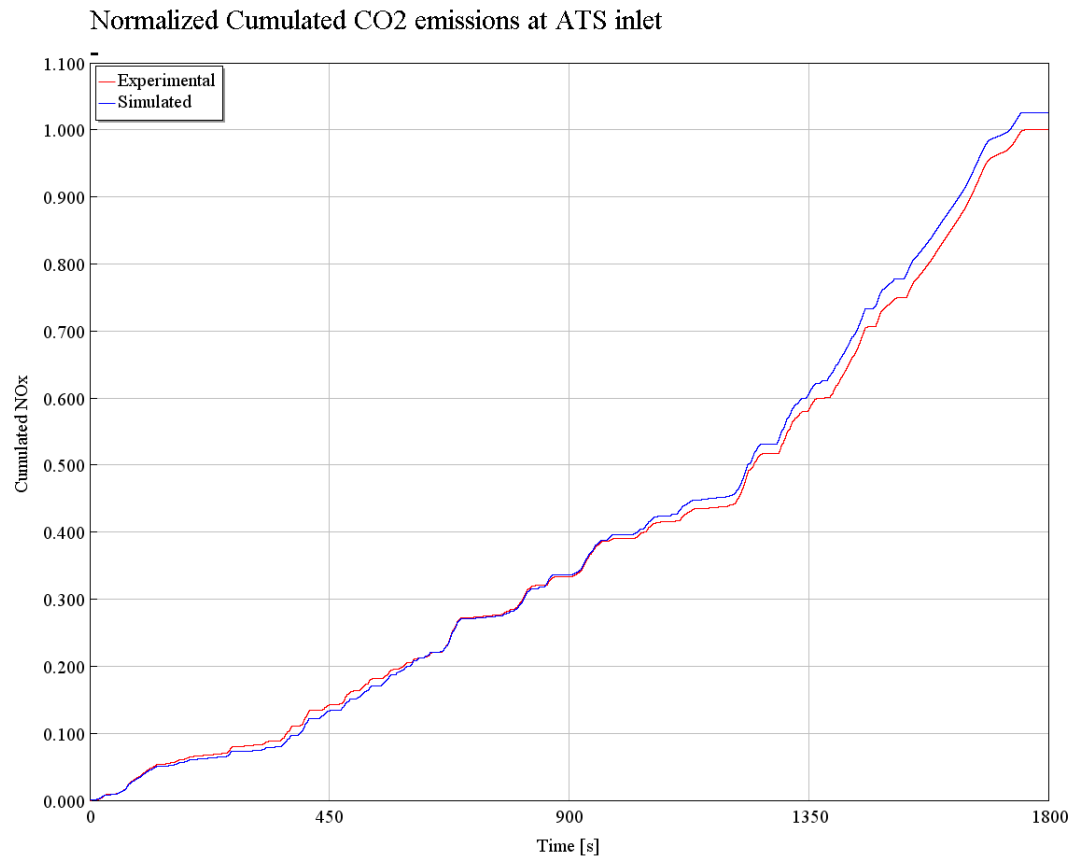


Figure 5.10 Predicted $CO_2$ (cumulated)

# 6. Conclusions

## 6.1   Summary and conclusions

An almost complete model of a CNG engine has been built and calibrated in this work (only ATS and tailpipe excluded). The engine was a 6 cylinders heavy-duty SI CNG fuelled for which both steady-state and transient condition have been analysed. Starting from the analysis of the combustion profiles, given by the Three Pressure Analysis, frictions and heat exchange have been adjusted. TPA has been possible since pressure traces and temperatures were available from experimental tests made on the actual engine.

Once the frictions and the heat transfer rates have been calibrated, the study continued finding a good predictive combustion model. SITurb was the only model already present in GT-Power that could have been used for this task. Unfortunately, the model highlights the impossibility of reproducing the combustion profiles through it. The profiles were in fact lagging in the development of the kernel, i.e. immediately after the spark, with respect to the experimental and after, due to the accumulated delay (hence energy still not released), once the flame was enough developed, it increased the profile slope reaching a peak higher than the experimental, to balance the energy deviation. No combination of calibration multipliers could solve this issue, that was caused by the incorrect modelling of the CNG turbulent speed performed by the software. To overcome it, a semi-empirical model exploiting the experimental combustion profiles obtained through the TPA has been then implemented: the profiles corresponding to the 25 experimental points have been used to build a table from which the software could take the right profile depending on engine speed and torque. Furthermore, GT-Power was automatically able to interpolate these profiles creating a continuous map of combustion profiles. Thank to that procedure, it has been possible to validate the engine model also in the WHTC.

$NO_x$, CO and $CO_2$ emissions have been then calibrated, starting from the steady-state conditions. $NO_x$ and $CO_2$ predicted emissions have given good results, matching the experimental values within a little margin of error, while for the CO errors where much larger. The reasons have to be found into the model used for the CO prediction, based on the equilibrium of oxidation into $CO_2$ kinetically controlled, hence based on the energy of the gases in the expansion and exhaust phases. The parameters that could be adjusted

are not enough to well describe the different kinetics and energy release occurring in a CNG engine that, although operated with homogeneous mixture, it hasn't the same behaviour of a gasoline one (as already seen during the combustion calibration). Transient results follow what already achieved in the steady-state, with $NO_x$ and $CO_2$ close to the experimental and CO very far, verifying that the engine is actually well simulated.

The results, although still not compatible with the aim of the project, i.e. creating a model that could substitute the experimental tests, are pretty reassuring on the potential that this type of study have. Finally, it has been verified that GT-Power model called SITurb is currently not suitable to be used for CNG fuelled engines and hence needs to be improved.

## 6.2   Future works

First, improve the combustion model by introducing an external routine, that can properly simulate the flame propagation of the CNG mixture, could extend the field of use of this model. With a complete predictive model so obtained, will be possible to perform evaluations on prototypes design, testing them directly in the model, without the necessity of built them and hence reducing cost of material, construction and time.

Then, enhance the CO calibration, eventually adding another external routine for its prediction, will bring additional benefits for the other emission compounds simulation, such as NOx and CH4, that haven't been accounted for in the work but are still present and of fundamental importance. A good prediction of all the emission compounds, could open the route to a coupling between engine model and ATS model. The complex model that will be obtained, could give a great help in the research of new compromises for emissions reduction, unlocking the possibility to operate both on the engine and in the ATS system at the same time. In that situation, design solutions that could have different behaviours if combined with each other with respect of being applied individually, could be easily evaluated and tested.

Finally, it will be useful to evaluate the transient behaviour of the model on more driving cycles, different from the WHTC. It will strengthen the accuracy of the model underlining

potential errors that haven't showed up before. The model obtained, although not completely immature, needs to be upgraded to be seriously useful as substitute of a test rig. It will take time, but the premises are reassuring.

Natural gas engines are largely studied nowadays and will be of fundamental importance in the development of near future vehicles, both heavy and light duty, due to their lower impact on the environment.